# Development of Advanced Artificial Solid Electrolyte Interphases for Lithium Metal Anodes

Dem Fachbereich Biologie und Chemie der
Justus-Liebig-Universität Gießen vorgelegte Dissertation
zur Erlangung des akademischen Grades
Doktor der Naturwissenschaften

- Dr. rer. nat. -

**Bastian Krauskopf**

- September 2023 -

| | |
|---|---|
| Dean / Dekan | Prof. Dr. Thomas Wilke |
| 1. Gutachter / 1st Reviewer | Prof. Dr. Jürgen Janek |
| 2. Gutachter / 2nd Reviewer | Prof. Dr. Bernd M. Smarsly |
| Eingereicht / Submitted | 21. September 2023 |
| Disputation | 18. Januar 2024 |

## Eidesstattliche Erklärung

Die vorliegende Arbeit wurde im Zeitraum vom 02.01.2019 bis 24.06.2023 am Physikalisch-Chemischen Institut der Justus-Liebig-Universität Gießen unter Betreuung von Prof. Dr. Jürgen Janek angefertigt.

Ich erkläre: Ich habe die vorgelegte Dissertation selbstständig und ohne unerlaubte fremde Hilfe und nur mit den Hilfen angefertigt, die ich in der Dissertation angegeben habe. Alle Textstellen, die wörtlich oder sinngemäß aus veröffentlichten Schriften entnommen sind, und alle Angaben, die auf mündlichen Auskünften beruhen, sind als solche kenntlich gemacht. Ich stimme einer evtl. Überprüfung meiner Dissertation durch eine Antiplagiat-Software zu. Bei den von mir durchgeführten und in der Dissertation erwähnten Untersuchungen habe ich die Grundsätze guter wissenschaftlicher Praxis, wie sie in der „Satzung der Justus-Liebig-Universität Gießen zur Sicherung guter wissenschaftlicher Praxis“ niedergelegt sind, eingehalten.

Gießen, 21.09.2023

Bastian Krauskopf

*Ich weiß jetzt, dass es unerheblich ist, wie jemand geboren wird.*
*Wie man mit dem Geschenk des Lebens umgeht,*
*macht einen zu dem, was man ist.*

Mewtu

# Kurzfassung

Die Elektrifizierung des Transport- und Verkehrssektors ist ein wichtiges Ziel zur Reduzierung von $CO_2$-Emissionen im Rahmen der weltweiten Bemühungen zur Bekämpfung der globalen Erwärmung. Trotz immer höherer Reichweiten bleibt die dennoch begrenzte Reichweite und vergleichsweise lange Ladezeiten von Elektrofahrzeugen (EVs), auch bekannt als „Reichweitenangst“, ein Hauptgrund für ihre langsam steigende Verbreitung. Zur Lösung dieser Problematik ist es laut Experten entscheidend, die Energiedichte von Batterien auf 500 Wh/kg und 1000 Wh/L zu erhöhen. Die derzeitige Lithiumionen-Batterietechnologie kann diese Werte aufgrund ihrer physikalisch-chemischen Grenzen jedoch nicht erreichen. Lithiummetall-Batterien bieten eine vielversprechende Alternative, da sie potenziell höhere Energiedichten und Leistungsdichten bieten können. Im Gegensatz zu konventionellen Lithiumionen-Batterien mit Graphitanoden verzichten Lithiummetall-Batterien in der Anode auf Trägermaterialien wie Graphit und erhöhen dadurch die spezifische Kapazität des Anodenmaterials. Allerdings stehen Lithiummetall-Batterien vor Herausforderungen wie unerwünschten Reaktionen zwischen der Lithiummetall-Anode (LMA) und dem Elektrolyten, die beide Komponenten beeinträchtigen, sowie ungleichmäßigem Lithiumwachstum auf der Elektrodenoberfläche, was zu einer verringerten Batterielebensdauer führt.

Im Zuge dieser Arbeit wurden verschiedene Ansätze zur Erzeugung einer stabileren Grenzfläche zwischen LMA und dem flüssigen Elektrolyten untersucht, um Degradationsreaktionen und ungleichmäßige Lithiumabscheidung zu unterbinden. Der erste Teil der Arbeit beschäftigte sich mit auf Polymeren basierenden Schutzschichten, die per Spin-Coating auf die Anoden aufgetragen wurden. Die so behandelten Elektroden wurden in symmetrischen Überführungszellen hinsichtlich Überspannung und Zyklenstabilität untersucht. Dabei wurde festgestellt, dass durch die Zugabe von Metallkomplexen zum Polymer die Überspannung stark verringert werden konnte und dass beispielsweise eine hybride Schutzschicht aus Polyethylenoxid und dem Feststoffelektrolyten $Li_6PS_5Cl$ zu einer hohen Zyklenstabilität führt, wobei allerdings die Verträglichkeit von Polymer, Feststoffelektrolyt und Lösungsmittel untereinander problematisch sein kann.

Im weiteren Verlauf dieser Arbeit wurde per Dip-Coating die natürliche Passivierungsschicht der Lithiumelektroden modifiziert, um eine künstliche Grenzfläche mit verbesserter Homogenität, Leitfähigkeit und Stabilität zu erhalten. Dabei wurde untersucht, auf welche Art und Weise die für das Dip-Coating eingesetzten Reagenzien mit Lithium bzw. mit der Passivierungsschicht reagieren und wie dies die Leistungsfähigkeit der Elektroden beeinflusst. Dafür wurden zusätzlich zu den Überführungsexperimenten oberflächenanalytische Methoden wie Röntgenphotoelektronen-spektroskopie (XPS) und Flugzeit-Sekundärionen-Massenspektrometrie (ToF-SIMS) angewandt.

Dabei zeigte sich, dass Modifikationen durch halogenhaltige Reagenzien, die auf der Elektrodenoberfläche beispielsweise zu LiCl oder LiBr reagieren, zu stark verbesserter Lithiumauflösung und -abscheidung führen. Aber auch die Kombination einer Stickstoff- und Phosphorhaltigen Verbindung mit einem sterisch gehinderten Alkohol resultierte in einer dünnen und homogenen Oberflächenschicht, die hoch ionisch leitfähiges $Li_3N$ enthält und sowohl in symmetrischen Zellen als auch in Lithium-Schwefel-Zellen zu verbesserten Eigenschaften in Bezug auf Lebensdauer und Kapazitätsverlust führt.

Die Ergebnisse dieser Arbeit erweitern das Wissen um die Möglichkeiten für Schutzbeschichtung und die Oberflächenmodifikation von LMAs. So wurden wichtige Parameter deutlich, die in Bezug polymerbasierte Schutzschichten beachtet werden müssen: Die Stabilität des Feststoffelektrolyten gegenüber dem Lösungsmittel, die Stabilität des Lösungsmittels gegenüber Lithium und Reaktionen zwischen Polymer und Feststoffelektrolyt. In Bezug auf das Dip-Coating der Elektroden stellte sich heraus, dass zum Beispiel durch die gezielte Nutzung prädestinierter Abgangsgruppen (Cl, Br) und die Veränderung der Reaktivität durch die Auswahl des Lösungsmittels oder die Kombination von Reagenzien es möglich ist, gewünschte Eigenschaften oder chemische Zusammensetzungen an der Elektrodenoberfläche zu erreichen.

# Abstract

The electrification of the transport and traffic sector is an important goal for reducing $CO_2$ emissions as part of worldwide efforts to combat global warming. Despite increasing ranges, the limited range and relatively long charging times of electric vehicles (EVs), also known as *range anxiety*, remain a major reason for their slow adoption. Experts believe that increasing the energy density of batteries to 500 Wh/kg and 1000 Wh/L is crucial to address this issue. However, the current lithium ion battery technology cannot achieve these values due to its physical and chemical limits. Lithium metal batteries offer a promising alternative as they potentially offer higher energy and power densities. Unlike conventional lithium ion batteries with graphite anodes, lithium-metal batteries eliminate carrier materials like graphite in the anode, thereby increasing the specific capacity of the anode material. However, lithium-metal batteries face challenges such as unwanted reactions between the lithium metal anode (LMA) and the electrolyte, which affect both components, as well as uneven lithium growth on the electrode surface, leading to reduced battery life.

In this study, various approaches were examined to create a more stable interface between LMA and the liquid electrolyte to prevent degradation reactions and uneven lithium deposition. The first part of the study focused on polymer-based protective layers applied to the anodes using spin-coating. The treated electrodes were investigated in symmetrical transfer cells regarding overvoltage and cycling stability. It was found that adding metal complexes to the polymer significantly reduced overvoltage, and, for example, a hybrid protective layer consisting of polyethylene oxide and the solid electrolyte $Li_6PS_5Cl$ led to high cycle stability, although the compatibility between the polymer, solid electrolyte, and solvent can be problematic.

In the further course of this study, the natural passivation layer of the lithium electrodes was modified via dip coating to obtain an artificial interface with improved homogeneity, conductivity, and stability. The way in which the reagents used for dip-coating reacted with lithium or the passivation layer and how this influenced the performance of the electrodes was examined. In addition to the symmetric cell tests, surface analytical methods such as X-ray photoelectron spectroscopy (XPS) and time-of-flight secondary ion mass spectrometry (ToF-SIMS) were applied.

It was found that modifications using halogen-containing reagents that react with the electrode surface, for example, to form LiCl or LiBr, resulted in significantly improved lithium dissolution and deposition. Combining a nitrogen and phosphorus-containing compound with a sterically hindered alcohol also resulted in a thin and homogeneous surface layer containing highly ionically conductive $Li_3N$, leading to improved properties in terms of lifespan and capacity loss in both symmetrical cells and lithium-sulfur cells.

The results of this study expand knowledge about the possibilities of protective coating and surface modification of LMAs. Important parameters were identified that need to be considered in relation to polymer-based protective layers: the stability of the solid electrolyte towards the solvent, the stability of the solvent towards lithium, and reactions between the polymer and the solid electrolyte. Regarding the dip-coating of the electrodes, it was recognized that desired properties or chemical compositions on the electrode surface can be achieved, for example, by selectively utilizing suitable leaving groups (Cl, Br) and modifying reactivity through the choice of solvent or combination of reagents.

# Table of Contents

# 1 Introduction

Starting with the commercial introduction of lithium ion batteries in 1991, the market for rechargeable batteries was dominated by lead-acid, nickel-cadmium (Ni-Cd) and nickel-metal hydride (Ni-MH) batteries. From today's point of view, these electrochemical energy storage techniques offer unsatisfactory low energy densities of 20-40 Wh/kg for lead-acid, up to 60 Wh/kg for Ni-Cd and up to 100 Wh/kg for Ni-MH batteries with Ni-Cd and Ni-MH being considered the state-of-the-art for portable electrochemical energy storage all throughout the 1990s whereas Ni-MH was seen as a promising advancement. Having a volumetric energy density equally high as lithium ion batteries in 2001 (340 Wh/L), Ni-MH batteries were even used as energy storage for hybrid electric vehicles.[1–3] However, in the following few years of the early 2000s, rapidly sinking manufacturing costs and opposingly rising capacity and energy density of lithium ion batteries (LIBs) quickly led to the (almost) obsolescence of alkaline rechargeable battery technologies such as Ni-Cd and Ni-MH as market leaders for portable power sources.[4,5] As a result of continuous research and development, modern LIBs can easily reach values as high as 265 Wh/kg resp. 635 Wh/L or more for their energy density.[6] Comparing these values with the energy densities mentioned at the beginning, it shows the almost inconceivable progress made in the last 30 years. Resulting from this merit, LIBs are not only the № 1 choice for handheld or portable electronic devices but also for grid electricity storage/buffering and, of course for electric vehicles (EVs).[5]

As it is a global effort to reduce $CO_2$ emissions in order to slow down global warming, the electrification of transport is one major goal.[7] However, despite the fact that ordinary EVs can drive 400-600 km with one single battery charge, the "short" range is still a major hindrance for higher EV adoption having even developed an own term: *range anxiety*, or in German: *Reichweitenangst*.[8,9] One way to achieve higher EV ranges is to increase the batteries' energy density,[7] for which respected experts have set a goal of 500 Wh/kg and 1000 Wh/L at cell level.[10,11] However, these values cannot be realized with the current *jack of all trades*, the conventional lithium ion battery technology, as said values would surpass its physicochemical limit.[12–14]

While consequently improvements in power- and energy density are hardly possible for ordinary lithium ion batteries, lithium metal batteries offer a promising alternative.[10,15] In a classic lithium ion battery, the anode is made of graphite, into which lithium ions are inserted and removed. At maximum degree of intercalation, one lithium ion requires six carbon atoms as a carrier material. By eliminating the ballast of the graphite, the specific capacity of the anode material can be increased more than tenfold from 372 mAh/g to 3860 mAh/g whilst having the lowest of all electrochemical potentials. Especially induced by the latter, lithium is an extremely reactive metal, which means that in a lithium metal battery, undesirable reactions between the lithium metal anode

and the electrolyte will cause degradation of both components.[16] Furthermore, lithium tends to grow unevenly on the electrode surface during electrochemical plating which results in mossy or dendritic lithium growth causing continuous consumption of the electrolyte and therefore reduced battery durability[17]. At worst, a lithium dendrite can penetrate through the separator creating a short circuit between anode and cathode resulting in thermal runaway bearing serious fire hazard.[18] Despite the fact that for example all solid state batteries (ASSBs) potentially offer the highest level of operational safety by using non-flammable solid electrolytes, their production would require a drastically higher use of limited resources like lithium. This means higher production cost and higher environmental footprint of ASSBs whilst liquid electrolytes offer the best combination of resource friendliness and high ionic conductivity.[6,15]

Due to the aforementioned high lithium metal reactivity, there is always a passivation layer on top of the lithium metal surface simply from production and storage.[19,20] When in contact with a liquid electrolyte, the lithium will as well react with the electrolyte components (organic solvents, such as carbonates and ethers; conducting salts like $LiPF_6$ or LiTFSI) forming a so called *solid electrolyte interphase* (SEI for short).[16,21] As the term implies, the SEI itself is equivalent to a solid electrolyte which allows permeation of $Li^+$ ions between anode and (liquid) electrolyte during charge and discharge of the battery. However, since the "natural" SEI is more of a self-organized layer, its structure is inhomogeneous[22] and the lithium ion flux is not uniform, which means that fresh lithium is constantly being exposed to the electrolyte, which in turn leads to degradation reactions. Ideally, the SEI should comprise high lithium ion conductivity, low electronic conductivity, chemical stability and beneficial mechanical properties like high young´s modulus and strong adhesion.[23,24]

In this work, various liquid-based and therefore scalable approaches for the modification of lithium metal anodes are developed and tested. Polymer- and polymer/solid electrolyte hybrid coatings were applied by spin coating while SEI modifications towards artificial SEIs (ASEIs) using reactive precursor chemicals were executed by dip coating. To understand the effects of these coatings and modifications, the electrodes were tested in symmetrical cells and were thoroughly analyzed regarding their chemical composition at the electrode surface. This way it was possible to gather deeper understanding on the choice of reagents, tuning their reactivity and the coating compositions.

# 2 Fundamentals

## 2.1 The Lithium Ion Battery

The functional principle of a commercially available lithium ion battery (LIB) lies in the intercalation of lithium resp. lithium ions in the electrodes. When the battery is charged, electrons are transferred from the cathode to the anode via an external circuit, which also causes the lithium ions to migrate through the electrolyte to the anode. According to IUPAC, in any electrochemical reaction, the anode is defined as the place of the oxidation. Therefore, the common nomenclature (negative electrode = anode, positive electrode = cathode) is technically only correct during cell discharge as the oxidation/reduction processes are inverted during cell charge.[25] In this work, nevertheless, only the negative electrode is referred to as the anode and the positive electrode as the cathode, in accordance with established literature.[6] The anode consists of graphite, in which 1 lithium atom per 6 carbon atoms is intercalated in the fully charged state. During the discharge process, the intercalated lithium in the anode releases its electrons again, which flow into the cathode via the external circuit and the electrical consumers. For clarification, the here described functional principle is schematically depicted in figure 2. The driving force for this is the negative free enthalpy of the discharge reaction, i.e. the transfer of lithium from the lithiated graphite to the delithiated cathode. In the classic case, the cathode material consists of a layered oxide in the form $LiMO_2$, often $LiCoO_2$ (LCO). The voltage of the battery, like that of every electrochemical cell, depends directly on the Gibbs free energy $\Delta_r G$ of the reaction taking place according to equation 1. In the case of the reaction (scheme 2) taking place in a battery as it is depicted in figure 2 this results in an open cell voltage $E$ of approximately 4 V.[26]

$$E = -\frac{\Delta_r G}{zF} \tag{1}$$

$$LiC_6 + Li_{(1-x)}CoO_2 \rightarrow Li_{(1-x)}C_6 + LiCoO_2 \tag{2}$$

As direct contact between cathode and anode results in a short circuit and destruction of the cell, the electrodes are divided by a porous separator that is soaked with the liquid electrolyte. The electrolyte typically comprises $LiPF_6$ as the conductive salt which is dissolved in a mixture of ethylene carbonate (EC) and another carbonate such as dimethyl carbonate (DMC, see figure 1 for chemical structures). The ion conducting and electron blocking properties of these non-aqueous electrolytes enable the $Li^+$ solvation and transport between the electrodes while limiting self-discharge of the batteries.[27]

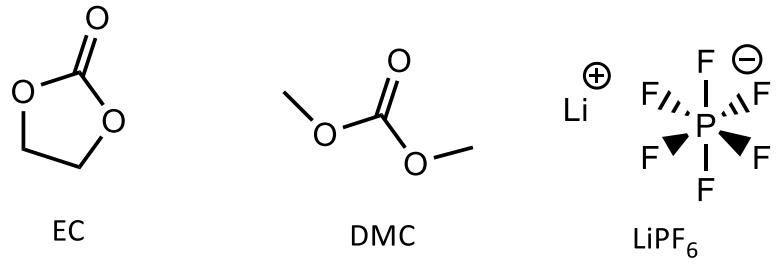


**Figure 1: Chemical structure of EC, DMC and $LiPF_6$ (left to right).**

The fundamentals of rechargeable lithium batteries have been laid in 1976 by Stan Whittingham as he introduced $TiS_2$ as the cathode material against a Li metal anode resulting in a cell voltage of ca. 2.5 V.[28] Further research by John Goodenough et al. in 1981 led to an increase of the cell voltage to 4 V by introduction of the oxide type cathode material $Li_xCoO_2$[29] which caused stark increase in energy density since it is proportional to the respective cell voltage. Today´s intercalation mechanism in both electrodes resp. the so-called rocking-chair chemistry was completed in 1985 when Akira Yoshino et al. established the use of carbonaceous anodes resulting in highly reliable batteries.[30] Since the commercialization in 1991 by Sony, the lithium ion battery has become the world´s number 1 electrochemical energy storage for consumer electronics[31] resulting in Whittingham, Goodenough and Yoshino being awarded the Nobel Prize for chemistry in 2019.

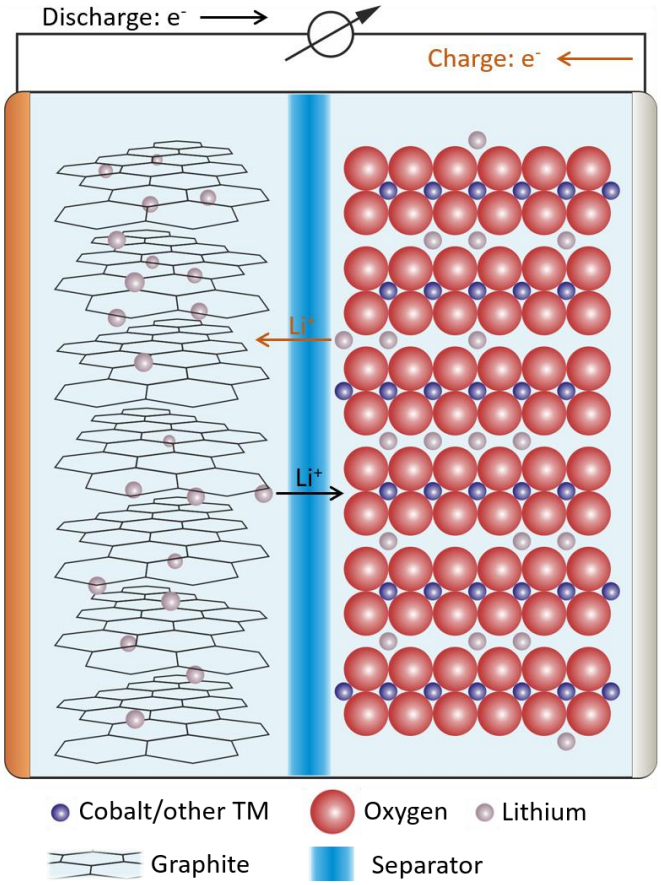


**Figure 2: Schematic design of a lithium ion battery consisting of a graphite anode and a lithium cobalt oxide cathode. For the sake of clarity, the electrolyte is not shown in detail.**

In terms of capacity, the price of LIBs has fallen by 97% between 1991 and 2021.[5] With regard to raw material costs, there is also a particular focus on the replacement of the problematic resource cobalt in the area of cathode materials. In so-called NCM ($LiNi_{1-x-y}Co_xMn_yO_2$) or NCA ($LiNi_{1-x-y}Co_xAl_yO_2$) cathodes, 70-90% of the cobalt can be replaced by nickel, manganese or aluminum with practically the same or even better performance[26,32] which is why they are already widely used in electric vehicles (EVs).[33] For the same cost-optimization reason alternative, cobalt-free LIB cathode concepts such as LNO ($LiNiO_2$), LMO ($LiMnO_2$) and LFP ($LiFePO_4$) are perceiving high interest in research and development. Especially LFP batteries are already well-developed and established delivering high lifetimes and low production costs. However, due to their low specific capacity, LFP batteries are mostly present in low-end electric vehicles.[34,35]

## 2.2 Alternative battery concepts

Since the development and improvement of LIBs has been constantly going on, their volumetric and gravimetric energy densities are quickly approaching the theoretical limits which logically cannot be surpassed.[13] However, with every step of asymptotically advancing towards these limits,

there is a risk that the operational safety of the battery may become compromised.[36] To overcome those limitations (see fig. 3 for a comparison of estimated energy densities) in terms of energy- and power density as well as potential safety issues, so-called post-LIBs such as lithium metal (LMB), lithium sulfur (Li-S), lithium air (Li-$O_2$) and all-solid-state batteries (ASSB) are intensively being researched and developed bearing concepts for new cathode, anode and electrolyte materials. All of the mentioned technologies require a lithium metal anode for ideal performance.[37–40]

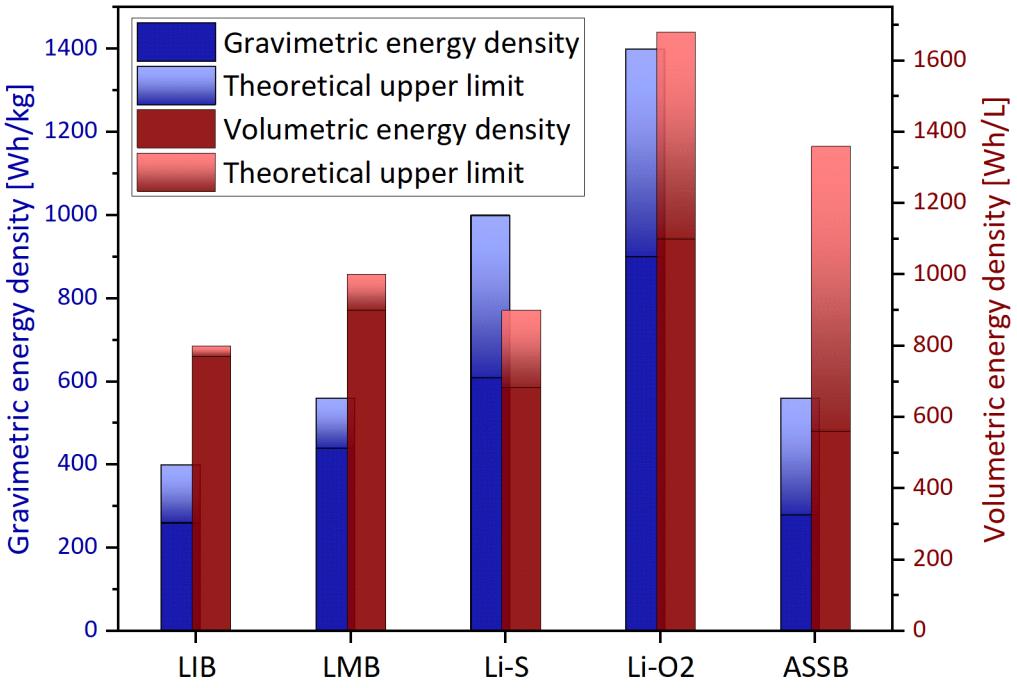


**Figure 3: Comparison of the respective volumetric and gravimetric energy densities of lithium based battery concepts.**[10,12,13,40–46]

### 2.2.1 The Lithium Metal Battery

In contrast to lithium ion batteries (LIBs), lithium metal batteries (LMBs) utilize pure lithium metal instead of graphite as anode material. As the lithium metal anode (LMA) does not contain any hosting material, it stands out having a particularly high theoretical capacity of 3862 mAh/g which is more than tenfold higher than the capacity of the graphite anode (372 mAh/g). This advantage allows the saving of volume and weight in the battery and can therefore increase the energy- and power density.[47] Apart from that, lithium metal has the lowest electrochemical potential which is most commonly denoted as - 3.04 V vs. the standard hydrogen electrode (SHE). While technically correct, this particular value is misleading since the SHE potential is defined in an aqueous system having a hydrogen ion activity at unity,[48–50] therefore this information cannot be transferred to non-aqueous battery systems without concern.

As depicted in figure 5, LMBs can be manufactured using the same cathode materials as commonly used in LIBs. Next to the carbonate/$LiPF_6$ electrolyte system mentioned before, another electrolyte system based on lithium bis(trifluoromethanesulfonyl)imide (LiTFSI) solved in 1,3-dioxolane (DOL) and dimethoxyethane (DME) is widely used in research (see figure 4 for the chemical structures).[10,51]

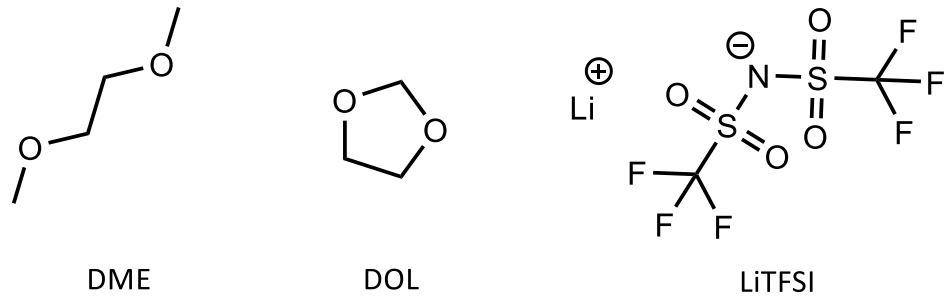


**Figure 4: Chemical structure of DME, DOL and LiTFSI (left to right).**

A special variety of the LMBs are so-called *anode-free* cells which are not assembled with an additional Li reservoir at the anode utilizing exclusively the lithium that becomes extracted from the prelithiated cathode material during charging. However, not all types of cathodes in lithium batteries are installed in the lithiated (discharged) state, as is the case with classic LIB cathodes (NCM, LCO, LFP). Conversion-type batteries such as lithium-sulfur or lithium-air batteries, for example, are almost exclusively built in a charged state by design, which means that a lithium reservoir remains necessary for future battery concepts.[52–55] The detailed characteristics and issues concerning the LMA will be discussed in section 2.3.

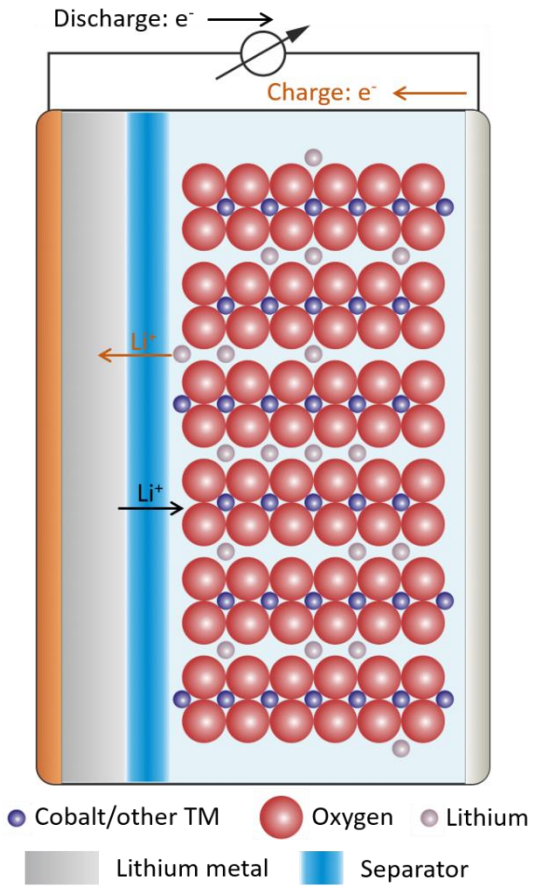


**Figure 5: Schematic design of a lithium metal battery with a lithium cobalt oxide cathode. For the sake of clarity, the electrolyte is not shown in detail.**

In fact, the first reversible lithium batteries such as the systems developed by Whittingham and Goodenough were lithium metal batteries and the company Moli Energy Ltd. started producing $Li^0|MoS_2$ batteries for pocket telephones in the 1980s.[28,29,48] However, the formation of Li dendrites on the anode upon charging led to severe safety issues such as fires resulting in a total product recall in 1989.[56] Since then, lithium metal anodes could not be established in the mass market until today.

### 2.2.2 The Lithium-Sulfur Battery

Sulfur is one of the earth´s most abundant elements and since its elemental form is produced *en masse* as a by-product of the desulfurization of natural gas and crude oil refining products, the development of lithium-sulfur batteries is of strong interest.[57,58] The cathode of lithium-sulfur (Li-S) batteries consists of elemental sulfur, binder materials (polymers) and conductive additives such as carbon nanotubes. Given the high theoretical electrochemical capacity of the sulfur as cathode material (1675 $mAh/g_s$)[44,59], Li-S batteries can potentially reach energy densities of 600-1000 Wh/kg[40,43] and 700-900 Wh/L.[40,42,45] The chemical reaction occurring at the cathode that gives the Li-S battery its driving force is the stepwise reduction of the Sulfur ($S_8$) via so-called

polysulfides ($Li_2S_8$, $Li_2S_5$, $Li_2S_2$ et cetera, summarized as $Li_2S_n$) to the final discharge product $Li_2S$ giving the cell an average operation voltage of 2.1 V.[44,60] In summary, the discharge reaction can be expressed according to scheme 3:

$$16\ Li + S_8 \rightarrow 8\ Li_2S \qquad (3)$$

The comparably low cell voltage with respect to standard LIBs is the reason why although the electrochemical capacity of the sulfur cathode is roughly 8 times higher than that of a NCM cathode (up to 200 mAh/g)[33], the Li-S battery energy density is "only" about twice as high because the energy density is the product of discharge capacity and discharge voltage. Furthermore, other components such as binders, conductive carbon, electrolyte, anode and cell cases have a higher influence on the gravimetric energy density compared to LIBs. One major challenge in the Li-S battery development is the polysulfide shuttle effect. As the term implies, the polysulfides that form as intermediate products of the cathode reaction can dissolve in the electrolyte and are able to shuttle between cathode and anode leading to low Coulomb efficiency and self-discharge of the cell.[61,62] A more detailed insight into this phenomenon will be given in section 2.3.2.

### 2.2.3 The Lithium-Air Battery

The lithium-air battery is a unique variety amongst the alternative lithium battery concepts. While all the other concepts need to include the cathode active material (CAM) into the cell and therefore their capacity and energy density is, *inter alia*, limited by the CAM, Li-air batteries can potentially utilize an almost infinitely large cathode: the oxygen in earth´s atmosphere.[63] Li-air batteries comprise besides the lithium metal anode and the electrolyte a cathode that will enable the diffusion of atmospheric $O_2$ into a mesoporous material (often times a carbon mesh)[41] where it can react together with the lithium ions and the electrons coming from the current collector forming different lithium-oxygen compounds as discharge products depending on the design of the battery: $Li_2O$ or $Li_2O_2$ using non-aqueous electrolytes, resp. LiOH using aqueous electrolytes.[64,65] Apart from the major hurdles associated with the interface of electrolyte and air at the cathode, the issues concerning the use of LMAs in this kind of batteries are most similar to the ones for LMBs and Li-S batteries, such as uneven lithium deposition, dendritic growth, parasitic side reactions and also the shuttling of other atmospheric gases through the electrolyte to the anode[64,66] (all of which will be explained in detail in section 2.3 *ff.*). Despite all the challenges, Li-air batteries are of high interest in research due to their outstanding high potential energy density that could even match the volumetric energy density of gasoline/petrol.[40]

### 2.2.4 All-Solid-State Batteries

While the LIB alternatives discussed in the previous sections are characterized by novel electrode materials, the special feature of all-solid-state batteries (ASSBs) is the electrolyte, which is not in the form of a liquid solution as is usually the case, but is instead an ionically conductive solid material. Advanced examples of these *solid electrolyte* (SE) called materials such as lithium germanium phosphorus sulfide ($Li_{(4-x)}Ge_{(1-x)}P_xS_4$, LGPS), lithium lanthanum zirconium oxide ($Li_7La_3Zr_2O_{12}$, LLZO), lithium thiophosphate ($Li_3PS_4$, LPS) or argyrodites ($Li_6PS_5X$, X = halogen) are widely used in battery research and are able to reach lithium ion conductivity values up to 1-10 mS/cm which is in the same range as common liquid electrolytes.[67–69] In ASSBs, the solid electrolyte not only acts as the ion conductor, it also takes the role of the separator preventing direct contact between the electrodes. Therefore, the basic design of an ASSB only needs 3 parts: a cathode composed of a mixture of CAM and SE, a thin layer of SE as separator, and an anode which ideally would be lithium metal.[70] This compact design principle leads to especially high volumetric energy density (cf. figure 3) while the gravimetric energy density suffers from the high specific mass of the solid electrolytes as well as the CAMs (NCM, NCA, etc.).[13] One major advantage of ASSBs is the fact that in SEs, there is no charge polarization during battery charging which possibly enables higher current densities and therefore quicker charging.[69] However, the SEs are not able to compensate volume changes during cycling as good as liquid electrolytes, which may lead to contact loss at the electrolyte/electrode interfaces and high interface resistances making the application of external pressure often times necessary.[70,71] Also, most solid electrolytes are not stable against chemical reduction by the lithium metal anode leading to the formation of undesired interphases.[72] Depending on the electronic conductivity of the interphase reaction products, the growth of said interphase may stop after several nanometers (electron insulating) but it also can continuously keep growing if the reaction products comprise electronic conductivity.[73,74]

## 2.3 The Lithium Metal Anode

As the lithium metal anode (LMA) is the crucial component of lithium metal batteries, it was already shortly introduced in section 2.2.1. The key advantage of the LMA lies in its numbers; having a particularly low density $\rho$ of 0.53 g/cm³ and low molar mass $M$ of 6.94 g/cm³ results in high theoretical gravimetric capacity $C_g$ = 3862 mAh/g that can be calculated from the Faraday constant $F$ ($F$ = 96485.3 C/mol resp. 26801.5 mAh/mol) according to equation 4 assuming that every lithium atom will release one electron.[75]

$$C_g = \frac{F}{M} \tag{4}$$

Lithium metal has the lowest standard half-cell potential of all elements, but in the context of lithium-based batteries it is more appropriate to use the redox pair $Li^0$ vs. $Li^+$ as a reference for the electrode potential. The electrode potential of the LMA is therefore 0 V vs. $Li^+/Li$. This information may seem redundant at first glance, but the electrode potential of any other possible electrode material that could be used as an anode is higher than this value. If it is also desired to be able to compare the electrode potentials in different solvents, the standard hydrogen electrode, which is practically always referred to, must not be used as the reference electrode, but rather the redox pairs $Rb/Rb^+$, ferrocene/ferrocenium or cobaltocene/cobaltocenium, since the solvate sheath has no great influence on the solvation energy and thus on the electrode potential with these large ions.[76–78] It follows that batteries with LMAs have a higher cell voltage, which also leads to a higher energy density, since the cell voltage is the measure of the energy transferred per electron.[11] Apart from the weight and volume saving properties and therefore potentially higher energy content of LMBs, there are several obstacles preventing their establishment in the mass market to this day. Since the LMA does not have a host structure like graphite or silicon, the LMA undergoes drastic (theoretically infinite) volume change upon charging and discharging which causes mechanical stress at the electrode/electrolyte interface.[79] At this very interface, the electrolyte inevitably becomes reduced by the lithium metal leading to the formation of the solid electrolyte interphase (SEI). While the SEI on graphite anodes is stable and even considered beneficial,[80,81] the uneven deposition and dissolution of lithium metal electrodes leads to an unstable SEI resulting in even stronger irregularities during battery cycling. This behavior mainly causes the drawbacks of the LMA such as low coulomb efficiency, high capacity fading and safety concerns. The origins of these issues will be illuminated in the following: Repeated exposure of fresh lithium to the electrolyte through an unstable SEI provokes ongoing reactions at the electrode surface which cause lower Coulomb efficiency and capacity fading due to loss of active lithium and electrolyte consumption.[17] Coulomb efficiency (CE) describes the ratio of the amount of charge in the discharge step to the amount of charge in the previous charge step and is therefore a measure of the reversibility of the electrode reaction(s). For a lifetime of 1000 charging and discharging processes (cycles) while retaining more than 80 % of the initial capacity, the CE of the electrodes must be above 99.95 %, if not 99.99 %. This value has so far only been achieved over individual cycles using a lithium metal anode and not over the entire cell life. Often the reported coulomb efficiency of LMAs is 99.0-99.5 %.[82] A more pronounced uneven deposition may result in the growth of mossy or dendritic lithium resp. generally spoken high surface area lithium.[83] In this case, parts of the lithium metal can become electronically isolated from the anode whereby this so-called *dead lithium* is not available for the electrochemical reactions anymore yielding in further capacity decay.[84] The most severe risk of dendritic lithium growth would be the onset of a short circuit by a dendrite growing through the entire electrolyte creating direct electric contact between both electrodes despite the fact that lithium is, like the other representatives of the alkali metals, a

comparably soft metal.[18] This event can possibly cause thermal runaway of the cell and even fire as already mentioned in section 2.2.1. A measure of the mechanical strength or elasticity of a material is the shear modulus *G*, which is defined as the ratio of the mechanical shear stress to the relative shear strain of a physical object. Its value for lithium metal is 3.4 – 4.3 GPa which is significantly lower than the shear modulus of other metals like Gold (28 GPa) or Iron (81.9 GPa).[85,86]

In research, very thick lithium anodes are mostly used, allowing the loss of active lithium to be compensated to a certain extent.[87–89] If the focus of the research is on the cathode, for example, it can make sense to use an excess amount of lithium and electrolyte to exclude these as possible error sources. In anode research, however, this is not purposeful, as the loss of active lithium is not noticeable when there is a large lithium surplus, as not all of the lithium in the electrodes is cycled. In order for the advantage of the higher specific capacity of the lithium metal to come into play, the LMAs must in fact be very thin, ideally less than 50 µm.[10,14]

### 2.3.1 The Solid Electrolyte Interphase

Just like many metals tend to form layers of oxidative products (so-called passivation layers) on the surface,[90] lithium metal is practically always covered with a passivation layer that forms during storage. It can also be intentionally created during production as the (natural) passivation layer will have an influence on the electrochemical capabilities degradation stability of the lithium electrode.[19,20,91,92] When installed in a cell, liquid electrolytes are able to partly dissolve the passivation layer comprising mostly LiOH, $LiCO_3$ and $Li_2O$ which enables surface reactions at the lithium metal/electrolyte interface leading to the formation of the solid electrolyte interphase (SEI). Given the fact that the SEI offers low electron conductivity close to electronic isolation and sufficient lithium ion conductivity, the SEI acts just as the name indicates as a solid electrolyte avoiding direct contact between the highly reactive electrode and the electrolyte.[21,93] Therefore, the presence resp. the formation of a stable SEI is highly desired because it can possibly stop ongoing detrimental reactions at the anode surface that would lead to loss of lithium and electrolyte consumption.[16] A comparison of different electrolyte compositions found a correlation between the increase in thickness of the SEI through contact with the electrolytes and the Coulomb efficiency. The more the SEI swells in the electrolyte, the lower the Coulomb efficiency due to the loss of active lithium.[94] Factors that influence the growth and thickness of the SEI include kinetic and thermodynamic factors such as electrolyte diffusion through the SEI, ionic and electronic conductivity and the chemical potential (difference) at the interface.[95–97] As the crucial step of the electrolyte reduction by lithium metal is the electron transfer from the electrode to the electrolyte species, the SEI electronic conductivity has the major influence on the SEI thickness assuming a dense layer since a low electron conductivity leads to stronger potential drop over the interphase

inhibiting further electrolyte reduction.[98] It is also possible that electrons are transported through the SEI via the diffusion of radicals and further reduce the electrolyte.[99] However, all these assumptions will only apply to a limited extent to a real lithium metal anode, as a natural SEI does not have a homogeneous structure, but is made up of a variety of components.[22] In addition, the uneven deposition and dissolution of the LMA during electrochemical cycling causes mechanical stress that can cause the SEI to crack or parts of it to detach or dissolve which results in ongoing lithium and electrolyte consumption. Also the inhomogeneous structure of the SEI means that its conductivity is neither homogenous across the surface, so at regions with higher ion conductivity there will be preferential lithium plating and stripping.[79,100,101] Figure 6 gives a schematic overview of the possible challenges that occur from a faulty SEI during battery cycling.

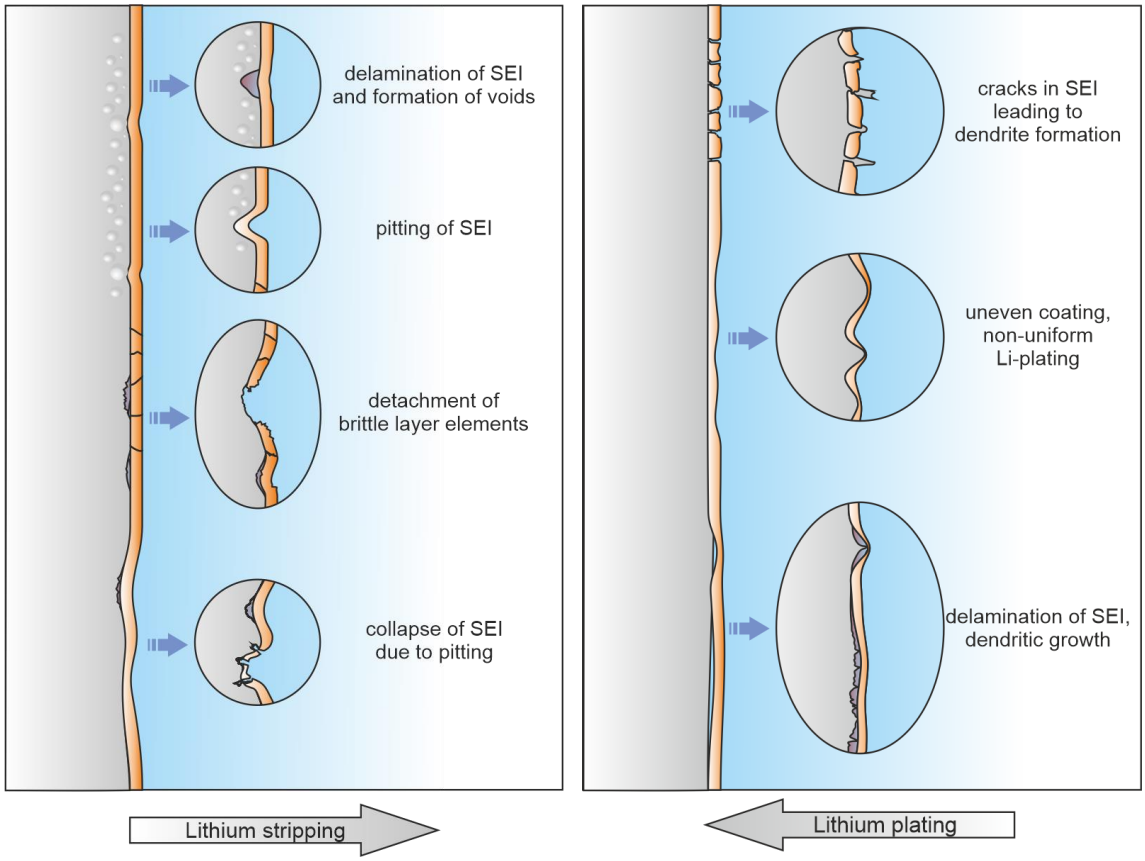


**Figure 6: Graphic summary of possible SEI failure mechanisms and their consequences.**

Considering the SEI ionic conductivity, it is difficult to determine exact values as the exact area and thickness of the interphase often remain unknown. In contrast, the areal resistivity (denoted in Ω cm²) can also be used to compare the electrochemical impact of (inter-)layers as for this value, the layer thickness is not needed. Detailed analysis of the ionic conductivity in doped and pure $Li_2O$ (one of the main SEI components, $\sigma \approx 10^{-12}$ S/cm) and comparison of the resulting areal resistivity ($10^6$ Ω cm²) with experimental data of SEI areal resistances ($10^1$-$10^3$ Ω cm²) showed that the SEI conductivity must be at least 3 to 5 orders of magnitude higher than the bulk conductivity of $Li_2O$.

This means that other processes are involved in the lithium ion conduction through the SEI.[102] Building on this finding, *Guo* and *Gallant* synthesized artificial SEIs from $Li_2O$ and LiF, respectively, to accurately determine their ionic conductivities directly on the lithium electrode. It turned out that the conductivities of the artificial, single-component SEIs were also several orders of magnitude higher than the respective bulk conductivities. One explanation for this behavior is that the potential of the lithium metal in the thin SEI changes the process or path of $Li^+$ diffusion and therefore affects $Li^+$ conduction.[101,103] Besides an estimation of the thickness of the SEI to be 5-40 nm (formed in $LiClO_4$ in propylene carbonate), measurements by *Churikov* yield similar values for the conductivity of the SEI. He also explains the origin of the comparatively high ionic conductivity on the basis of a charge carrier injection into the SEI at an applied electrochemical potential.[104]

#### *2.3.1.1 SEI Composition*

In order to gather better understanding of the SEI composition, *Peled* et al. introduced a model describing the SEI structure as a mosaic of lithium salts such as $Li_2O$, LiF, $Li_2CO_3$ and organic components like organic carbonates and polyolefins in 1997. They also proposed a layered structure within the mosaic in which the inorganic salts are close to the lithium electrode and the organic components are closer to the electrolyte.[22] Additional to the lithium salts that may come from the natural passivation layer on top of lithium metal, LiF and the organic components are the decomposition products from the organic solvents and conductive salts that make up the electrolyte.[105] Since the establishment of these models, the mechanism of SEI growth on both graphite and lithium metal anodes has been continuously investigated. It is to be emphasized that the growth of SEI on the two types of anodes mentioned is basically considered to be very similar due to the almost identical electrode potential.[22,106] In 2022, *Walter* et al. published kinetic Monte Carlo simulations on the decomposition of ethylene carbonate (EC), one of the most common electrolyte solvents, in contact with a negative electrode. The results revealed that upon contact of EC with the electrode, first, there will be the formation of a SEI layer mostly comprising $Li_2CO_3$ and minor organic lithium salt amounts. As this surface reaction continues, it changes due to the electronic insulation and distance from the initial electrode surface towards the preferential formation of organic lithium salts and minor inorganic fractions. The simulations also proposed ongoing reactions forming inorganic SEI components from organic SEI components as well as EC decomposition at the SEI/electrolyte interface. The results of this study both explain and confirm *Peled*'s layer model, which was published 25 years earlier.[106] However, liquid electrolytes comprise a mixture of chemical compounds making the SEI formation mechanism more complex and consequently, different electrolyte systems show different reaction behavior, for example

EC/DMC/$LiPF_6$ electrolyte shows reactivity with an artificial SEI consisting of $Li_2O$, which is generally regarded as passivating, while DOL/DME/LiTFSI electrolyte shows no reactivity.[107] *Fiedler* et al. investigated for the latter mentioned electrolyte system the individual compositions of the reaction layer formed upon immersion resp. galvanostatic current load of Li metal in DOL/LiTFSI and DME/LiTFSI solutions using complementary XPS and SIMS techniques. It was shown that the DME electrolyte quickly reacts with the Li substrate forming a thin passivation layer whose growth stalls early, even under galvanostatic load, but whose composition changes over time to inorganic salts such as LiF and LiOH. The film-forming reaction of the DOL electrolyte upon immersion appears to be slower yet more persistent resulting in continuous growth of the SEI. Contrary to the observations regarding DME, the DOL-SEI that forms under galvanostatic load is drastically different which is distinguished by a porous structure and a significantly increased growth rate.[108]

#### *2.3.1.2 SEI Growth Mechanism and Rate*

Regarding the SEI growth rate, it is generally recognized that the SEI formation is a transport-controlled reaction that depends on the diffusion of the reactive species through the SEI. Whether the SEI growth rate depends on the conduction of electrons, the diffusion of the electrolyte or the diffusion of radicals through the SEI, the dependence of the layer thickness over time $t$ is always dependent on $t^{0.5}$ (sqrt($t$)). Furthermore, across shortest distances there is the possibility that the SEI layer growth depends on electron tunneling through the SEI, in which case the time dependence would be ln($t$).[99,109,110]

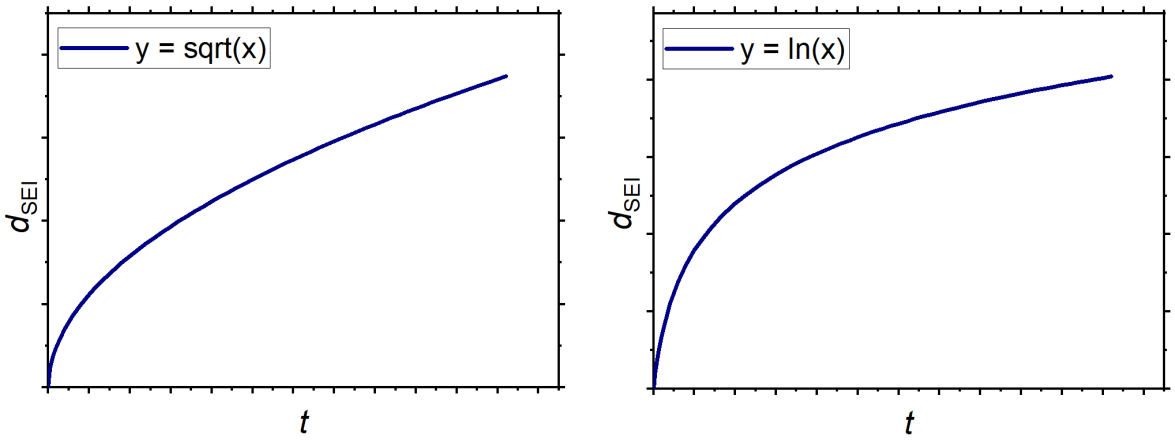


**Figure 7: Qualitative comparison of a square root (sqrt) dependency (left) vs. logarithmic dependency (right). Due to the close similarity of the curves, it can be difficult to discriminate between different processes.**

This $t^{0.5}$ assumption has its origin in the description of the surface layer growth on the basis of *Fick*'s 1st law, which assumes a steady state of reactant concentrations. For this reason, this model applies in a satisfactory degree of approximation only to SEI growth during storage (so-called

calendrical aging). The expansion of the SEI can, for example, be tracked indirectly via the measurement of the cell resistance or the capacity loss. Simulations confirm the $t^{0.5}$ dependence of the SEI growth and also the increasing growth rate with increasing state of charge. They also indicate that the growth of the inner SEI practically stops after some time, while only the outer, porous SEI continues to grow thereafter.[111] When the electrochemical cell is cycled, however, the boundary conditions such as reactant concentration gradients or inhomogeneities become drastically changed leading to a significant mismatch of the $t^{0.5}$ model.[95] For carbon electrodes, measurements revealed that the SEI growth during cycling is dependent on the *C*-rate (proportional to the current density) and also that the growth predominantly occurs during plating due to different possible reasons: electrode expansion and SEI cracking, high overpotential from high $Li^+$ desolvation energy barrier, and higher charge carrier concentration all during lithiation.[112] Theoretical computations showed that the large differences in the charge carrier concentration ($Li^+$ and $e^-$) within the SEI during lithiation and delithiation is the main reason for the asymmetry in the SEI growth.[113] As became clear in the previous section, the structure of the SEI differs significantly depending on the solvent and electrolyte salt used, and the rate of SEI formation can therefore also differ greatly. Thus, it can be assumed that a porous SEI, which also allows electrolyte diffusion, grows much faster and thicker than a dense SEI,[108,114] which depends exclusively on the (low) electron conductivity, with both still following the $t^{0.5}$ dependency.

In literature it is often emphasized that in an ideal case, the SEI would comprise high and homogenous ionic conductivity, low electronic conductivity, high mechanical strength, strong adhesion to the electrode and chemical stability.[23,115] However, for LIBs comprising graphite anodes there is strong computational and experimental evidence showing that radical diffusion (mostly Li atoms resp. Li interstitials) through the SEI plays a major role in long-term SEI growth. As the electrode potential of the anode is dependent on the state of charge (SOC), and the expected loss of capacity due to radical diffusion-induced SEI growth depends on this, *Single* et al. were able to predict the calendrical ageing of commercial NCA cells accurately using this model. Meaning that in ASEI design this aspect must be considered aswell.[99,109] So far, for lithium metal anodes/batteries there are barely any publications regarding radical diffusion[116] making it questionable whether this phenomenon only occurs on graphite electrodes.

### 2.3.2 Dendrite Formation

Irregular lithium structures that form during uneven electrodeposition on the LMA surface are often generalized under the term *dendrites* which stems from the Greek word *δέντρο* (déntro) for tree. However, these uneven lithium deposits come in many different shapes that are described as globules (beads), whiskers, mossy, fiber- or needle-like, bush- or tree-like.[117,118] Dendrites are a

challenge in both liquid and solid electrolytes because once a dendrite begins to form on the electrode surface, its growth is self-reinforcing since at the tip of the dendrite the distance to the opposite electrode is smallest and therefore the electric field is strongest there, causing cathodic deposition to occur preferentially at the dendrite tip.[119] The onset and speed of dendrite growth is dependent on many parameters such as diffusion of both cations and anions through the bulk electrolyte.[120] The morphology of these irregular lithium deposits depends on the applied current density. Contrary to early models,[120] whisker-like structures will already grow at low current density, below a certain threshold, fiber-like structures known as needle-like dendrites or whiskers develop. Unlike tree-like dendrites, these structures seem to originate from their roots and they will not penetrate the separator causing short circuits.[121] At high current density, the lithium ions at the electrode interface deplete, resulting in dendrites that resemble trees and grow from the tips. Lastly, at current densities between the two aforementioned limits, mossy-like dendrites form. The growth mechanism of these dendrites is believed to be a hybrid of tree-like dendrites and whiskers. While no definitive conclusions have been reached regarding the nature of dendrite evolution, as partly mentioned before, tip-induced growth appears to be due to the increased ionic and electronic fields around the dendrite's tip, while bottom-induced nucleation seems to be caused by defects in the SEI and the lithium electrode below it.[122] However, even if a shorting of the cell can be avoided by choosing the right parameters, there will still be the issue of lithium loss and electrolyte consumption caused by inhomogeneous lithium plating and stripping[123] which causes much more cell failures through cell dry out than through short circuits since in academic research the used current densities are relatively low.[121] Studies by *Steiger* et al. were also able to identify other factors that influence the morphology of lithium deposition. They found that electrodeposition in $LiPF_6$/EC/DMC electrolyte leads to a stronger branching of the lithium, while in LiTFSI/DOL/DME the lithium is deposited in a more spherical shape, which they attribute to the different compositions of the SEIs. Furthermore, they found that lithium, like other metals, generally tends to be deposited in a non-uniform, needle-shaped manner, as demonstrated in a physical vapor deposition experiment.[124]

A parameter often mentioned in connection with dendrite growth is the so-called *Sand's time* ($\tau$). Henry Sand originally worked on the determination of diffusion coefficients in 1901[125], but by transforming the proposed equations, they can also be used to determine the time (= *Sand's time*) at which the cation concentration at the anode is zero and dendrite growth begins. The onset time can be calculated according to eqn. 6 under the prerequisite that the applied current density $J$ surpasses the limiting current density $J_{lim}$ as described in eqn. 5. Here, $e$ is the elemental charge, $D$ is the $Li^+$ diffusion coefficient, $t_{Li+}$ is the transference number, $c_0$ is the bulk electrolyte concentration and $l$ is the distance between the electrodes.[51,126,127]

$$J_{\text{lim}} \geq \frac{2ec_0D}{(1-t_{\text{Li}^+})l} \tag{5}$$

$$\tau = \pi D\left(\frac{ec_0}{2J(1-t_{\text{Li}^+})}\right)^2 \tag{6}$$

Although these formulae do not take the existence of an SEI, which makes the prediction of dendrite growth much more complex, into account, one can see the influence of the contributing factors on the limiting current density and the onset time: to avoid or delay dendrite formation, the electrolyte should comprise high diffusivity, a high lithium transference number and a short distance between the electrodes. In a modification of the equations shown above (e.g. replacing the electrode spacing by the SEI thickness, omitting the transference number), it is nonetheless also possible to describe dendrite formation at the SEI/lithium metal interface, which means that the same conditions mentioned for the bulk electrolyte apply to the SEI in order to prevent dendrites as shown by *Maraschky* and *Akolka*.[128]

### 2.3.3 Cross-talk Effects of Cathode Materials on the Lithium Metal Anode Surface

A thoroughly studied electrode cross-talk resp. crossover effect is the polysulfide shuttle effect that occurs in Li-S batteries. As the charge and discharge reactions in the sulfur cathode happen stepwise via the so-called polysulfide intermediates, these non-polar polysulfides can partly dissolve in the liquid electrolyte and migrate between the electrodes.[129,130] This shuttling of dissolved polysulfide molecules creates several drawbacks for Li-S cells. One purpose of every battery electrolyte is the electronic isolation and spatial separation of the electrodes, so that the charge and discharge reactions are solely enabled by electron flow through an external closed circuit. When a polysulfide molecule (e.g. $Li_2S_6$) migrates towards the anode, it will be reduced by reacting with lithium ions and the corresponding electrons forming $Li_2S$ and a shorter chain length polysulfide that is still soluble in the electrolyte. This reduction of the sulfur species is technically a discharge of the cathode which logically should only occur inside or at the cathode, not at the anode surface.[131,132] The results of this unintended internal cell discharge are low Coulomb efficiency and high self-discharge rates of Li-S batteries.[133] Moreover, said effect leads to the accumulation of lithium sulfide on the LMA surface which is an undesired SEI component due to its low ionic conductivity.[134] In order to mitigate the polysulfide shuttle effect, *Mikhaylik* introduced the addition of lithium nitrate ($LiNO_3$)[135] which quickly became a standard component for Li-S electrolyte as $LiNO_3$ reacts together with dissolved sulfur compounds at the anode surface modeling a more favorable SEI composition.[129,136] However, uneven lithium deposition still causes ongoing exposure of fresh lithium to the electrolyte provoking continuous consumption of $LiNO_3$.[62,137]

While the aforementioned polysulfide shuttle effect has been known and thoroughly studied for a long time, the possible crossover of transition metal (TM) ions from conventional cathode materials to the LMA was practically neglected.[46] By contrast, the influence of the interaction of dissolved cobalt, manganese and nickel ions on graphite anodes has already been extensively studied and the results unanimously show a negative influence on the properties of the batteries.[138–141] In 2019, *Betz* et al. were amongst the first authors to conduct a systematical study on the influence of TM ion dissolution and crossover on the lithium metal anode. This study, that compared NCM, LFP and $LiNi_{0.5}Mn_{1.5}O_4$ (LNMO) cathodes, revealed the presence of manganese on the LMA surface after cycling with an LNMO cathode, and the different cathodes had clear influence on the Li electrode overpotential as well as on the LMA morphology. To be precise, the dissolution of manganese resp. the presence of manganese in the electrolyte leads to higher lithium anode overpotential and alters the LMA deposition morphology from nodule-like structures to a bead-shaped surface.[142] Further studies show that the manganese inside the SEI is not being reduced to $Mn^0$ metal but stays in the form $Mn^{+II}$ while strongly influencing the SEI evolution as the formation of LiF which is considered beneficial is decreased.[143] Nickel accounts for the largest proportion of transition metals in modern, widely used NCM cathodes. Different studies using NCM cathodes with different nickel contents could not demonstrate a negative effect of the migration of $Ni^{2+}$ ions from the cathode to the LMA; the incorporation of nickel into the SEI could be shown, but in negligible amounts.[46,142,144] Only the artificial addition of nickel ions to the electrolyte leads to reduced capacity, increased cell resistance, increased SEI growth and increased decomposition of the electrolyte due to the formation of Ni metal on the anode surface.[46] Interestingly, the studies of *Langdon* and *Manthiram* show an anode to cathode crossover effect when using LiFSI (lithium bis(fluorosulfonyl) imide) conductive salt in combination with NCM cathodes indicating that FSI anions are defluorinated at the LMA and the remaining fluorine-deficient FSI decomposition products cross over to the cathode where they become oxidized and form the cathode electrolyte interphase (CEI). This effect leads to higher fluorine content in the SEI and therefore even higher anode stability when using NCM cathodes compared to symmetrical cells.[144,145] For the third TM occurring in NCM, cobalt, there are no studies on the effect that a possible cobalt ion crossover has on the lithium metal anode. For Li-S cells, however, the addition of TM (Zn, Cu, Ni, Co or Mn) acetate salts into the electrolyte resulted in higher Coulomb efficiency and enhanced rate capability for every investigated TM additive which is explained by the formation of a transition metal sulfide-containing SEI that reduces the polysulfide shuttle effect and provides a more homogeneous lithium deposition.[146] With regard to the aspired stabilization of the LMA, these findings illustrate that at least the addition of reactive additives can lead to significantly different outcomes depending on the cell chemistry.

Lithium-air batteries are possibly the most complicated system with regards to crossover effects from cathode to anode as $O_2$, the cathode active material makes up 21 % of earth's atmosphere

while the other air constituents ($N_2$, Ar, $CO_2$, $H_2O$) can dissolve in the electrolyte and migrate towards the LMA just as $O_2$ itself can do, too.[147] For better comparability with the other battery systems, this small overview will only focus on non-aqueous Li-air batteries. Naturally, the noble gas Ar will not react with any battery component. Also, the influence of $N_2$ on the LMA and the SEI is negligible during operation although it makes up the largest part of the atmospheric gases.[64] Whether the transport of $O_2$ to the anode has got a beneficial or a detrimental effect on the anode stability and performance is under debate.[64,148,149] For one, a study by *Lee* et al. could show that the presence of $O_2$ in the electrolyte can break up the native passivation layer of the lithium metal and induce ongoing decomposition reactions of the DMSO/LiTFSI electrolyte (DMSO = dimethyl sulfoxide) during storage even without applying any charging or discharging.[150] On the other hand, *Qiu* et al. and *Wang* et al. found that in tetraglyme/LiOTf resp. tetraglyme/LiTFSI (tetraglyme = tetraethylene glycol dimethyl ether; LiOTf = lithium trifluoromethanesulfonate) electrolyte systems, oxygen prevents ongoing SEI formation reactions and leads to a more compact and homogenous anode morphology after cycling.[149,151] Systematic observations by *Haas* and *Janek* led to a possible explanation for this discrepancy in reports concerning the influence of oxygen. They could show that the plating of fresh lithium electrodes under $O_2$ atmosphere leads without exception to higher Coulomb efficiency compared to plating and/or cycling under Ar atmosphere. However, when using commercial Li foil comprising a natural passivation layer, an altered SEI formation mechanism will cause a less stable SEI under oxygen atmosphere which is the reason for literature reports of its negative influence on electrode performance.[152] Despite the low concentration of $CO_2$ in air, it is present in Li-air battery electrolytes not only by solvation of atmospheric $CO_2$ but also originating from side reactions inside the cell leading to the formation of lithium carbonate ($Li_2CO_3$) on the anode surface as well as on the cathode. While the formation of $Li_2CO_3$ on the cathode is an unwanted reaction, it is considered a beneficial component of the anode SEI due to its stabilizing properties.[92,148,153] Water contaminations from air humidity or other sources are most widely considered as detrimental especially for lithium metal anodes due to the strong tendency of alkali metals to react with $H_2O$ resulting in the formation of the metal hydroxide. Since the reaction of $H_2O$ with lithium metal does not lead to a passivated surface, the parasitic reactions will continue until complete degradation of the anode.[114,154,155] It is worth noting that the influence of atmospheric gases on the LMA in the installed state is very similar to the results of the lithium storage experiments by *Otto* et al..[20] Lastly, in the research of Li-air batteries so-called redox mediators which are supposed to reduce the charging overpotential at the cathode are investigated. These soluble redox mediator species are likewise able to shuttle towards the anode resulting in the degradation of both the LMA and the redox mediator which is accelerated through a destabilization of the SEI.[156–158] In ASSBs, such chemical crossover from electrode to electrode practically does not occur due to the solid electrolyte and its low diffusivity for any chemical species with the

exception of lithium ions.[159] However, first studies have proven TM interdiffusion from the NCM cathode into the bulk solid electrolyte leading to electro-chemo-mechanical degradation.[160]

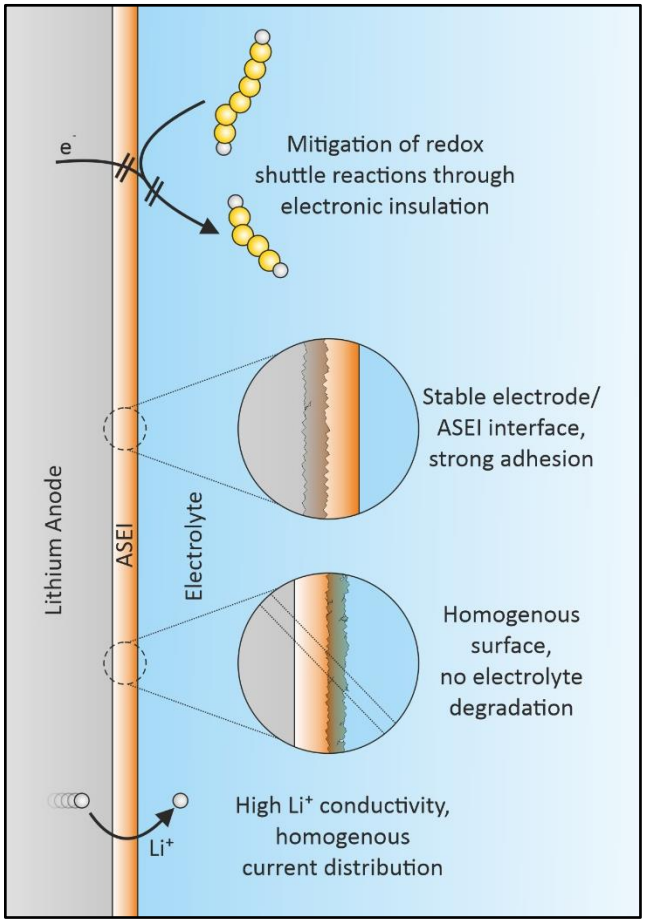


**Figure 8: Summary of desired ASEI properties.**

In summary, nearly every problem that is associated with lithium metal anodes such as dendrite growth, electrolyte consumption, lithium loss, dead lithium, cross-talk or shuttle effects could potentially be solved by the properties outlined in figure 8: A permanently mechanically stable artificial SEI (ASEI) that comprises high $Li^+$ conductivity and minimal electronic conductivity as these supposedly simple requirements would inhibit uneven lithium growth and therefore exposure of lithium metal to the electrolyte and the dissolved species inside. Furthermore, the lack of electronic conductivity would prevent ongoing reduction reactions on top of the ASEI.[98] However, highly mobile unwanted contaminants like $H_2O$ might still be able to permeate such an ideal ASEI and induce ongoing parasitic reactions[20] which is especially problematic for Li-air batteries as they are quasi-open towards the atmosphere and its humidity.[64] This leads to the conclusion that Li-air batteries might need a different, perhaps more complicated LMA protection concept whereas LMBs and Li-S batteries could share the same protection strategy.

## 2.3.4 Protection of the Lithium Metal Anode Surface

### *2.3.4.1 Properties of potential ASEI components and coatings*

The goal of numerous researchers and was and is to create an artificial SEI (ASEI) resp. a protective layer comprising the aforementioned beneficial properties in order to inhibit the adverse effects resulting from lithium loss, electrolyte consumption and dendrite formation. There are several hypotheses including the corresponding microscopic explanations about what type of material would be a desirable SEI component. Alloys that can form upon contact of other metals like aluminum, indium or silicon with the LMA or metal coatings comprising silver or even gold can offer stability of the LMA against air and suppress the formation of dendrites due to the lithiophilic surface, high lithium diffusion and homogenous current density.[24,161–163] Organic resp. short alkyl chain based protective layers are said to prevent electrolyte decomposition, lower the interfacial resistance an constrain the LMA volume changes.[164] Aromatic functional groups, on the other hand, give mechanical toughness and flexibility to the SEI through their distinct π-π interactions.[165] $Li_3N$ and $Li_3P$ are compounds of high interest for their outstanding lithium ion conductivity and protection from detrimental side reactions.[166–168] LiF and LiCl are considered to prevent dendrite formation due to their high surface diffusion for lithium and to give the SEI mechanical strength preventing cracks and electrolyte consumption.[103,169–171] With regard to LiF, a comparison of ex situ and in situ (through additives) generated LiF in the SEI demonstrated that the ex situ layers are unstable and the formation of LiF in situ leads to more significant improvements, which also means that the additive is used up over time.[105] This can be explained by the findings that the supposedly LiF-forming additives do not form homogenous films but rather form single crystallites on the SEI[172] whilst the positive effect of these additives may come from their quick polymerization resulting in the formation of compact and flexible SEI films.[173] On the other hand, the observation that fluoroethylene carbonate, a frequently used additive, releases harmful HF inside the cell at temperatures above 45 °C might speak against the use of LiF-forming additives.[174] Nevertheless, a study by the group of Archer revealed that any kind of lithium halide (LiF, LiCl, LiBr and LiI) is capable of significantly enhancing the surface mobility of lithium when incorporated into the SEI.[175] All the binary lithium compounds mentioned above additionally have in common that they are stable towards reduction by elemental lithium[72] which would make them attractive as a component of an anode protection layer. However, often times data and information about specific characteristics such as ion conductivity and diffusion in LiF for example, are contradictory, misinterpreted, incomplete or incorrectly cited;[105,176–178] making literature search particularly difficult. Another compound class of interest are phosphazenes which are defined by a phosphorus/nitrogen backbone with alternating single and double bonds (c.f. figure 37). These have

already been having much attention by the battery research community on one hand for their use as electrolyte additives in order to reduce flammability and for SEI modification[179–183], on the other hand in form of polyphosphazenes as polymer electrolytes.[184,185] However, direct lithium metal anode modifications have been done scarcely.[186]

A well-functioning SEI must additionally comprise sufficient mechanical stiffness and flexibility at the same time. For homogeneous polymer electrolytes, mathematical calculations resulted in the much-cited *Monroe-Newman* model, according to which the shear modulus *G* of the electrolyte must at least be twice as high as the shear modulus of lithium in order to effectively prevent the formation of dendrites. Accordingly, *G* of the SEI must be at least 7-8 GPa.[86] However, since this value refers to a homogeneous layer while an SEI or ASEI is usually inhomogeneous and contains phase or grain boundaries, no generally valid predictions can be made with this model regarding the dendrite resistance.[126,187] Another mechanical parameter is the Young's modulus (modulus of elasticity, also denoted in Pa or GPa) *E* that describes a material's response to tensile or compressive stress. It measures the ratio of the stress applied to the material to the resulting strain (deformation) in the same direction. A computational study by *Liu* et al. focuses on the relationship between the conductivity of the SEI and the Young's modulus with regard to the formation of dendrites. The modelling showed that to prevent dendrites, not only the Young's modulus must be at least 4 GPa, but also the SEI conductivity must be more than 10 % of the electrolyte conductivity. In particular, since almost no SEI/ASEI materials achieve an ionic conductivity in the range of 10 % of the conductivity in comparison to a liquid electrolyte, the authors were unable to identify any literature-known example of an ASEI that meets both of these criteria.[188]

Apart from the single-component properties, there are also synergetic effects coming from the combination or contact of different SEI phases as was shown both theoretically and experimentally for the practically ubiquitous SEI compounds LiF and $Li_2CO_3$. At the contact interfaces between LiF and $Li_2CO_3$ grains, the concentration of lithium ions is enhanced while the electron concentration is reduced. Simultaneously, the Li defect concentration in the LiF crystal lattice is enhanced by the space charge effect overall resulting in higher ionic and lower electronic conductivity giving rise to better battery performance using LiF/$Li_2CO_3$-modified LMAs.[189,190] This synergetic effect of two different finely dispersed phases that is also called the *second phase effect* has further been reported for other systems such as $Li_3P$/LiCl mixtures and also ionic conductors that have been dispersed with insulating $Al_2O_3$ particles.[191,192]

In reality, artificial SEIs will always be multi-component layers as a modification through additives or dip coating, for example, leads to several reaction products.[110,174] A comparison of $LiBF_4$ and $LiBF_3CN$ as electrolyte additives revealed that the SEI resulting from the $LiBF_3CN$ additive, which consists of $LiN_xO_y$, $Li_3N$ and $Li_2O$, grows only half as thick as the $LiBF_4$-derived SEI (20 nm vs.

40 nm). This shows that a multi-component ASEI contributes to achieving homogenous lithium plating/stripping and enhanced capacity retention in full cells with NCM cathodes.[89]

#### *2.3.4.2 ASEIs vs. Protective coatings | in situ vs. ex situ*

After the previous section presented examples of the wide range of possible chemical compound classes that can improve the electrochemical properties of the lithium/electrolyte interface or interphase, this section will now present details about the different coating/modification techniques.

Generally speaking, the broad variety of methods to acquire an ASEI or protective layer can be divided into *ex situ* and *in situ* techniques. In situ modifications of the SEI can only be achieved via the addition of certain reagents to the electrolyte or by (partly) replacing the electrolyte solvents or conducting salts. This way the SEI forming reaction upon cell assembly and cycling can be altered towards more desired reaction products for higher cell performance and stability.[24,170,181,193,194] In batteries with an intercalation cathode, for example, vinylene carbonate, fluoroethylene carbonate and ethylene sulfite are used; also, inorganic additives can be added, such as aluminum trichloride.[195] For ex situ techniques, on the other hand, there are practically unlimited possibilities for the fabrication of protective layers or ASEIs. These methods stretch across all matters of state beginning at solid state lamination processes[196–198], liquid-based spin coating[17,78], dip coating[199,200], spray coating[164] or drop casting[186], gas phase reactions[201,202] and atomic layer deposition (ALD)[176,203] up to plasma[204,205] and sputter coatings.[162,206] Wet chemical processes offer a broad spectrum for coating lithium anodes with the help of solvent-based substances or mixtures of substances. The direct protective coatings on lithium with two-dimensional "phosphorene" and with aluminum oxide nanoparticles through spin coating are known.[78,207] Furthermore, lithium has already been coated with a composite of $Al_2O_3$ and a polymer using a doctor blade.[208] Other wet chemical processes such as spin coating of silicone polymers, spray coating of metal oxide precursors and dip coating have already been successfully tested and published on other electrode materials.[209–211] These methods are also likely to be transferable to the application of elemental lithium and enormously expand the possibilities for creating protective layers. In addition, the solvent-based techniques are very promising in terms of scalability, for example in "roll-to-roll" processes. One further method of optimizing the electrochemical performance of the LMA is based on the principle of not to change the surface chemistry but to change the surface morphology by nanostructuring.[212,213]

While on one hand there are approaches that require the used chemicals such as electrolyte additives or coating agents reacting to some extent with the LMA and/or the SEI, there are on the other hand approaches that involve coating the lithium with polymers, solid electrolytes or hybrid

combinations thereof.[207,214,215] These coatings move a little away from the concept of artificial SEI and should therefore be called protective coatings, even though the two terms are often used synonymously. The polymers used are often polyethylene oxide (PEO) or polyvinylidene difluoride (PVDF), some of which contain conducting salts.[216] The aim many of polymer coatings is to achieve a defined intermediate layer and to suppress dendrite growth according to the *Monroe-Newman* model.[86,217] A widely researched solid electrolyte that is applied by radio frequency (RF) sputtering for protective coatings of LMAs is lithium phosphorus oxynitride, or "LiPON" for short, which is highly stable against lithium and therefore prevents degradation reactions as well as polysulfide shuttling.[115,218] The coating of Li anodes via RF sputtering is a well-known method also for other materials such as $Li_3PO_4$, carbon, silicon, and $Al_2O_3$, all of which lead to improved electrochemical properties.[163,206,219–221] Sulfide type solid electrolytes, which are used in the construction of all-solid-state batteries, have also been tested as protective coatings.[222] Combining polymer and (ceramic) solid electrolytes in a hybrid coating is suggested by recent research as a measure to enhance their mechanical characteristics through embedding solid electrolyte particles into a polymer matrix. Such hybrid or composite electrolytes are expected to exhibit higher elastic stiffness while still remaining the flexibility and adhesion of the polymer.[223] The processes for the production of hybrid electrolytes are partly solvent-based,[224] which means that lithium electrodes can also be coated directly with the solute intermediates of the production process to achieve a stable hybrid interlayer between LMA and liquid electrolyte.

# 3 Experimental

## 3.1 Coin Cell Fabrication

All symmetrical cells were constructed using CR2016 coin cell cases, 2 layers of polyolefin separators (25 µm, Celgard LLC, USA) and 50 µL electrolyte (1 M LiTFSI (99.95 %, Sigma-Aldrich GmbH, Germany) + 0.25 M $LiNO_3$ (≥ 99.0 %, Sigma-Aldrich GmbH, Germany) in DOL/DME (1/1) (both Sigma-Aldrich GmbH, Germany). DOL and DME had been stored over 3 Å molecular sieves having $H_2O$ contents of less than 0.4 ppm and 1.2 ppm, respectively. LiTFSI and $LiNO_3$ were dried in a Büchi vacuum oven at 120 – 130 °C for 48 h each. The water content of the resulting electrolyte was determined by Karl-Fischer titration to be < 22 ppm which is a typical value.[225,226]

The Li-S cells were prepared at Fraunhofer IWS in Dresden by Florian Hofmann in an argon filled glovebox ($p(H_2O)/p$ < 0.1, $p(O_2)/p$ < 0.1 ppm). The cells were assembled in CR2016 coin cells using S/C-electrodes as cathode (diameter: 12 mm), Li foil without and with coating as anode (diameter: 13 mm), a 12 µm thick PE separator, a 1000 µm thick stainless steel spacer (Fraunhofer IWS) and 1.5 M lithium bis(trifuoromethane)sulfonimide (LiTFSI, Gotion, Inc.) in tetramethylene sulfone (TMS, Kishida Chemical Co., Ltd.) and 1,1,2,2-tetrafluoroethyl-2,2,3,3-tetrafluoropropyl ether (TTE, Daikin Chemical Europe GmbH) (v, 1:1) as electrolyte.[62] The electrolyte amount was based on an electrolyte / sulfur ratio of 10 µl $mg_S^{-1}$. The cells were characterized with a BaSyTec CTS test system (BaSyTec GmbH). The cells were cycled in the voltage window between 1.5 – 2.6 V. For formation, the cells were first discharged at C/20 (1C = 1672 mAh $g_S^{-1}$) and charged at C/10. Afterwards, they were charged and discharged at C/10.

## 3.2 Lithium Metal Electrode Modification

### 3.2.1 Spin Coating

The solutions for the spin coating process were made by first dissolving the polymer in the solvent under continuous stirring. If necessary, the closed vials were placed on a heating plate to accelerate the polymer dissolution at roughly 50 – 60 °C. After complete dissolution of the polymer, the metal complex resp. the solid electrolyte powder was added at room temperature. In case of the metal complexes, the solutions were ready for spin coating after a few minutes of stirring. In case of the argyrodite solid electrolyte, the suspensions were vigorously stirred for at least 15 hours to ensure

good homogenization. All of these steps are performed under argon atmosphere. Some polymer/argyrodite suspension vials were double sealed in pouch foil to avoid contamination by air and water and were placed in an ultrasonic bath outside the glovebox for 5 hours in order to achieve even higher dispersion. For the coating, the vials were transferred into the glovebox again. During the coating, it was made sure to always keep the suspensions stirring and to extract them as quickly as possible to avoid precipitation.

With regard to the manufacturer and purity of the chemicals, the following specifications are given:

- Indium acetylacetonate, ≥ 99.99 %, Sigma-Aldrich GmbH, Germany
- Chloro(1,5-cyclooctadiene)copper(I) dimer, 95 % Sigma-Aldrich GmbH, Germany
- Dichloro(1,10-phenantroline)copper(II), 98 % Sigma-Aldrich GmbH, Germany
- Polystyrene (PS), average $M_W$ ~250000, pellets, Acros Organics, Belgium
- Polyvinylidene difluoride (PVDF), average $M_W$ ~534000, powder, Sigma-Aldrich GmbH, Germany
- Polyvinylidene difluoride (PVDF), average $M_W$ ~180000, beads, Sigma-Aldrich GmbH, Germany
- Polyethylene oxide (PEO), average $M_W$ ~300000, powder, Sigma-Aldrich GmbH, Germany
- Poly(vinylidene fluoride-co-hexafluoropropylene) (PVDF-HFP), average $M_W$ ~400000, pellets, Sigma-Aldrich GmbH, Germany
- $Li_6PS_5Cl$, NEI Corporation, USA
- Tetrahydrofuran (THF) anhydrous, ≥ 99.9 %, inhibitor-free, Sigma-Aldrich GmbH, Germany
- Dimethylformamide (DMF), ≥ 99.9 %, Sigma-Aldrich GmbH, Germany
- Ethyl acetate (EtOAc) anhydrous, 99,8 %, Sigma-Aldrich GmbH, Germany
- Tris(*N*,*N*-tetramethylene)phosphoric acid triamide (TNNT), ≥ 98.0 %, Sigma-Aldrich GmbH, Germany
- Acetonitrile (ACN) anhydrous, 99,8 %, Sigma-Aldrich GmbH, Germany
- 2-Methyl-2-butanol, > 99%, Sigma-Aldrich GmbH, Germany
- Propylene carbonate (PC), ≥ 99.0 %, Sigma-Aldrich GmbH, Germany
- Dimethyl sulfoxide (DMSO) anhydrous, ≥ 99.9 %, Sigma-Aldrich GmbH, Germany

Lithium electrodes (Ø = 13 mm) were freshly punched from 30 µm thick lithium sheets (Honjo Metal Co., Ltd (Japan) > 99.0 w%) and placed on the 13 mm spinning die of a SCI-20 spin coater (Novocontrol Technologies GmbH & Co. KG). If not otherwise stated, 4 droplets of spinning solution or dispersion were placed in the center of the lithium electrode followed by starting the spinning at 100 Hz rotational speed. After few seconds, the spin coater is turned off and the coated

electrode is carefully peeled off the spinning die. Especially if the spinning fluid had a low viscosity, the coating was conducted twice to ensure a covering coating.

### 3.2.2 Dip Coating

#### *3.2.2.1 Preparation of the Anodes discussed in chapter 4.2*

Hexachlorophosphazene (NPCl), Tris(diethylamino)phosphine (TDP) and Dichloro(diethylamino)phosphine (DDP) were purchased from Sigma-Aldrich GmbH (Germany) with a purity of 97 % for DDP and TDP and 99 % for NPCl. Lithium electrodes (Ø = 13 mm) were freshly punched from 30 µm thick lithium sheets (Honjo Metal Co., Ltd (Japan) > 99.0 w%) and subsequently submerged in 9.1 % or 16.7 % (w/w) solutions of the reagents in heptane (anhydrous, 99%, Sigma-Aldrich GmbH, Germany) or tetrahydrofuran (THF, anhydrous, ≥ 99.9 %, inhibitor-free, Sigma-Aldrich GmbH, Germany). During the dip coating, the vials were swayed occasionally. If not stated otherwise, the electrodes were removed from the solutions after 30 minutes and were carefully placed on Kimtech wipes to dry under argon atmosphere.

#### *3.2.2.2 Preparation of the Anodes discussed in chapter 4.3*

A 5 % and a 10 % (by mass) solution each of 3-(trifluoromethoxy)-aniline (98 %, Sigma-Aldrich GmbH, Germany), 4-(trifluoromethoxy)-anisole (98 %, Sigma-Aldrich GmbH, Germany) and 1,2-dibromo-tetrachloroethane (97 %, Sigma-Aldrich GmbH, Germany) in heptane (99 %, Sigma-Aldrich GmbH, Germany) was prepared. In addition, a 20% solution of 1,2-dibromo-tetrachloroethane in heptane was prepared. 30 µm thick lithium foils (Honjo Metal Co., Ltd (Japan) > 99.0 w%) were punched out and dip coated. For this purpose, the foils remained in a solution for 30 minutes and were then rinsed in heptane.

#### *3.2.2.3 Preparation of the Anodes discussed in chapter 4.4*

Lithium electrodes (Ø = 13 mm) were freshly punched from 30 µm thick lithium sheets (Honjo Metal Co., Ltd (Japan) > 99.0 w%) and subsequently submerged in a solution of 5 % tris(*N*,*N*-tetramethylene)phosphoric acid triamide (TNNT, ≥ 98.0 %, Sigma-Aldrich GmbH, Germany) and 10 % tert-pentanol (> 99%, Sigma-Aldrich GmbH, Germany) (w/w) in heptane (99 %, Sigma-Aldrich GmbH, Germany). After 15 minutes of dip coating, the electrodes were taken out of the coating solution and were either rinsed with fresh heptane to clean the surface from residual reagents, then shortly left to dry on lint-free Kimtech wipes in order to avoid contamination or

directly put on Kimtech wipes and carefully left to dry at RT under Ar atmosphere for 1 hour. All steps were performed in an argon glovebox ($p(H_2O)/p < 1$ ppm , $p(O_2)/p < 1$ ppm).

## 3.3 Electrochemical Experiments

### 3.3.1 Cycling Experiments

The electrochemical experiments were conducted in a temperature chamber at 25°C with a battery cycler system Series 4000 from Maccor or VMP300 electrochemical testing unit (BioLogic). All plating/stripping experiments (1 mAh/cm² per step) were performed using the same cycling protocol (5 cycles at 0.1 mA/cm², 10 cycles at 0.2 mA/cm², 10 cycles at 0.5 mA/cm², then at 1.0 mA/cm² until cell failure). For SEM imaging, some cells were cycled in a shorter protocol comprising 1 cycle at 0.1 mA/cm² followed by 25 cycles at 1 mA/cm² (declared as *short cycling*).

### 3.3.2 Impedance Spectroscopy

All electrochemical impedance spectroscopy (EIS) measurements were performed with a VMP300 potentiostat (BioLogic). Potentiostatic electrochemical impedance spectroscopy (PEIS) was performed at OCV using an AC amplitude of 5 mV in the frequency range from 7 MHz or 3 MHz to 0.1 Hz with 15 points/decade and 5 measures per frequency.

## 3.4 Analytics

### 3.4.1 Scanning Electron Microscopy

SEM measurements were performed in a Merlin high-resolution scanning electron microscope (SEM, Carl Zeiss AG). For sample transfer, an argon-filled Leica EM VCT500 shuttle (Leica Microsystems) was used. The samples were attached to the sample holder using nonconductive double-sided tape and were sputter coated with 4 nm platinum to avoid charging effects.

#### *3.4.1.1 Energy dispersive X-ray Spectroscopy*

The EDX analysis utilized a windowless XMAX EXTREME EDX detector (Oxford Instruments), which was connected to a Merlin high-resolution scanning electron microscope (SEM, Carl Zeiss AG). To transfer the samples, a Leica EM VCT500 shuttle (Leica Microsystems) filled with argon gas was employed. The electron acceleration voltage ranged from 2 to 4 kV. EDX spectra were

obtained using mapping of random sample surface areas. The software AZtec 4.3 (Oxford Instruments) was utilized to automatically quantify the elements of interest. X-ray emission depths were determined using simulations conducted with *Casino* software version 2.51. Unless otherwise specified, nonconductive double-sided tape was used to attach the samples to the sample holder.

### 3.4.2 X-ray Photoelectron Spectroscopy

XPS measurements were carried out with a PHI VersaProbe II instrument (ULVAC-PHI, Inc.). All samples were transferred to the instrument in an argon-filled transfer vessel. Monochromatic Al $K_\alpha$ radiation (1486.6 eV) was used; the power of the X-ray source was 100 W, and the beam voltage was 20 kV. The examined areas were 0.13 $mm^2$. For depth profiling, $Ar^+$ ions with accelerating voltages between 1 and 2 kV were applied, using the following sputter steps: surface, (1) 3 min 1 kV, (2) 8 min 2 kV, (3) 5 min 2 kV, (4) 10 min 2 kV, (5) 15 min 2 kV. For the survey spectra, a pass energy of 93.9 eV, and for the detail spectra, a pass energy of 23.5 eV were used. Data evaluation was carried out with the software CasaXPS (version 2.3.18, Casa Software Ltd). All data were calibrated in relation to the signal of adventitious carbon at 284.8 eV or to the O 1s lithium oxide signal at 528.5 eV if no carbon was present. A Shirley background was used, and all spectra were fitted with a GL line shape. All samples were electrically isolated with nonconductive double-sided tape (tesa) for the measurements.

### 3.4.3 Time of Flight Secondary Ion Mass Spectrometry

ToF-SIMS measurements were conducted using a ToF.SIMS 5 instrument (IONTOF GmbH), which is equipped with a 25 kV Bi cluster primary-ion gun for analysis and a 20 kV gas cluster ion beam (GCIB) for depth profiling. All samples were transferred from the glovebox to the instrument with an argon-filled Leica EMVCT500 shuttle (Leica Microsystems). Depth profiles on lithium foils were measured in spectrometry mode (bunched) which provides a high signal intensity and a high mass resolution (40000 cts/s, full width at half maximum, FWHM $m/\Delta m = 5000$ @ $m/z = 17.00$ ($OH^-$)). Depth profiles in spectrometry mode were acquired with $Ar_{1500}^+$ cluster ions (10 keV, 10 nA, 300 × 300 $\mu m^2$) as sputter species and $Bi^+$ (1.2 pA, 100 × 100 $\mu m^2$) as primary ions. Between two sputter frames, analysis was performed after 2 s of pause time, in random raster mode, measuring two frames with 128 × 128 pixels and 1 shot/pixel. The cycle time for all measurements was 100 µs. All measurements were carried out in negative-ion mode. Data evaluation was carried out with the software SurfaceLab 7.2 (IONTOF GmbH).

# 4 Results and Discussion

## 4.1 Application of Metal-Complex/Polymer and Argyrodite/Polymer hybrid protective Layers by Spin Coating

In spin coating, a wide variety of substrates can be coated by applying a defined amount of a solution to the substrate, which is then spun off again by rapidly rotating the substrate. The centrifugal force acting on the solution coats the substrate uniformly and thinly. The advantage of spin coating over dip coating lies, for example, in the shorter contact time between substrate and coating solution and in the almost instantaneous solvent evaporation due to the rapid rotation.

In an effort to create a surface functionalization that ensures homogeneous lithium deposition and thus suppresses the formation of dendrites, the electrodes were coated with solutions containing indium acetylacetonate. The working hypothesis here was that maximum homogeneity would be achieved by complexing the indium ion in the solution and thus transferring this to the protective layer. A possible subsequent reduction of the indium ions to indium metal could then lead to a homogeneous, long-term stable lithium deposition. Initially, the electrodes were coated with a solution of 9 % $In(acac)_3$ (see figure 9 for chemical formula) in tetrahydrofuran (THF).

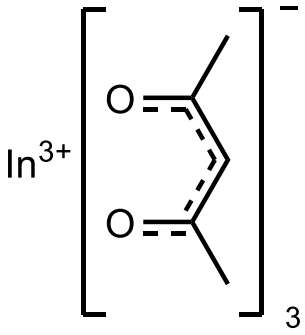


**Figure 9: Chemical formula of indium acetylacetonate ($In(acac)_3$).**

Using this coating solution, however, electrochemical studies showed no improvement in long-term stability. Appropriately treated electrodes were analyzed by scanning electron microscope (SEM) and energy dispersive X-ray spectroscopy (EDX, see figures 10 and 11) to investigate the surface condition as well as the elemental composition. The investigations showed that the surface of the electrodes as well as the elemental distribution was partly inhomogeneous and that overall only little indium was deposited on the surface.

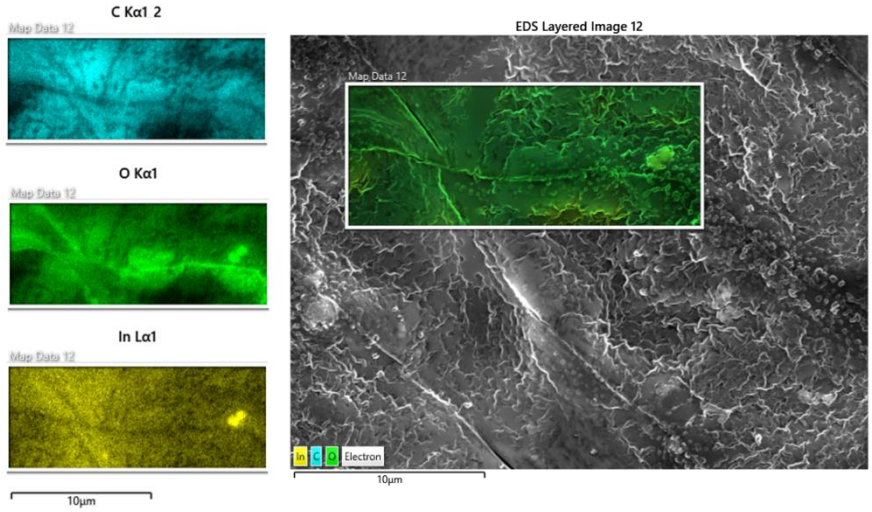


**Figure 10: Combined SEM and EDX imaging of the In(acac)$_3$ (without polymer) treated lithium electrode shows a porous structure and some fissures of the coating.**

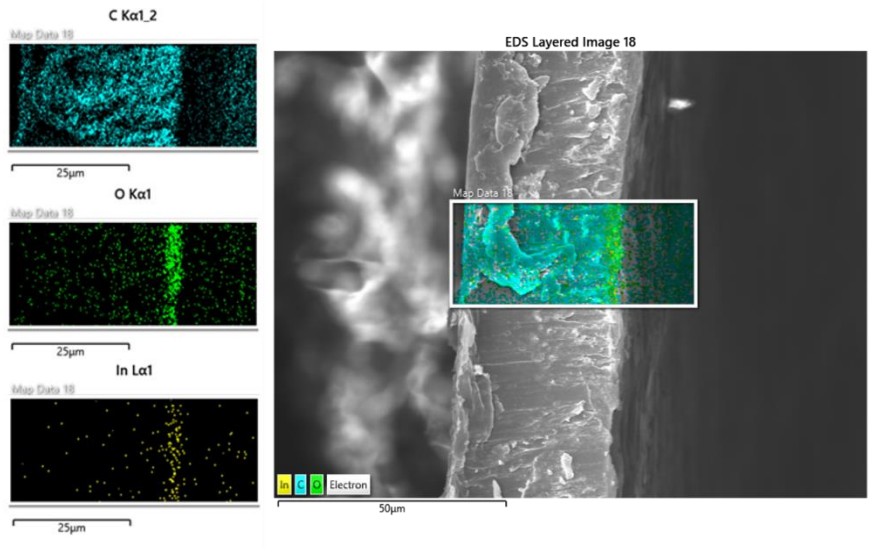


**Figure 11: Combined SEM and EDX imaging of a cross sectioned sample coated with In(acac)$_3$ in THF shows only weak indium signals which means there is little indium on the electrode surface.**

To increase the "loading" of the electrode surface with indium, solutions were created for the following coatings in which polystyrene (PS) was added to the indium complex solution as a binder material. In order to approach an appropriate ratio of indium complex and polymer, the coating solution compositions (9 % PS/1.5 % In(acac)$_3$; 5 % PS/5 % In(acac)$_3$; 1.5 % PS/9 % In(acac)$_3$, all in THF) were compared in electrochemical tests. While the symmetrical cells built with lithium electrodes that were coated with both higher polymer amounts showed high overpotentials, the 1.5 % PS/9 % In(acac)$_3$ spin coating led to improved electrochemical properties. Thus, the plating/stripping experiments ran stably for 200-250 hours (see figure 12) and the calculated interfacial resistance was consistently in the range of 120 - 140 Ωcm² (see table 1).

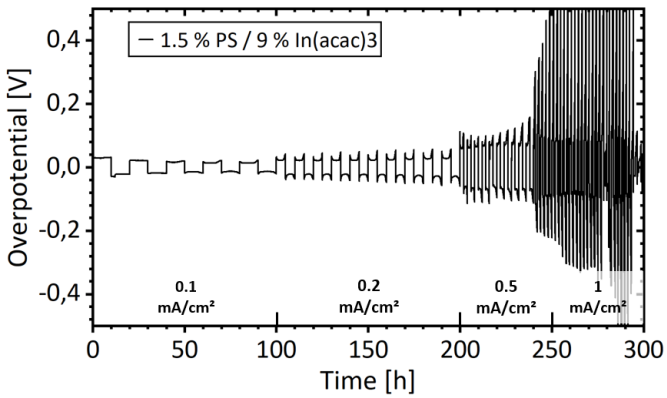


**Figure 12: Overpotential profile of a symmetrical cell using electrodes spin coated with PS and $In(acac)_3$ using THF as solvent. Measurement was performed at $T$ = 25 °C.**

**Table 1: Average overpotentials and resulting cell resistances for the first 3 current density steps as depicted in fig. 12. Contrarily to the anode modifications in chapter 4.4, for example, the cell resistance is not decreasing during cycling but rather stays constant.**

| Step | Current density / (mA/cm²) | Overpotential / mV | Cell resistance / Ωcm² |
|---|---|---|---|
| 1 | 0.1 | 14 | 140 |
| 2 | 0.2 | 24 | 120 |
| 3 | 0.5 | 70 | 140 |

These electrodes were also examined using SEM and EDX. SEM images of cross-sections of the samples clearly showed that the use of the PS as a binder allowed significantly more coating material to be deposited on the electrode surface (fig. 13). The signals of the EDX investigation belonging to the indium are clearly more pronounced than in figure 11. A morphological examination of the sample (fig. 14) could show that the surface of the coating itself is very flat and homogeneous, but the polystyrene is brittle and has a strong tendency to form cracks. In addition, identically coated electrodes stored in fully assembled symmetrical cells for several weeks (without cycling) were examined to determine if the $In(acac)_3$/PS coating dissolved in the used electrolyte.

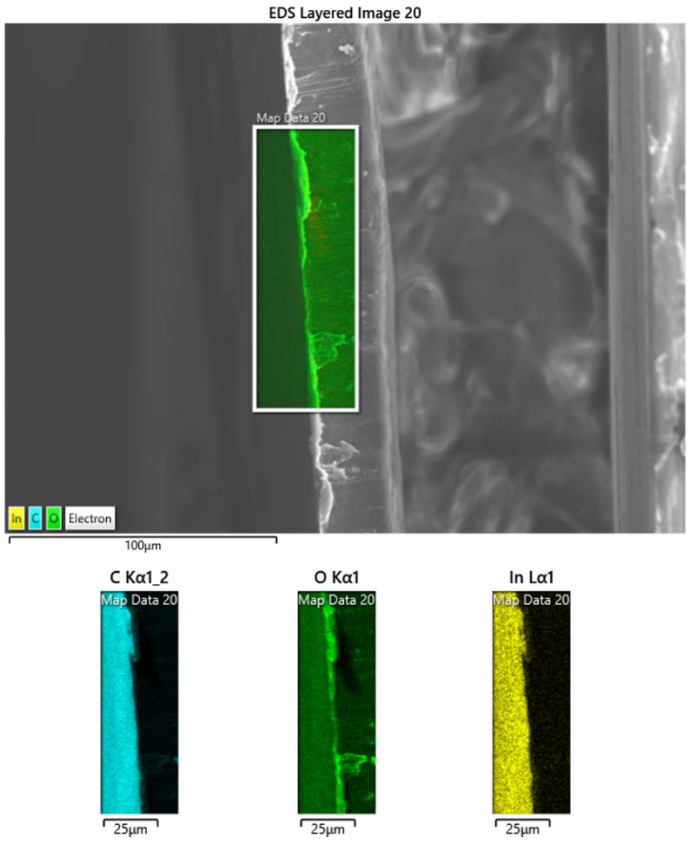


**Figure 13: Cross section of a $In(acac)_3$/PS spin coated lithium foil. Compared to the sample without PS as binder (fig. 11) the indium signal is significantly stronger and more pronounced.**

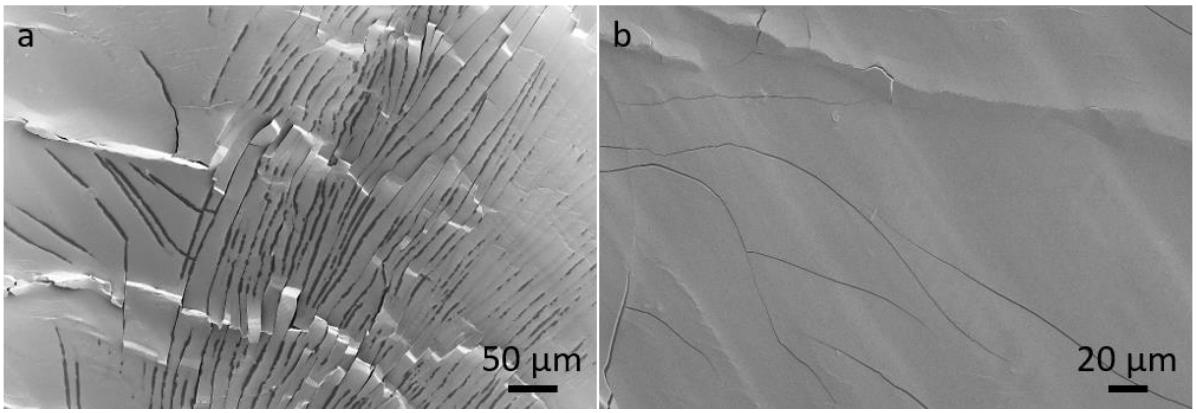


**Figure 14: Top view of a $In(acac)_3$/PS spin coated lithium foil. While the surface of the polymer coating is smooth and homogenous, there is a high tendency to forming cracks. a) 500 x magnification; b) 1000 x magnification.**

The results of the SEM examinations of the electrodes from the storage experiment (fig. 15) strongly indicate that the $In(acac)_3$/PS protective layer used in the DOL/DME electrolyte at least partially dissolves. The surface of the electrodes appears significantly changed; thus, the previously flat morphology of the polystyrene is much more heterogeneous, and moreover, cracks could no longer be observed. The disappearance of the cracks due to the dissolution of the protective layer could be an explanation for the enhanced electrochemical properties of the cells. Nevertheless, an alternative

polymer that is insoluble in the electrolyte was sought for in the following, partly because the cell performances were not satisfactory reproducible either (compare figures 12, A1 and A2).

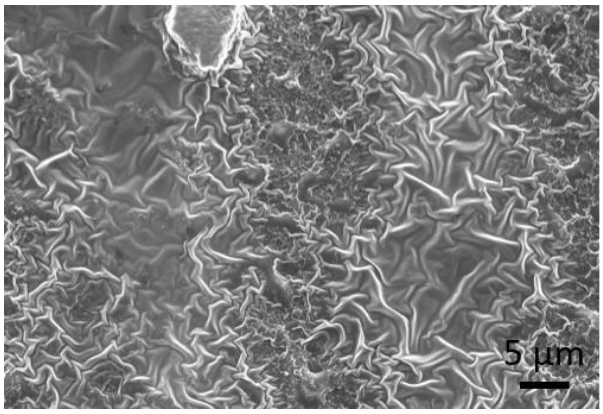


**Figure 15: The clearly changed surface morphology of the PS based protective coating indicates a partial dissolution in the electrolyte.**

Polyvinylidene difluoride (PVDF) is a commonly used binder material in battery applications because it is not soluble or swells only slightly in common battery electrolytes.[227] For this reason, it was selected to further develop the concept of combining a polymer binder with a metal complex.

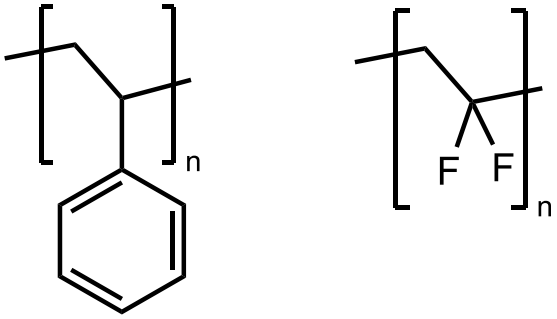


**Figure 16: Chemical structure of polystyrene (PS, left) and polyvinylidene difluoride (PVDF, right).**

First, the solubility of PVDF (powder, molecular weight = 534k) in the solvents THF and dimethylformamide (DMF) was compared; the comparison showed that the polymer dissolved only with difficulty and not completely in THF. In DMF, however, it dissolved much better. Also, the comparison SEM micrographs of lithium foils spin coated with 1.5% PVDF solutions show that with THF as solvent, small particles, which presumably were not completely dissolved, remain on the surface (fig. 17 a), while the sample with DMF as solvent does not have such particles (fig. 17 b). Overall, the PVDF surface is nevertheless clearly different from that of the PS, as it exhibits a fine, fiber-like structuring, while the PS surface is very smooth (see fig. 14).

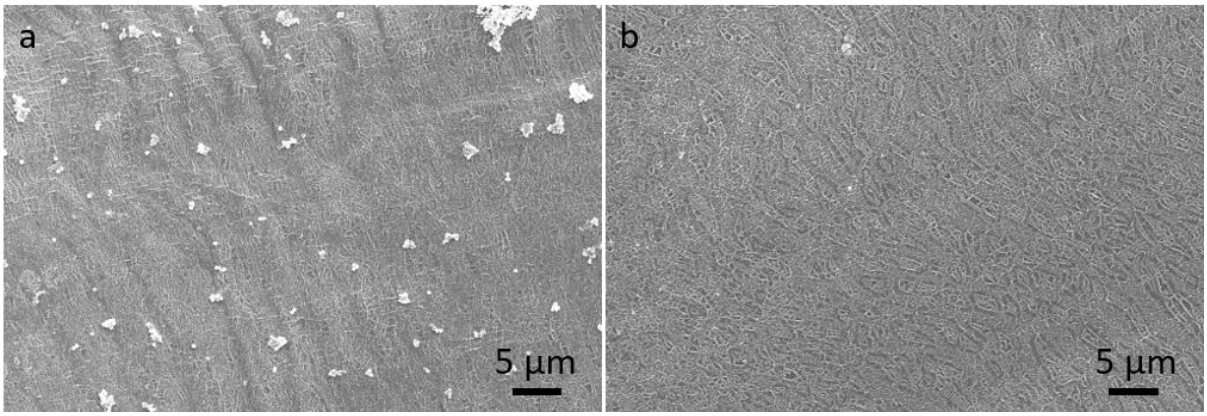


**Figure 17: Comparison of PVDF-coated lithium foils using a) THF and b) DMF as solvents.**

Furthermore, as depicted in figure 18, cross-sections of the PVDF-coated lithium foils were analyzed by SEM and EDX. The thickness of the PVDF layer could be determined to be about 3 µm and especially based on the fluorine signals in the EDX imaging it could be proven that the PVDF coating adheres to the lithium surface.

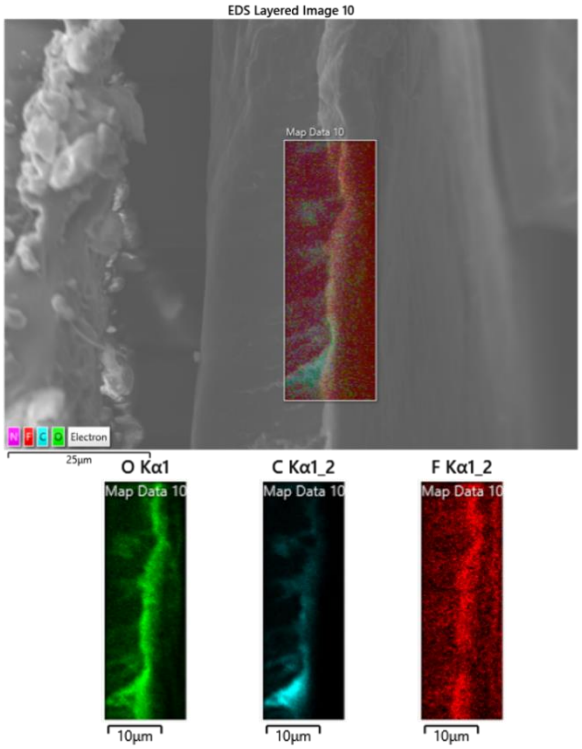


**Figure 18: Cross section and EDX elemental mapping of a PVDF coated lithium foil showing high fluorine accumulation on the electrode surface coming from the PVDF.**

Electrochemical tests of spin coated electrodes using PVDF and $In(acac)_3$ in combination were carried out for both THF and DMF as solvents of the spin coating solution. Despite the problematic

solvation of PVDF powder in THF, the coatings were also able to achieve stable plating/stripping and low overpotential for up to 220 - 250 hours (figs. 19; A3).

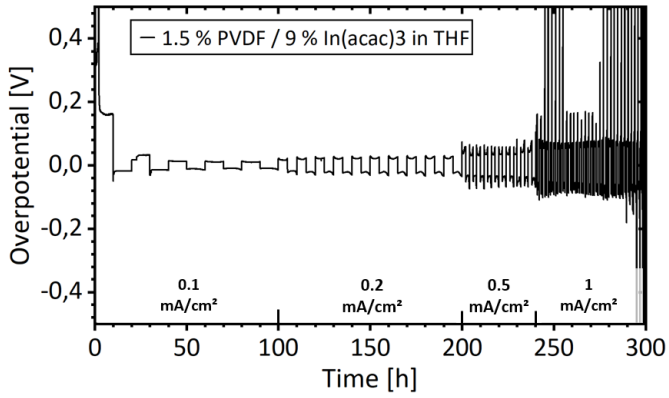


**Figure 19: Overpotential profile of a symmetrical cell using electrodes spin coated with PVDF and $In(acac)_3$ in THF. Measurement was performed at $T$ = 25 °C.**

Using DMF as solvent of the spin coating solution led to quick dissolving of the PVDF power and the solution was clear and homogenous after the subsequent addition of the indium complex. However, the coatings did not lead to better electrochemical performance compared to the PS/$In(acac)_3$/THF nor the PVDF/$In(acac)_3$/THF coatings as there appeared early voltage spikes and the overpotential rose very high already around 200 h. Also, a higher amount of polymer (3 % PVDF) for higher viscosity of the coating solution did not lead to satisfactory improvements (see figs. 20, 21 and A4). All of the electrochemical tests mentioned above were started directly after cell assembly. However, as can be seen e.g. in figures 19 and 21, the first half cycle often shows high overpotential which was thought to be caused by incomplete penetration of the polymer layer by the liquid electrolyte.

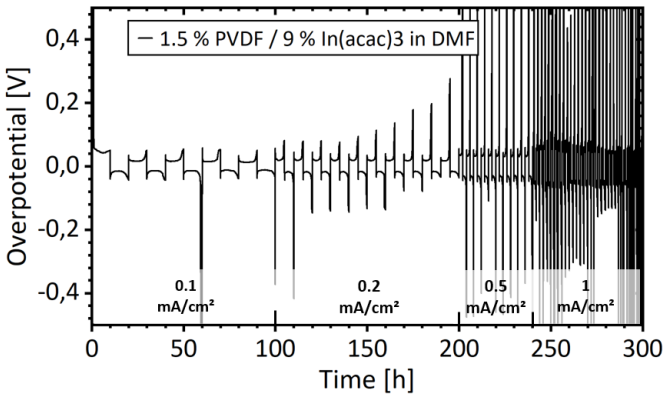


**Figure 20: Overpotential profile of a symmetrical cell using electrodes spin coated with PVDF and $In(acac)_3$ in DMF. Measurement was performed at $T$ = 25 °C.**

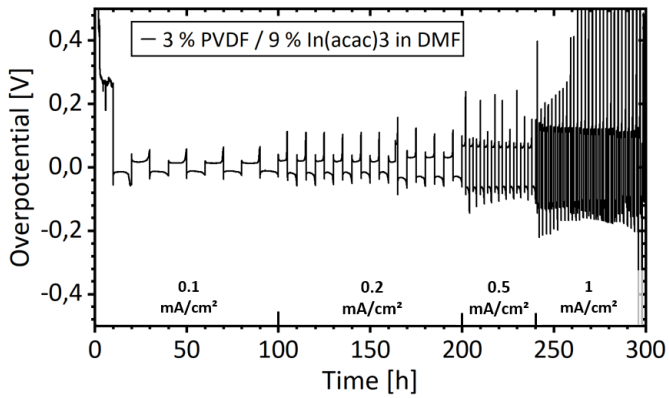


**Figure 21: Overpotential profile of a symmetrical cell using electrodes spin coated with PVDF and $In(acac)_3$ in DMF. Measurement was performed at *T* = 25 °C. Note the higher PVDF content.**

For this reason, further cells were constructed and stored for 24 resp. 72 hours prior to electrochemical cycling so there is enough time for the electrolyte to wet and penetrate the protective coatings. While some of these stored or aged cells showed the highest life times of up to 280 hours (see fig. A5), these results were not reproducible as 2/3 of the cells had short circuits after the storing procedure. With regard to the coatings carried out with DMF as a solvent, it must also be mentioned that during spin coating, the short contact time of the solvent with the lithium metal already led to a discoloration of the lithium surface, which means that DMF is less stable towards lithium than THF. For this reason, the spin coatings were carried out as quickly as possible. Apart from indium acetylacetonate, protective coatings with 2 different copper complexes (a copper (I) and a copper (II) complex, chloro(1,5-cyclooctadiene)copper(I) dimer and dichloro(1,10-phenantroline)copper(II)) were also investigated, but these did not improve the electrochemical properties. Just as at the beginning of the investigation series the spin coating was first tested with an $In(acac)_3$ solution without polymer, the corresponding polymers were also dissolved without the metal complex and the electrodes were coated with them. Spin coatings with 10 % PS in THF, 1.5 % PS in THF, 1.5 % PVDF in THF, 1.5 % PVDF in DMF and 3 % PVDF in DMF were tested, none of which led to improved electrochemical properties or reproducible results.

To briefly summarize this part of the work, a completely new concept for the protective coating of lithium metal anodes was developed here. The concept is based on the spin coating of combined solutions of polymers and metal complexes, which were chosen instead of simple metal salts to ensure maximum solubility in organic solvents and thus to obtain the distribution of polymer and metal ions in the protective layer as homogeneously as possible. This first study showed that the combined coatings led to improved electrochemical properties of the electrodes, in contrast to coating only with the polymers or only with the metal complexes. DMF as a solvent was found to be rather unsuitable for the coatings, despite the better solubility of PVDF, presumably because it already reacts with the lithium during the coating. The coatings with PS or PVDF and $In(acac)_3$ in THF showed more significant improvements in the plating and stripping overvoltage, although the

solubility of PVDF in THF proved to be problematic. This could be further optimized in the future, for example by using PVDF with a shorter chain length or by dissolving the polymer in THF under heating.

Furthermore, another type of polymer-based protective coatings was investigated: polymer-inorganic hybrid coatings. The aim of these investigations was to find a suitable combination of polymer and solvent to create a functional and stable coating solution or suspension with the argyrodite $Li_6PS_5Cl$ (LPSCl), which could also be applied to the lithium metal electrodes via spin-coating. Based on the results of *Ruhl* et al.[67], a knowledge base regarding the stability of the argyrodite against certain solvents could already be relied upon. Additionally, the publications of *Wang* and *Zhang* et al.[228,229] provided promising reference points, as they were able to generate stable solutions of PVDF or PEO and LPSCl in ethyl acetate (at 55 °C) for the production of freestanding hybrid electrolyte layers.

Consequently, first attempts were made to replicate the solutions according to the publications. It turned out that it was not possible to dissolve PVDF (MW = 534k (powder) or MW = 180k (beads); MW = 300k was used in the publication[228]) in ethyl acetate, neither at 55 °C nor at higher temperatures. However, PEO could be successfully dissolved. Initially, solutions or suspensions with mass ratios of 1.5 % polymer and 13.5 % argyrodite (hereinafter abbreviated as *x*(polymer)/%:*x*(argyrodite)/%, in this case 1.5:13.5) were prepared. Despite the insolubility of PVDF powder in EtOAc, electrodes were coated with the suspension, but it did not lead to improved properties, whereas the coatings with PEO 1.5:13.5 in EtOAc resulted in a uniform plating/stripping overpotential for approximately 250 hours (fig. 22).

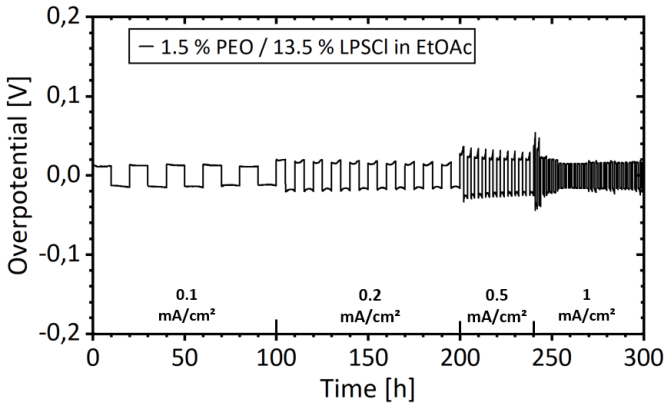


**Figure 22: Overpotential profile of a symmetrical cell using electrodes spin coated with PEO 1.5:13.5 in ethyl acetate showing remarkably low overpotential. Measurement was performed at *T* = 25 °C. The overpotential drop after 250 h indicates onset of short circuiting.**

Since the powdery LPSCl settled quickly without continuous stirring of the suspension, another solution with the composition 1.5:10 in EtOAc was placed in an ultrasonic bath for 24 hours to achieve better homogenization. The resulting solution exhibited significantly improved

homogeneity, while the cell performance did not differ significantly from the 1.5:13.5 coating without ultrasonication. The solubility of PVDF powder was improved by adding 10 % tris(*N*,*N*)-tetramethylene phosphoric acid triamide (TNNT) to the main solvent, EtOAc. However, the solution slowly discolored after adding the argyrodite, indicating degradation of the solid-state electrolyte. The cell tests of the electrodes coated with 1.5:13.5 or 3:12 in EtOAc + TNNT were not reproducible. Similarly, to improve the solubility of PEO, 10% acetonitrile (ACN) was added to EtOAc. It was found that the polymer dissolved faster than in pure EtOAc, and the cell tests of the electrodes coated with the 1.5:13.5 or 3:12 composition showed improved electrochemical properties with lifetimes ranging from 180 to 290 hours, although voltage peaks often occurred towards the end of the respective cycles as can be seen in figure 23.

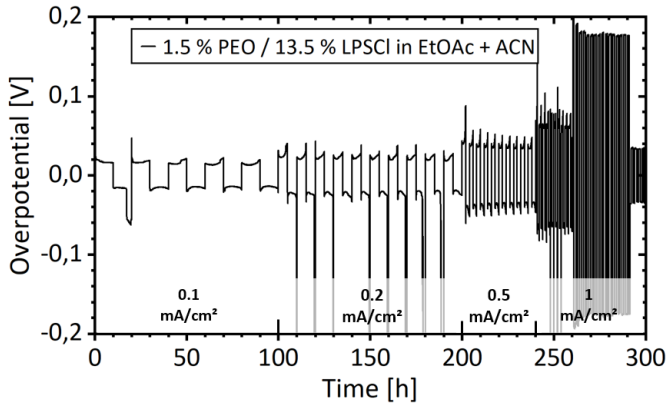


**Figure 23: Overpotential profile of a symmetrical cell using electrodes spin coated with PEO 1.5:13.5 in ethyl acetate and acetonitrile. Measurement was performed at *T* = 25 °C. While the voltage peaks between 100 and 200 hours indicate irregularities in plating and stripping, the voltage drop just before 300 h indicates a short circuit.**

To expand the range of tested solvents for PEO (chemical structure of PEO is depicted in fig. 29), commonly used solvents in battery applications such as THF and ACN[67], as well as DMF, were examined for their suitability in relation to PEO based coatings. Since the 3:12 composition in THF was very viscous and resulted in excessively increased cell overpotential, a solution with a composition of 1.5:10 was prepared and homogenized in an ultrasonic bath. The resulting coatings led to a moderately improved cell lifetime of 230 hours (see figs. 24 and A6).

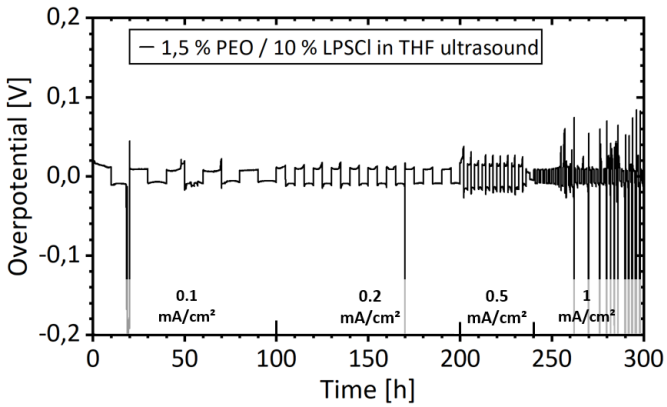


**Figure 24: Overpotential profile of a symmetrical cell using electrodes spin coated with 2 x 5 droplets PEO 1.5:10 in THF after ultrasonication. Measurement was performed at *T* = 25 °C.**

Acetonitrile as a solvent for PEO/argyrodite dispersions provided outstanding stability of the coating solutions or dispersions. Protective coatings with a composition of 1.5:13.5 resulted in varying cell test results, ranging from only 150 hours of stable plating and stripping up to 290 hours. The 3:12 composition exhibited further increased homogeneity, which positively affected the coating process and resulted in stable cycling with low overpotential for over 300 hours. The corresponding voltage plot can be seen in figure 25. Contrary to previous treatments of the coating solutions in the ultrasonic bath, no further improvement was achieved with the ACN/PEO/argyrodite combination (c.f. figure A7).

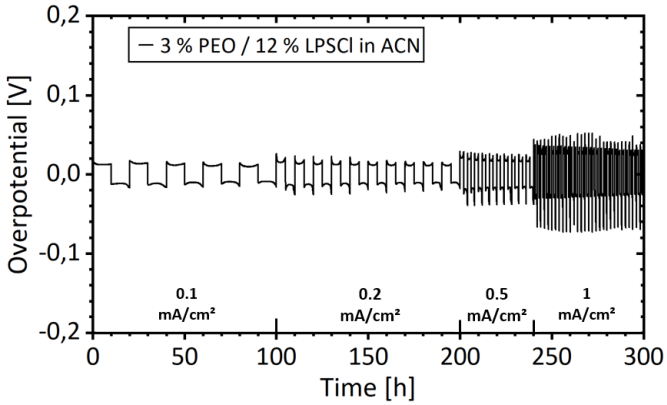


**Figure 25: Overpotential profile of a symmetrical cell using electrodes spin coated with 5 droplets PEO 3:12 in ACN. Measurement was performed at *T* = 25 °C. The small voltage peaks at the end of the higher current density cycles can also originate from measurement artifacts due to quick change of polarity.**

PEO also showed good solubility in DMF; however, the solution became very viscous after the addition of LPSCl in the 1.5:10 composition, while a reduced mass fraction of 1:7 resulted in a very thin solution. Both coatings did not improve the electrochemical properties, which was partly due to the difficulties in the spin coating process caused by their viscosities and also the known issue of lithium degradation in contact with DMF.

For PVDF, suitable solvents were also searched for (THF, 2-methyl-2-butanol, propylene carbonate, DMF, DMSO), of which only DMF and DMSO were able to dissolve PVDF (regardless of chain length). However, once the argyrodite was added to the polymer solution, the suspension began to discolor, eventually resulting in a purple to black viscous reaction product that was unsuitable for coating. Even a strong dilution of this product did not yield usable solutions. The same phenomenon was observed with poly(vinylidene fluoride-co-hexafluoropropylene) (PVDF-HFP) instead of PVDF. However, unlike PVDF, PVDF-HFP (for the chemical structure, see fig. 29) could be successfully dissolved in ethyl acetate, THF, and ACN. Hybrid coatings with PVDF-HFP and LPSCl in THF were performed using the compositions 3:12, 1.5:13.5, and 1.5:10, with the 3:12 composition resulting in multiple voltage peaks (see fig. A8). With the lower polymer fraction in the 1.5:13.5 coating, cycling durations of approximately 250 hours were achieved before voltage spikes occurred (fig. 26, A9). The 1.5:10 coating could not reach this value, with cycling durations of 220 to 240 hours (figs. 27 and 28).

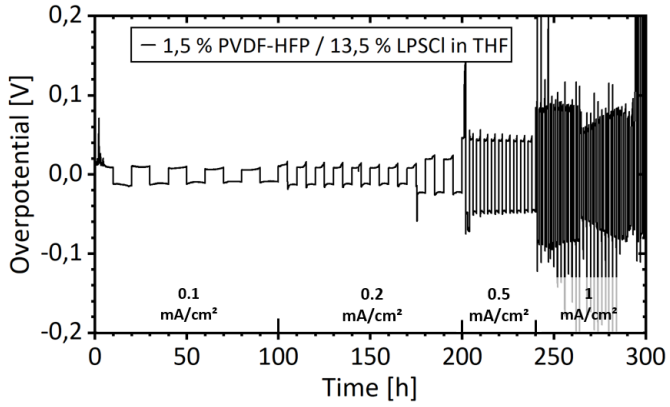


**Figure 26: Overpotential profile of a symmetrical cell using electrodes spin coated with PVDF-HFP 1.5:13.5 in THF. Measurement was performed at *T* = 25 °C. Note the sudden rise of overpotential at ca. 180 hours.**

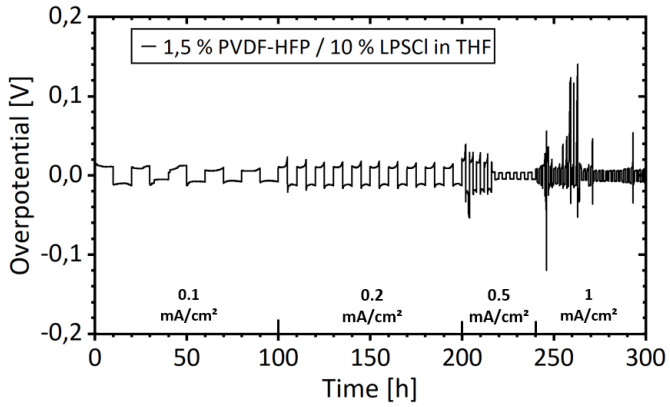


**Figure 27: Overpotential profile of a symmetrical cell using electrodes spin coated with 2 x 5 droplets PVDF-HFP 1.5:10 in THF showing a short circuit after roughly 220 hours. Measurement was performed at *T* = 25 °C.**

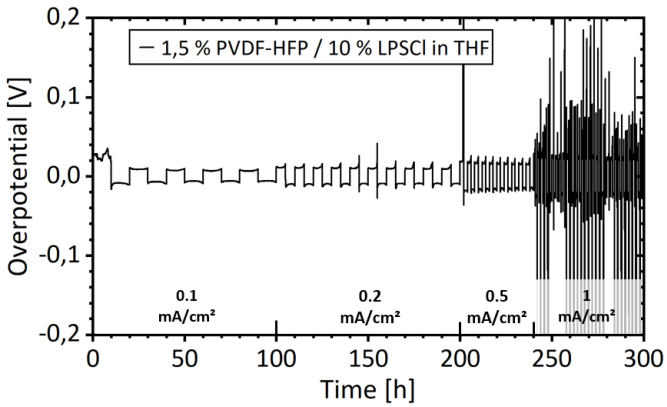


**Figure 28: Overpotential profile of a symmetrical cell using electrodes spin coated with 2 x 5 droplets PVDF-HFP 1.5:10 in THF displaying longer cycling stability than the cell shown before, however, not ending in a short circuit but in high overpotential peaks. Measurement was performed at *T* = 25 °C.**

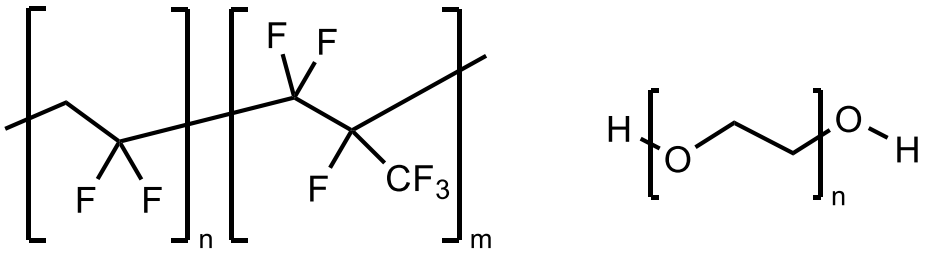

**Figure 29: Chemical structures of poly(vinylidene fluoride-co-hexafluoropropylene) (PVDF-HFP, left) and polyethylene oxide (PEO, right).**

A solution or dispersion of 3 % PVDF-HFP and 12 % LPSCl in acetonitrile exhibited a slight grayish discoloration but displayed a high degree of homogeneity, resulting in excellent spin coating performance. However, as depicted in figure 30, the electrochemical results were not convincing due to high voltage spikes and low lifetimes. Similar to the attempts to dissolve PVDF by adding TNNT to ethyl acetate, a coating solution was prepared using PVDF-HFP and EtOAc + TNNT as solvents to investigate if a slow discoloration or degradation would occur with the addition of LPSCl. Since discoloration occurred here as well, albeit slowly, the coatings were performed as quickly as possible. However, the voltage profiles of the symmetric conversion experiments (fig. 31) frequently exhibited voltage drops, indicating the possible formation of dendrites. Hybrid 12:3 protective layers using PVDF-HFP and pure ethyl acetate as a solvent showed some high cycle stability (fig. 32), although reproducibility was not always achieved.

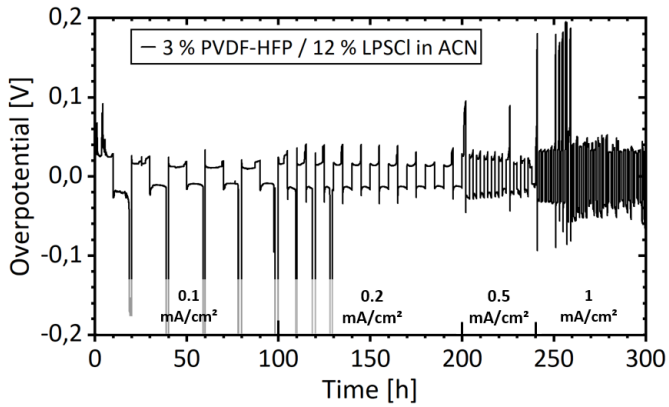


**Figure 30: Overpotential profile of a symmetrical cell using electrodes spin coated with PVDF-HFP 3:12 in acetonitrile. Measurement was performed at *T* = 25 °C.**

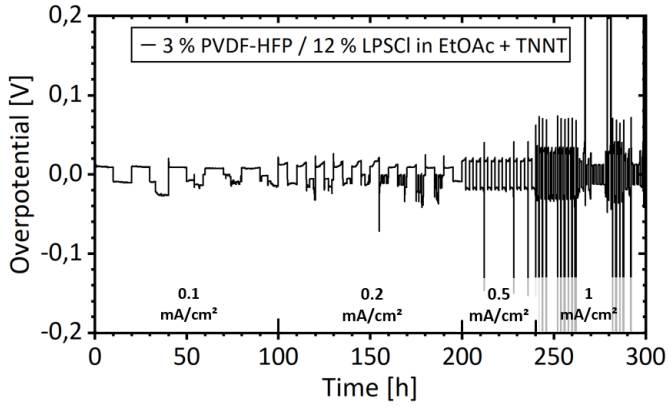


**Figure 31: Overpotential profile of a symmetrical cell using electrodes spin coated with PVDF-HFP 3:12 in ethyl acetate and TNNT. Measurement was performed at *T* = 25 °C.**

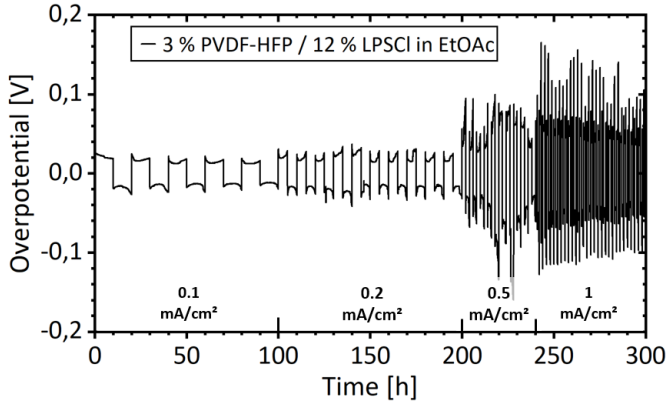


**Figure 32: Overpotential profile of a symmetrical cell using electrodes spin coated with PVDF-HFP 3:12 in ethyl acetate. Measurement was performed at *T* = 25 °C.**

Since the coating dispersion used in these experiments was very homogeneous, and the spin coating process proceeded smoothly, further cell tests were conducted using symmetric cells with electrolyte composition different from the previously used cells. Specifically, additional cell tests were conducted using DOL/DME/LiTFSI liquid electrolyte without the addition of lithium nitrate.

Interestingly, these cells exhibited nearly identical voltage profiles, which can be seen in figures 33 and 34, and long cycle stability of 270-300 hours.

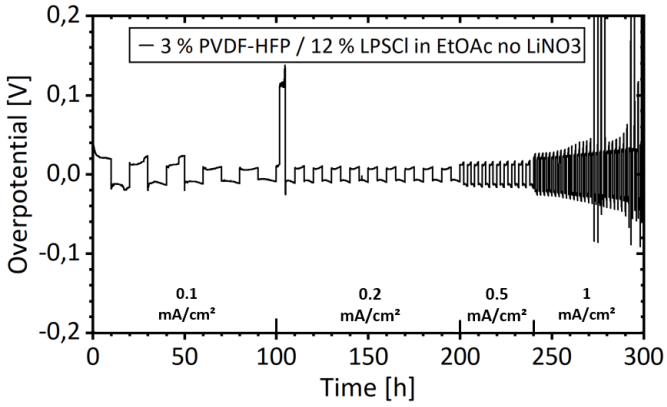


**Figure 33: Overpotential profile of a symmetrical cell using electrodes spin coated with PVDF-HFP 3:12 in ethyl acetate. Measurement was performed at *T* = 25 °C. The liquid electrolyte did not comprise lithium nitrate as additive.**

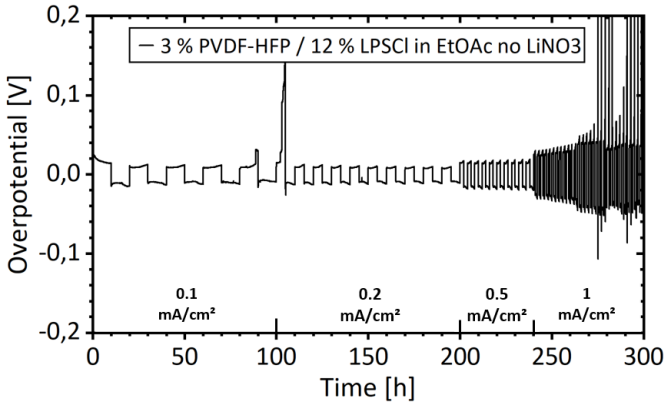


**Figure 34: Overpotential profile of a symmetrical cell using electrodes spin coated with PVDF-HFP 3:12 in ethyl acetate. Measurement was performed at *T* = 25 °C. The liquid electrolyte did not comprise lithium nitrate as additive.**

Due to the strong degradation of (per)fluorinated polymers PVDF and PVDF-HFP dissolved in DMF with LPSCl, a stability test was subsequently conducted by adding LPSCl powder to various solvents and observing any color changes in the solvent or argyrodite over several days. Interestingly, the only solvent that showed a significant reaction with LPSCl was DMSO as depicted in figure 35, which rapidly changed color, initially turning green and then dark brown. All other solvents (including DMF) did not exhibit significant discoloration, indicating that the decomposition reactions mentioned above only occur in the presence of dissolved fluoropolymers in DMF.


**Figure 35: LPSCl powder submerged in ethyl acetate, DMF, DMSO, propylene carbonate, 2-methyl-2-butanol, DOL, and DME (from left to right). While contact to DMSO instantly led to discoloration, all the other combinations did not change their optical appearance over several days.**

For the clarification of the degradation phenomenon, see figure 36: LPSCl as well as PVDF alone in DMF provide no color change. For reference, it is shown that PEO and LPSCl together in DMF change color indicating a degradation reaction. Only the PVDF (PVDF-HFP, too) and LPSCl in DMF will show this kind of reactivity resulting in a thick slurry. The reason for the degradation reaction possibly lies in the Lewis base character of DMF and the fact that PVDF will eliminate HF in presence of a base. However, in the tested system, this reaction seems to be alleviated or catalyzed by the presence of the LPSCl solid electrolyte.[230–232]


**Figure 36: Left: suspension of LPSCl in DMF, no discoloration. Center-left: solution of PVDF in DMF, no discoloration. Center right: dispersion of LPSCl in a solution of PEO in DMF (for reference), no discoloration. Right: dispersion of LPSCl in a solution of PVDF in DMF, discoloration and formation of a thick slime.**

Lastly, compatibility of $Li_6PS_5Cl$ with liquid electrolytes was investigated. Equivalent to the solvents, a small amount of solid electrolyte was submerged in the liquid electrolyte and stored for several days to see if a discoloration takes place. The liquid electrolytes used this survey were DOL/DME/LiTFSI with and without $LiNO_3$ and EC/DMC/$LiPF_6$. As depicted in figure A10, the samples in EC/DMC/$LiPF_6$ and DOL/DME/LiTFSI with $LiNO_3$ show no discoloration while the sample in DOL/DME/LiTFSI without $LiNO_3$ shows a slight yellow discoloration. Said discoloration possibly does not come from incompatibility between the liquid and solid electrolytes but from residual water content in the liquid electrolyte since LiTFSI salt is highly hygroscopic. This conclusion is supported by the observation that the LPSCl also turned yellow in an older sample of DOL/DME/LiTFSI with $LiNO_3$ that had higher $H_2O$ content than the freshly prepared one used in figure A10.

In summary, this part of the doctoral project started out as a trial to develop hybrid LPSCl/PVDF coatings for lithium metal anodes but it turned out quickly that the use of PVDF led to the dilemma of either being insoluble in the solvents or decomposing when dissolved. Table 2 shows an overview of all examined polymer-solvent combinations for LPSCl hybrid coatings. Using PVDF-HFP as binder material allowed successful coatings with acetonitrile, ethyl acetate and THF as solvents of which THF and ethyl acetate gave promising results in the cycling experiments.

**Table 2: Overview of the polymer/solvent combinations tested for suitability with $Li_6PS_5Cl$ powder for hybrid anode coatings.**

| | PVDF 534k Powder | PVDF 180k Beads | PVDF-HFP | PEO |
|---|---|---|---|---|
| **ACN** | | | Polymer dissolves<br>Cycling experiments | Polymer dissolves<br>Cycling experiments |
| **EtOAc** | Polymer does not dissolve<br>Cycling experiments | Polymer does not dissolve | Polymer dissolves<br>Cycling experiments | Polymer dissolves<br>Cycling experiments |
| **THF** | | Polymer does not dissolve | Polymer dissolves<br>Cycling experiments | Polymer dissolves<br>Cycling experiments |
| **EtOAc + ACN** | | | | Polymer dissolves<br>Cycling experiments |
| **DMF** | | Polymer dissolves, degradation<br>Coating not possible | Polymer dissolves, degradation<br>Coating not possible | Polymer dissolves<br>Cycling experiments |
| **EtOAc + TNNT** | Polymer dissolves, degradation<br>Cycling experiments | | Polymer dissolves, degradation<br>Cycling experiments | |

Polyethylene oxide (PEO) showed the highest versatility and made coatings with every of the selected solvents possible. Here, acetonitrile, ethyl acetate and THF as well showed promising improvements towards low overpotential and long cycling stability of the symmetric cells. Despite showing excellent solvation of PEO, DMF was not convincing as solvent because it does not seem

stable in contact with the lithium electrode. Further homogenization of the coating dispersions in an ultrasonic bath could further improve some of the coatings but not all of them.

## 4.2 Developing Phosphorus-, Nitrogen- and Chlorine containing protective Coatings for Lithium Metal Anodes

In the second part of this work, three different molecules are inspected for their suitability as reagents for the formation of an artificial SEI. Hexachlorophosphazene (NPCl), Tris(diethylamino)phosphine (TDP) and Dichloro(diethylamino)phosphine (DDP) all contain phosphorus and nitrogen while differing in the occurrence of chlorine resp. ethyl groups as can be seen in their structural formulae in figure 37. Assuming a chemical reaction between the used reagents and lithium metal resp. its natural passivation layer, the formation of phosphate- and nitrate-like species can be expected. Through complete reduction by the lithium metal, the phosphorus, nitrogen and chlorine originating from the coating agents may react to $Li_3P$, $Li_3N$ and LiCl, all of which have highly desired properties to be employed in an artificial SEI, such as high lithium ion conductivity[166,167], high lithium diffusivity[175], mechanical strength[169] and electrochemical stability against the low electrochemical potential of lithium. Especially the compound class of phosphazenes which are defined by a phosphorus/nitrogen backbone with alternating single and double bonds have already been having much attention by the battery research community on one hand for their use as electrolyte additives in order to reduce flammability and for SEI modification[179–183], on the other hand in form of polyphosphazenes as polymer electrolytes.[184,185] Direct lithium metal anode modifications have been done scarcely.[186]

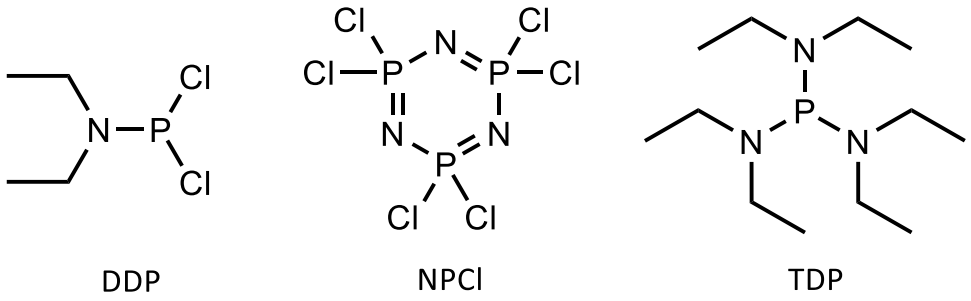


**Figure 37: Left to right: chemical structure of Dichloro(diethylamino)phosphine (DDP), Hexachlorophosphazene (NPCl) and Tris(diethylamino)phosphine (TDP).**

In figure 38, the plating/stripping overpotential of an untreated reference cell is depicted. The unstable appearance of the overpotential graph descriptively indicates unstable lithium dissolution and nucleation/deposition. At higher current densities beginning at 200 h (0.5 – 1 mA/cm²), the overpotential quickly rises and the cell quickly reaches the cut off potential of 5 V (out of scale) indicating cell failure. Figure 39 shows the cycling profile of a cell using electrodes that were treated

with 16.7 % DDP in heptane. In the first cycles, the lithium transport seems to be much more stable than in the pristine cell, however, after ca. 130 h a short circuit appears which was possibly caused by a dendrite that grew through the separator.

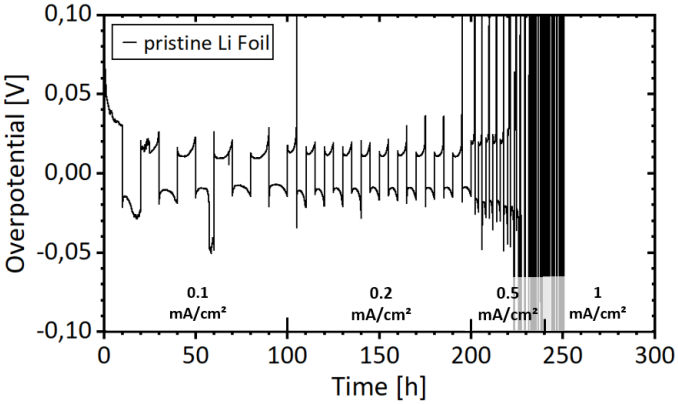


**Figure 38: Overpotential of a symmetric cell using two pristine Li metal electrodes. Measurement was performed at *T* = 25 °C. The occasional voltage spikes indicate a non-uniform lithium deposition/dissolution.**

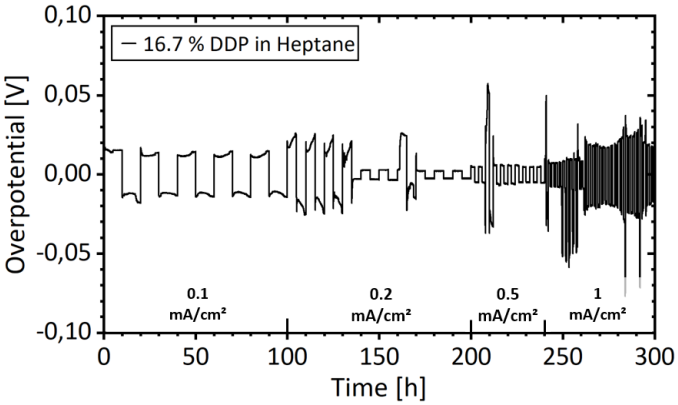


**Figure 39: Overpotential of a symmetric cell using two Li metal electodes after dip coating in 16.7 % DDP in heptane. Measurement was performed at *T* = 25 °C. After ca. 130 h the voltage suddenly drops which indicates a short circuit caused by a dendrite. The dendrite can loose contact from time to time which causes the sporadic voltage spikes.**

The dip coating of the electrodes with 16.7 % NPCl in heptane leads to the lowest recorded plating/stripping overpotential reported in this study (9 mV at 0.1 mA/cm², 16 mV at 0.2 mA/cm², 35 mV at 0.5 mA/cm², 63 mV at 1.0 mA/cm²) as well as the longest life span as can be seen in figure 40. The cell cycles in a stable manner for 350 h.

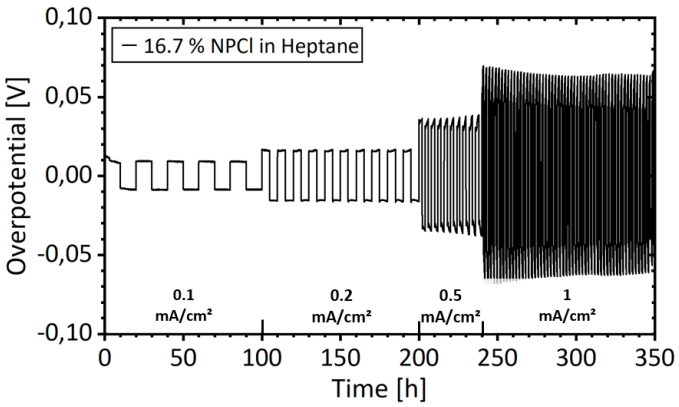


**Figure 40: Overpotential of a symmetric cell using two Li metal electodes after dip coating in 16.7 % NPCl in heptane. Measurement was performed at *T* = 25 °C. The cell shows stable plating/stripping over the course of 350 h or 80 cycles which is equivalent to 160 mAh/cm² of charge transport. The almost ohmic behaviour of the lithium transfer can be clearly seen, as the overvoltage increases with every increase in current density after 100 h, 200 h and 240 h, respectively.**

In the figures 41 and 42, the cycling profiles of symmetric cells that were built with TDP-coated Li electrodes. The cells differed in the used solvent for dip coating. While the coating in heptane led to comparably high and unstable overpotential, the use of THF resulted in much higher plating/stripping stability and lower overpotential. This shows that although THF is considered to have low reactivity with lithium[233], the solvent used for the surface coating plays a critical role just as the coating compound itself.

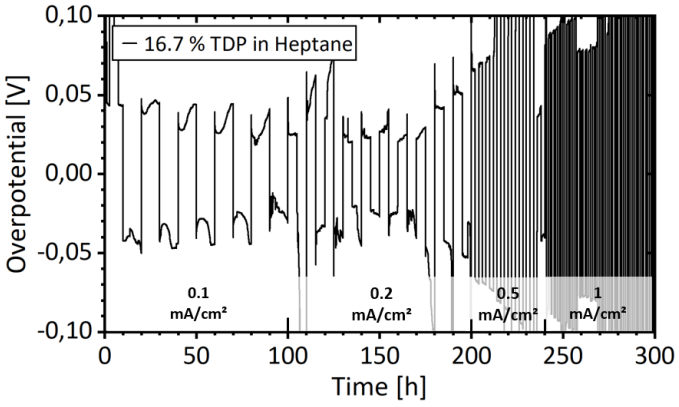


**Figure 41: Overpotential of a symmetric cell using two Li metal electodes after dip coating in 16.7 % TDP in heptane. Measurement was performed at *T* = 25 °C. The plating/stripping process shows high and unsteady overpotential indicating a highly resistive and uneven SEI.**

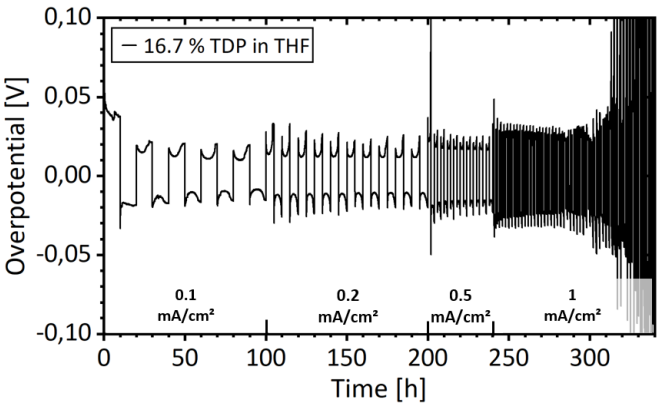


**Figure 42: Overpotential of a symmetric cell using two Li metal electodes after dip coating in 16.7 % TDP in THF. Measurement was performed at *T* = 25 °C. The cycling protocol runs stable for ca. 300 h. The wavy appearance of the overpotential graph is often seen in symmetric cells.[234] Rising overpotential after long cycling may indicate ongoing consumption of the electrolyte.**

Over the course of this study, much more cells than those exemplarily depicted in figures 38-42 were built and tested. Figure 43 gives an overview of all investigated types of dip coating regarding their cycling time and passed charge. This graphic presentation was chosen to emphasize the increase in the amount of charge that has passed over time due to the increasing current density. For example: after 240 hours, 50 mAh will be cycled back and forth, whereas after 300 hours it will already be more than double the amount (110 mAh). The outstanding performances of the 16.7 % NPCl in heptane (a) resp. 16.7 % TDP in THF (b) coatings are clearly visible. To emphasize the high reproducibility of the 16.7 % NPCl in heptane coatings, all 5 cells' cycling profiles are plotted together in the appendix figure A11. Furthermore, there are overpotential profile examples for every other coating depicted in figure 43 shown in A13-A17.

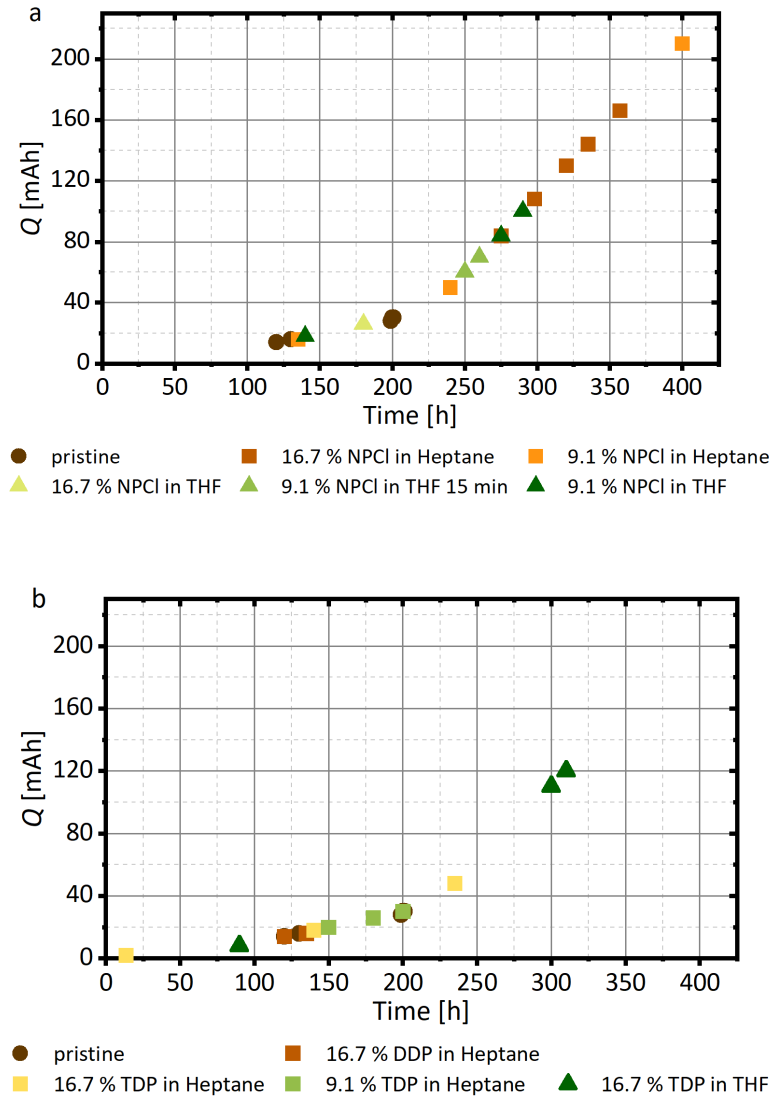


**Figure 43: Plots of the cycling time and charge flown of each cell built for this study. (a): Comparison of the NPCl coatings with the untreated cells. The high reproducibility of the 16.7 % NPCl in heptane coatings is particularly striking. (b): Comparison of the DDP and TDP coatings with the untreated cells. The coating with 16.7 % TDP in THF achieves comparable values to 16.7 % NPCl in heptane, but with lower reproducibility.**

With the aim of gaining knowledge about structure-property relationships on the tested lithium electrodes, the electrodes were examined in the SEM immediately after dip coating for each reagent used and compared with an untreated sample. The untreated lithium surface (fig. 44 a) shows a repetitive granular morphology with a size of the surface structures in the range of ca. 200 nm. In figure 44 b, the Li surface after treatment with 16.7 % DDP in heptane can be seen. The surface structure is strongly altered by the dip coating indicating a thick reaction layer with lager granular deposits and cracks on the surface. This thick and brittle surface might already be an explanation for the poor electrochemical performance of the cells built with these electrodes. The dip coating with 16.7 % NPCl in heptane (fig. 44 c), on the other hand, shows a very similar surface structure to the pristine sample meaning that the coating itself is thin and homogenous which is favorable for

fast and homogenous lithium transport. The coating with 16.7 % TDP in THF strongly altered surface morphology (fig. 44 d), but as the EDX observations show, there is almost no evidence of N or P signals and a surface reaction/phosphorus incorporation only occurred spot wise (see A18 and A19).

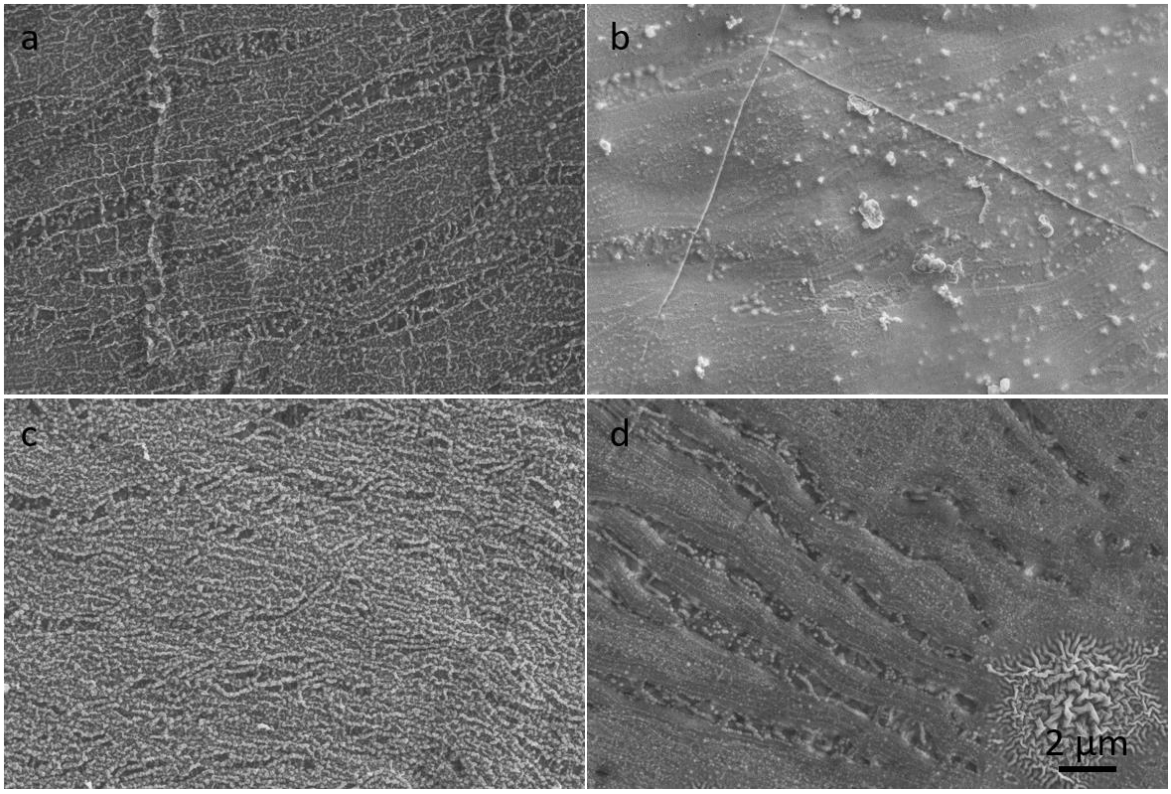


**Figure 44: SEM observations of Li electrodes before cycling under 15000x magnification: a) pristine Li foil. b) Li foil treated with 16.7 % DDP in heptane. c) Li foil treated with 16.7 % NPCl in heptane. d) Li foil treated with 16.7 % TDP in THF. The unusual structure on the bottom right was determined by EDX to be residual TDP from the coating process.**

*Post mortem* SEM observations of the electrodes were conducted on pristine cells and samples of the 2 best running coatings (16.7 % NPCl in heptane, 16.7 % TDP in THF). Figures 45 a) and b) display the *post mortem* surface of an untreated Li electrode after a short cycling protocol. The surface is full of craters and mossy/dendritic lithium while large areas seem to have not been affected by the plating/stripping at all. Similar to the pristine sample, the 16.7 % TDP in THF coating does not lead to a full surface utilization, as shown in figure 45 c) and d). The electrochemically active spots, however, show a completely different morphology, as the lithium deposits in form of roughly 5 µm sized beads. Figures 45 e) and f) show the electrode surface with 16.7 % NPCl in heptane coating after short cycling. The electrode surface shows a very large surface and, in contrast to the other *post mortem* samples, the complete electrode surface appears to contribute to the electrochemical reactions. The voltage profiles of the short cycling protocols for the NPCl/heptane and TDP/THF SEM samples can be seen in figure A20 and A21, respectively.

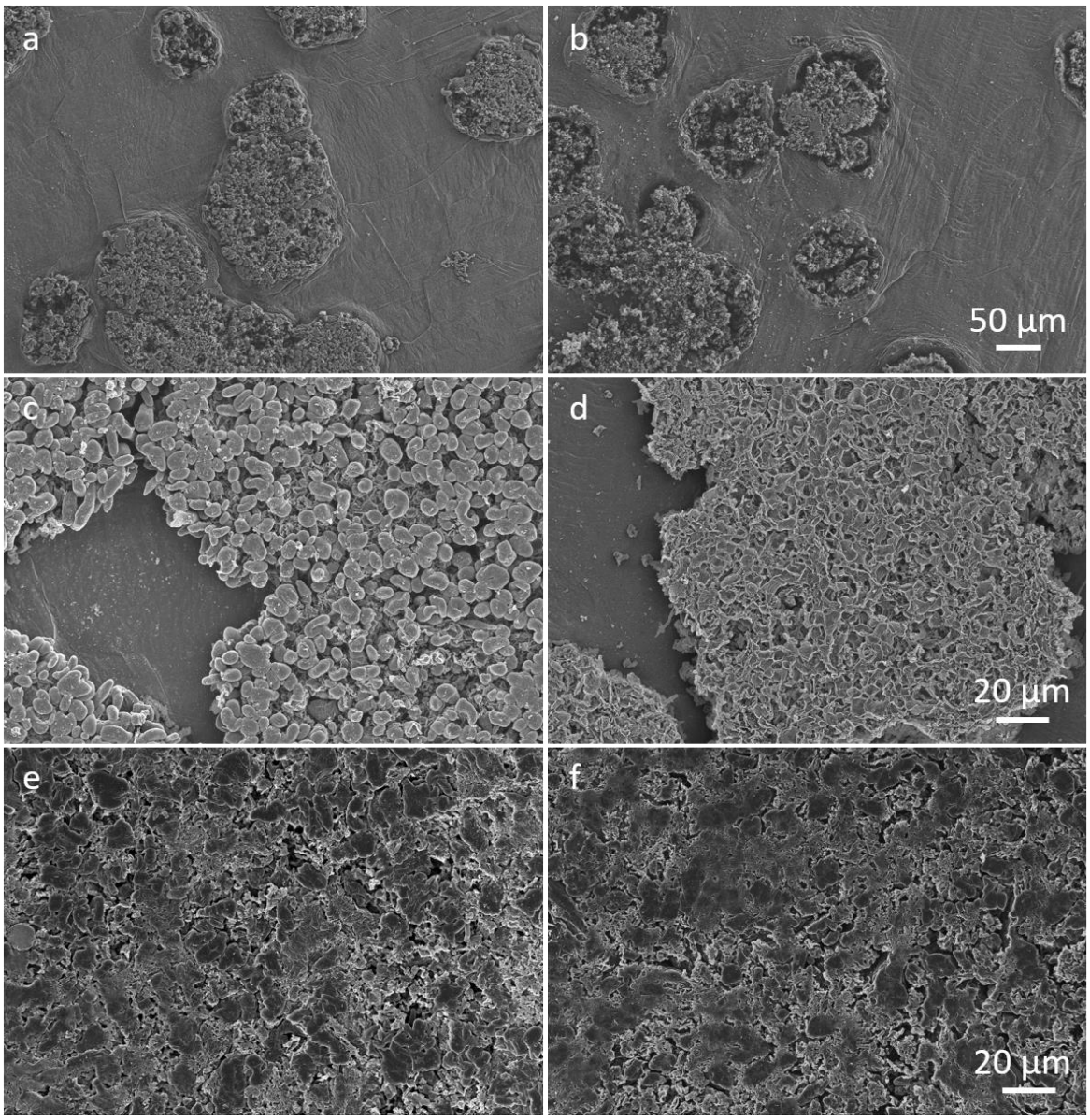


**Figure 45: Post mortem SEM observations of: a, b) unmodified Li electrode after short cycling under 500x magnification c, d) 16.7 % TDP in THF treated Li electrode after short cycling under 1500x magnification. e, f) 16.7 % NPCl in heptane treated Li electrode after short cycling under 1500x magnification. The pictures on the left are taken from the electrode that has been plated in the last step while the pictures on the right are taken from the electrode that has been stripped in the last step.**

Figure 46 shows post mortem SEM pictures of electrodes after long cycling. The TDP/THF treated electrode (fig. 46 a) comprises a much more uniform and denser surface leading to the conclusion that the surface utilization is significantly enhanced. Similarly, the surface of the NPCl/heptane treated electrode (fig. 46 b) is much more uniform after long cycling leading to the conclusion, that the high surface area lithium that emerges in the beginning grows together forming a denser surface over time.

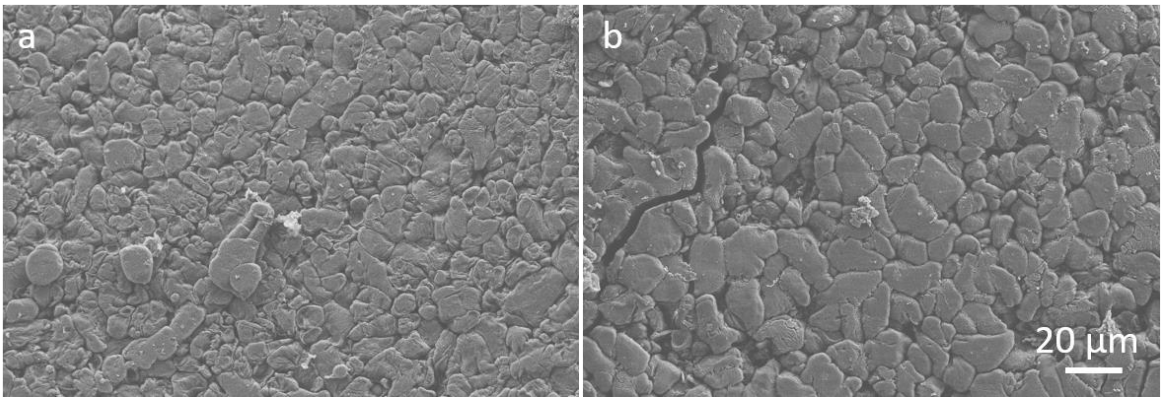


**Figure 46: a) Post mortem observation of a 16.7 % TDP in THF treated Li electrode after standard (long) cycling under 1500x magnification. b) Post mortem observation of a 16.7 % NPCl in heptane treated Li electrode after standard (long) cycling under 1500x magnification.**

Besides the EDX measurements, elemental quantification was carried out by analysis of XPS survey spectra. Figure 47 depicts the element concentration depth profiles of 5 different lithium electrodes after dip coating. All measured samples are qualitatively similar concerning the progression of the lithium, carbon and oxygen content as the Li and C signals are rising resp. dropping in accordance with untreated lithium foils (cf. table 4) whilst the oxygen content is rising contrarily after the first two sputter steps. Therefore, these 3 elements already show that the surface chemistry of the lithium foils has been altered as oxygen usually shows the highest surface concentration on pristine lithium.[19] Here, through the use of organic solvent-based coating liquids, carbon is the most present surface element. Focusing on the elements that were supposed to be incorporated into the SEI by the coating it stands out that the highest nitrogen and phosphorus contents come from the coatings using DDP in heptane resp. NPCl in THF. Especially for phosphorus, the other coatings practically do not lead to enhanced P content as the atomic concentration values are within the error range of the XPS quantification. Since TDP does not contain chlorine, the TDP coatings are not considered in the Cl quantification. It shows that the highest chlorine contents originate from the NPCl containing coatings.

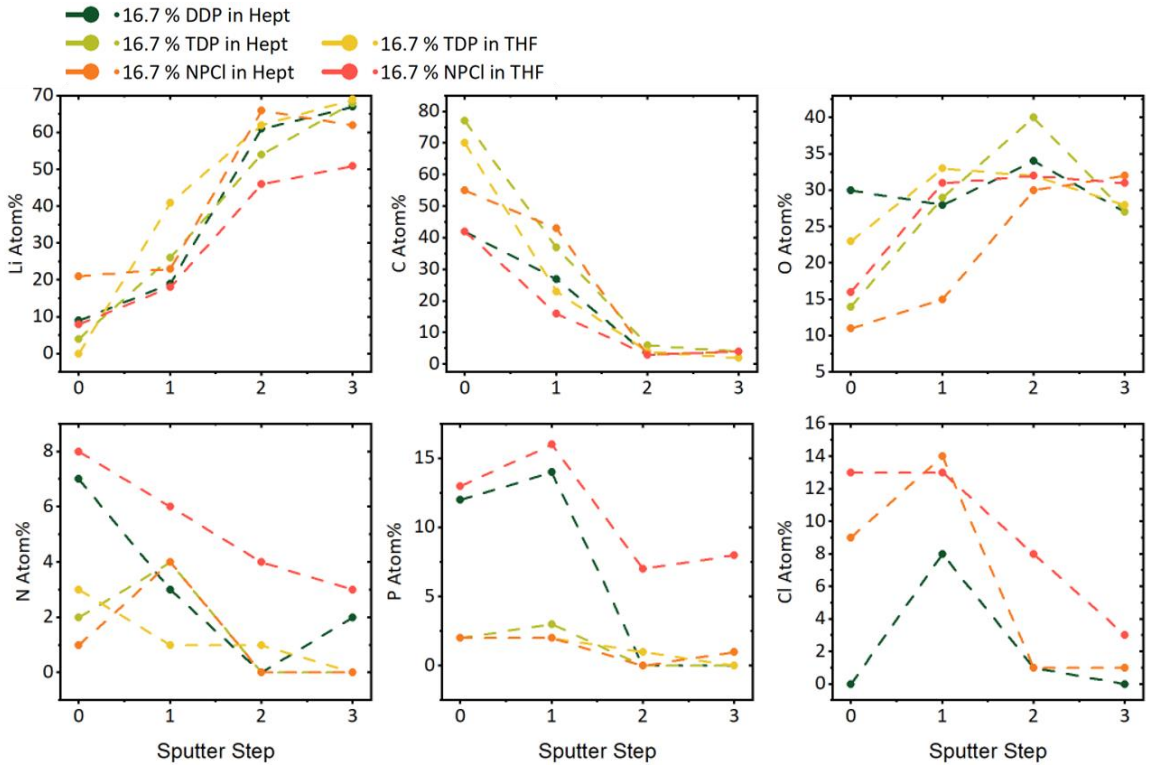


**Figure 47: Elemental distribution according to XPS measurements. Sputter step "0" depicts the measurements on the sample surfaces. As material is removed by the sputtering process, the subsequent measurements after the respective sputter steps match up to depth profiles of the sampled regions.**

Taking into account the electrochemical performance, the morphological changes observed by eye and SEM, and the XPS results, it is thus possible to draw some conclusions about the coatings and possibly also the choice of coating reagents. For example, the DDP/heptane as well as the NPCl/THF coating solutions show high reactivity resulting in strong surface changes up to the point of complete electrode degradation which also reflects in the poor electrochemical performance. The XPS analysis of these samples show, however, high concentrations of nitrogen and phosphorus (and chlorine), the elements that were initially anticipated to lead to better electrochemical performance. These findings will be analyzed precisely in the following.

Based on the broad analyses carried out on the lithium electrodes coated in this section, several insights were gained that can be applied to these coatings and also to the surface treatment of lithium electrodes in general. The reactivity of the reagents plays an important role, as the study shows. The observed different reactivities of the chemicals used is ultimately not surprising, as this can already be estimated from the molecular structure. DDP is the most reactive species of the compounds investigated, which is already noticeable in the fact that the substance has to be stored under refrigeration. It follows that using heptane as solvent, the molecule readily reacts with the lithium metal to form a thick ASEI, which also contains the desired elements (N, P, Cl), but the surface reaction is not self-limited, so the reaction proceeds too far and even impedes the performance of the electrode. With THF as solvent for DDP, no dip coating was possible, as the

lithium completely dissolved resp. decomposed after a short time. If further investigation of this compound as a coating reagent is considered, a lower concentration than the 16.7 % used here in both solvents should be selected in any case. The solution of NPCl in heptane leads to an ASEI in contact with lithium, which consists largely of LiCl. This behavior is also easy to understand, as NPCl is used in many reactions as a starting compound to replace the chlorine atoms with other substituents and thus produce the monomeric basis for polymer compounds such as MEEEP (poly[bis 2-(2-(2-methoxyethoxy)ethoxy)ethoxyphosphazene])[235].

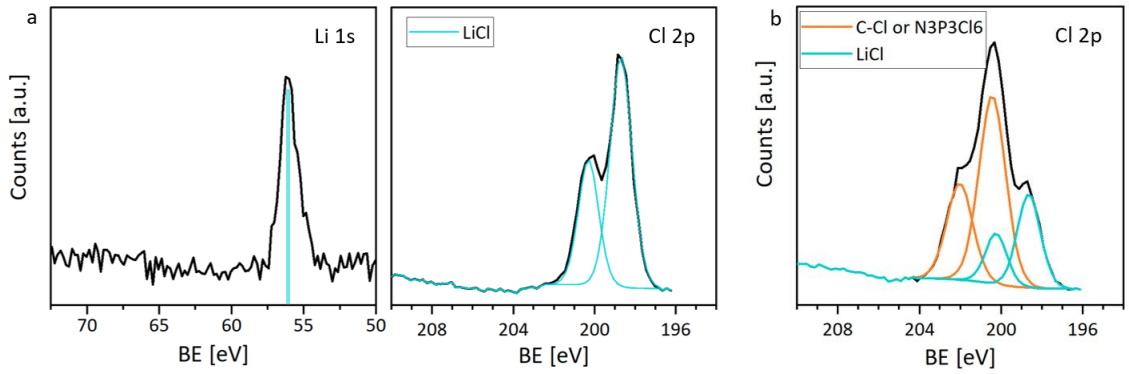


**Figure 48: a) Li 1s and Cl 2p detail spectra of a NPCl/heptane treated lithium surface. b) Cl 2p detail spectrum of a NPCl/THF treated lithium surface.**

In the coating process using heptane as solvent, it is almost exclusively the chlorine that reacts, while the phosphazene six-membered ring stabilized by aromaticity does not react further with the lithium. Figure 48 a shows the XPS detail spectra of lithium resp. chlorine measured on the sample surface. Both signals clearly indicate the presence of lithium chloride as both signals show the respective binding energies of 56 eV (Li 1s) and 198.6 eV (Cl $2p_{3/2}$)[236]. As there are no other strong lithium signals, this means that the vast majority of the surface lithium is in the form of LiCl. When THF is used as a solvent, the results of the analytics are significantly altered as can be seen in figure 48 b; the LiCl signal is strongly superimposed by a signal coming from a higher binding energy of roughly 200 eV for the Cl $2p_{2/3}$ peak. This peak can be attributed to covalently bound chlorine meaning that the signal either comes from residual NPCl that was incorporated into the ASEI or it has formed C-Cl bonds[237,238], possibly through reaction with THF polymerization products. Moreover, significant amounts of phosphorus and nitrogen can also be found on the electrode surfaces. Therefore, reactivity has also increased here with the use of THF towards a thicker ASEI similar to the 20% DDP in heptane coating. For this reason, further experiments were conducted for NPCl in THF with a lower concentration of NPCl (9.1 % instead of 16.7 %, dip coating for 30 minutes or 15 minutes). However, none of the NPCl/THF coatings could achieve as high cycle stability and reproducibility as 16.7 % NPCl in heptane.

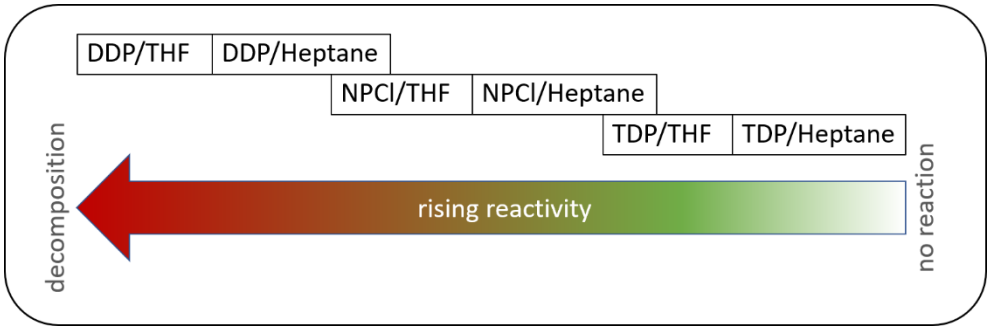


**Figure 49: Scheme of the reactivities for the investigated reagent/solvent combinations. Green color indicates the best level of reactivity regarding significant but non-destructive modification of the electrode surfaces.**

Furthermore, the low reactivity of the TDP can likewise be explained on the basis of the structural formula, since the phosphorus as well as the nitrogen atoms are sterically shielded by the ethyl groups, so that the reaction of the heteroatoms with e.g. lithium is impeded. Although there is hardly any difference between the TDP/heptane and TDP/THF treated samples in the XPS tests, it can be assumed that the reactivity of the coating solution was again increased by THF as a solvent, as the electrochemical properties were greatly improved as a result. The fact that the performance of the cells with 9.1 % and 16.7 % TDP in heptane does not differ greatly also suggests that the solutions do not significantly change the electrode either way. As the previous conclusions already suggest, in addition to the selection of reagents, the choice of solvent is of crucial importance for a successful coating of lithium metal anodes. In the present case, it was found that THF increases the reactivity of the coating solutions compared to heptane, allowing desired surface modifications to be achieved by tuning the coating solution's composition. As figure 49 suggests, the "sweet spot" for combinations of reagent and solvent concerning improvements in the electrochemical properties of the electrodes is found in the combinations NPCl/heptane and TDP/THF. The reason behind the higher reactivity using THF lies possibly in its higher polarity as this would stabilize and facilitate ionic processes that occur during the (A)SEI formation reactions. However, as it was already assumed in the context of possibly arising C-Cl bonds, the XPS detail spectra of both the TDP/THF and the NPCl/THF coated specimens show characteristic C 1s and O 1s binding energy peaks for polymerized THF at ca. 285 eV and 286 eV (C 1s) respectively 532-533 eV (O 1s, see figs. A22 and A23).[239–241] Especially, the spectra show that nearly all of the oxygen on the TDP/THF sample surface comes from the poly-THF that has formed during dip coating. This means that the possible incorporation into the SEI respectively the hypothetical decomposition products of selected solvents for dip coating must always be considered. In the case of THF/poly-THF this phenomenon is not necessarily malicious as the oxygen atoms in the polyether chains are capable of coordinating $Li^+$ ions and therefore facilitate their conduction.[242] Finally, the post-mortem SEM studies help to gain further understanding of the results of the SEI modifications. Without dip coating, large parts of the electrode surface apparently do not participate in the electrochemical plating/stripping, which can be seen from the fact that the lithium is only deposited and dissolved in several spots (fig. 45).

The coatings with TDP/THF and in particular NPCl/heptane increased the electrochemically active portion of the electrode surfaces, with NPCl/heptane being particularly prominent, as this coating allowed the entire surface of the electrode to participate in the plating/stripping after only a short cyclisation (fig. 45). Since the resistance and thus the overvoltage of the cell depends reciprocally on the effective electrode surface, this also explains the reduced overvoltages using the modified electrodes in the symmetrical cells. In the NPCl/heptane-treated cells, the significant proportion of LiCl in the SEI is probably the reason for the homogeneous and covering distribution of the electrochemically active sites on the electrode due to its high $Li^+$ diffusion[23,84,193]. As well as for the straight-line (fig. 40), non-wavelike course of the overvoltage as seen e.g. in comparison to the TDP/THF cells (fig. 42), since a straight-line course is a sign of a low activation barrier for nucleation during electrochemical plating.[84,243,244]

## 4.3 Halide based SEI Modifications

As the results of section 4.2 showed that the best anode performance and stability was linked to high chlorine incorporation into the SEI, further efforts were conducted to investigate halide based LMA coatings. 3-(trifluoromethoxy)aniline (3TA), 4-(trifluoromethoxy)anisole (4TA) and 1,2-dibromotetrachloroethane (DBTC) (see figure 50 for the chemical structure) were chosen to create fluorine resp. bromine containing ASEIs. The anodes were dip-coated for 30 minutes in solutions ranging from 5% to 20% in heptane, followed by rinsing with heptane. The coated electrodes were subjected to electrochemical tests in symmetrical cells and analyzed by ToF-SIMS, SEM, and EDX techniques.

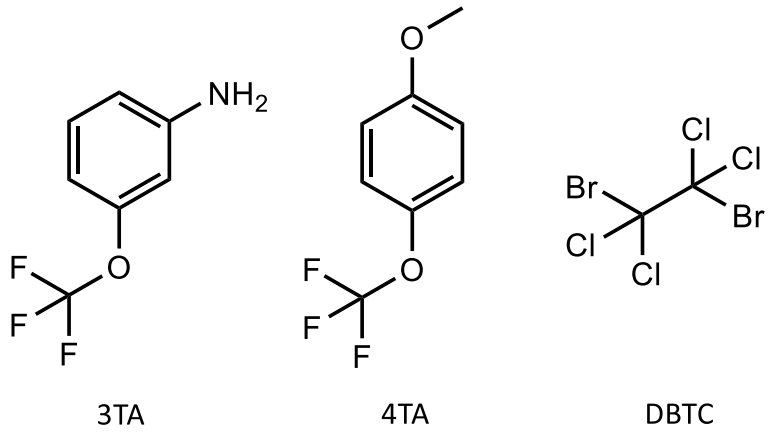


**Figure 50: Chemical structure of 3TA, 4TA and DBTC (left to right).**

The electrochemical tests of the modified lithium metal electrodes compared with untreated electrodes (cf. figs. 38 and 65 a) showed that the dip coating with 3TA leads to improved cycling behavior (lower plating and stripping overvoltage), while the 5 % solution (fig. 51) leads to a

stronger improvement than the 10 % 3TA solution in heptane (fig. 52). This shows, for example, in the lifespan of the cells, measured by the beginning of the sharp increase in the overvoltage; this begins at 240 hours with the 5 % coating and at around 200 hours with the 10 % coating.

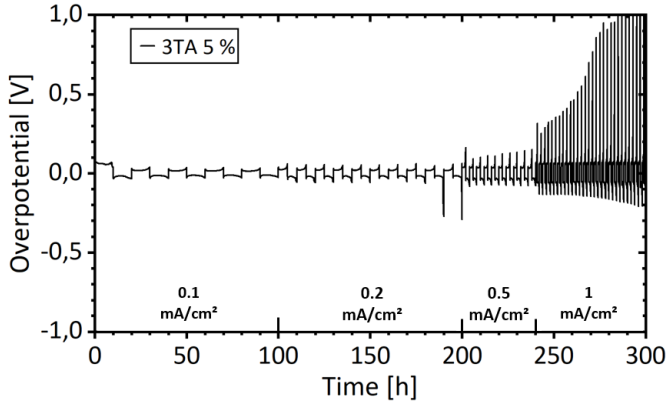


**Figure 51: Overpotential of a symmetric cell using two Li metal electodes after dip coating with 5 % 3TA in heptane. Measurement was performed at *T* = 25 °C.**

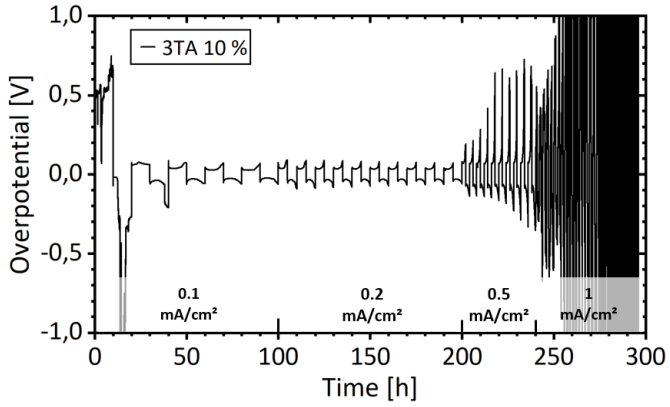


**Figure 52: Overpotential of a symmetric cell using two Li metal electodes after dip coating with 10 % 3TA in heptane. Measurement was performed at *T* = 25 °C.**

On the other hand, it was not possible to improve the electrochemical properties of the lithium electrodes with 4TA as a coating reagent, as shown in fig. 53 for the 10 % 4TA coating.

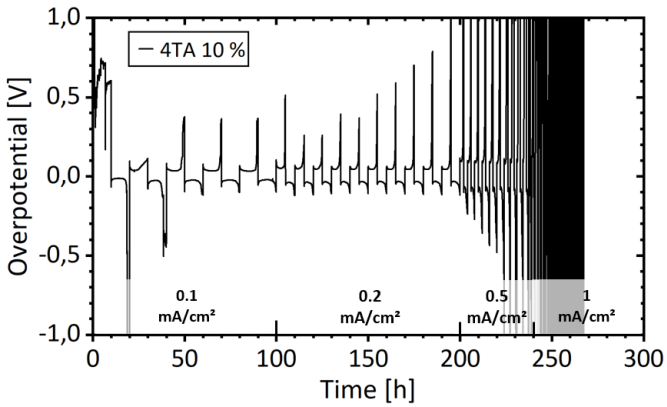


**Figure 53: Overpotential of a symmetric cell using two Li metal electodes after dip coating with 10 % 4TA in heptane. Measurement was performed at *T* = 25 °C.**

In contrast to the 3TA coatings, where the lower concentration led to better cycling results, the comparison of the coatings using 5 % DBTC (fig. 54) and 10 % DBTC (fig. 55) in heptane showed that the latter exhibited the lower overpotential (15 - 25 mV at 0.1 mA/cm²) and longer cell life (ca. 250 h).

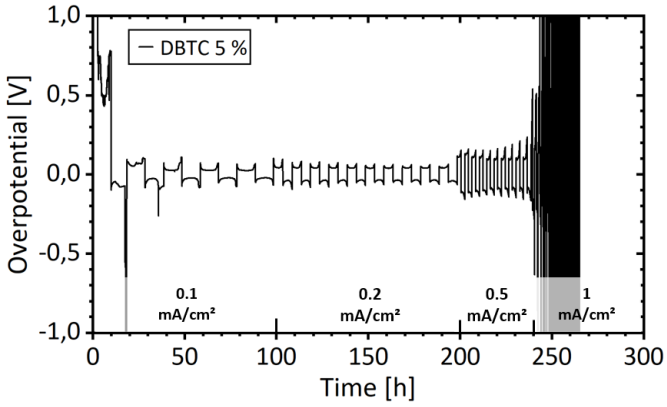


**Figure 54: Overpotential of a symmetric cell using two Li metal electodes after dip coating with 5 % DBTC in heptane. Measurement was performed at *T* = 25 °C.**

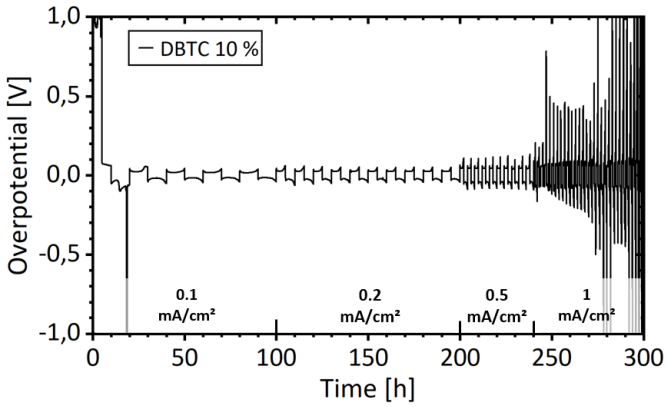


**Figure 55: Overpotential of a symmetric cell using two Li metal electodes after dip coating with 10 % DBTC in heptane. Measurement was performed at *T* = 25 °C.**

For this reason, a further series of tests with 20 % DBTC in heptane for dip coating was conducted; it turned out that this concentration was already close to the saturation limit. As depicted in figure 56, in the plating and stripping experiment, the electrodes immersed in 20 % DBTC in heptane showed the highest cycle stability (up to 300 h), the lowest overvoltage (10 - 15 mV at 0.1 mA/cm²) and the highest reproducibility of all tested 3TA, 4TA and DBTC coatings.

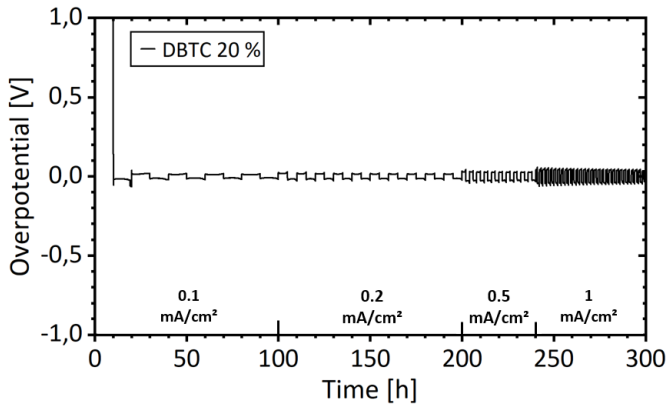


**Figure 56: Overpotential of a symmetric cell using two Li metal electodes after dip coating with 20 % DBTC in heptane. Measurement was performed at *T* = 25 °C.**

One common feature that most of the symmetrical cells in this series showed was the high overvoltage in the first cycle. The reason for this observation may be that the ASEI was not yet fully formed at the beginning of the cycling. In order to gain insights into the structure-property relationships of the modified lithium electrodes, the surfaces of the electrodes were examined under a scanning electron microscope (SEM) after dip coating. Figure 57 shows a comparison of the electrode surfaces at 10000x magnification. There appears to be an obvious similarity between the 10 % 3TA and 20 % DBTC coatings and between the 10 % 4TA and 10 % DBTC coatings, respectively. It is remarkable the apparent similarity of the first two coatings (fig. 57 a and d) with both the untreated lithium foil and the 20 % NPCl coating from the previous chapter (cf. fig. 44 a and c), especially as this thin and homogenous surface alternation is linked to the best cell performances of each sub-study.

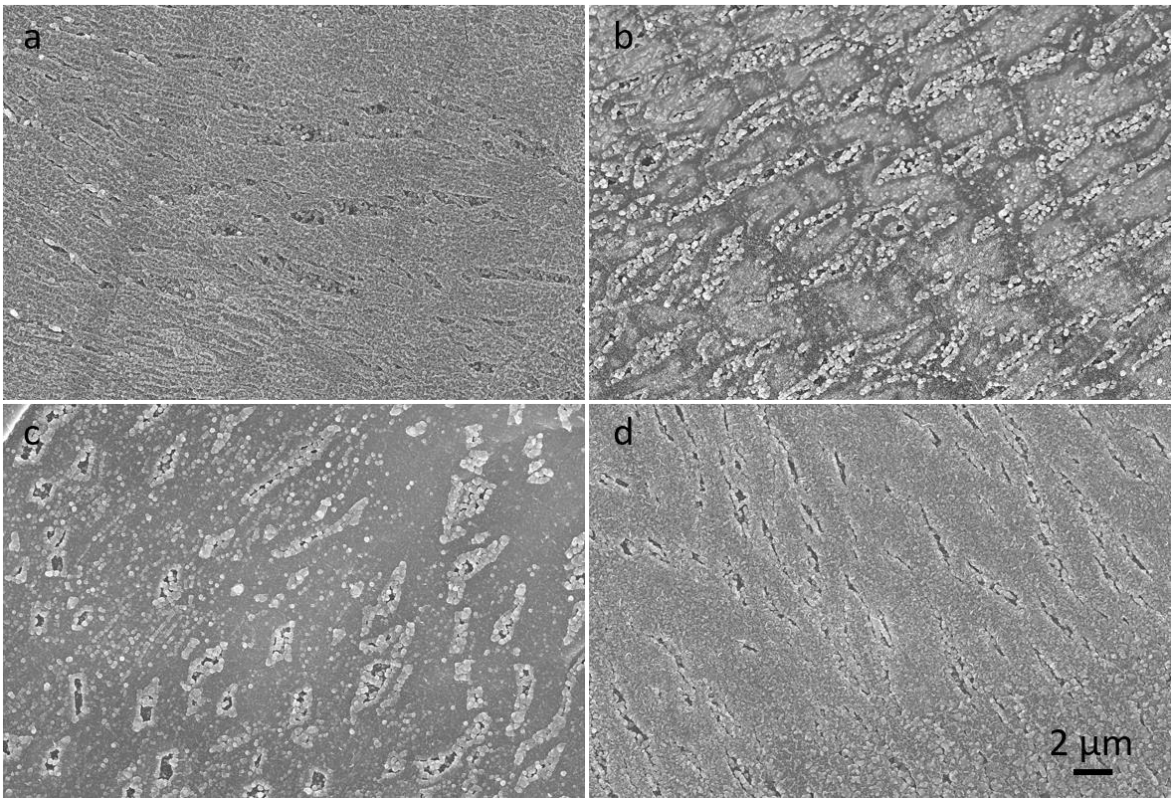


**Figure 57: Comparative SEM images of electrode surfaces after dip coating in 10 % 3TA (a), 10 % 4TA (b), 10 % DBTC (c) and 20 % DBTC (d) at 10000x magnification.**

Figure 58 shows a further magnification (25000x) of the electrode samples, allowing further details of the surface morphology to be identified. The surfaces of the 10 % 4TA and 10 % DBTC electrodes are quite inhomogeneous with larger structures, grains of ca. 200 nm size and also holes in the range of 1 µm. The coatings with 10 % 3TA and 20 % DBTC, on the other hand, resulted in more homogeneous surface morphologies with a finer surface structure with repeating patterns of < 100 nm in size. These coatings are not perfectly covering either, but the same structure can be seen underneath the gaps. Accordingly, the improved electrochemical performance of the latter two coatings can be explained, among other things, by the improved homogeneity of the surface.

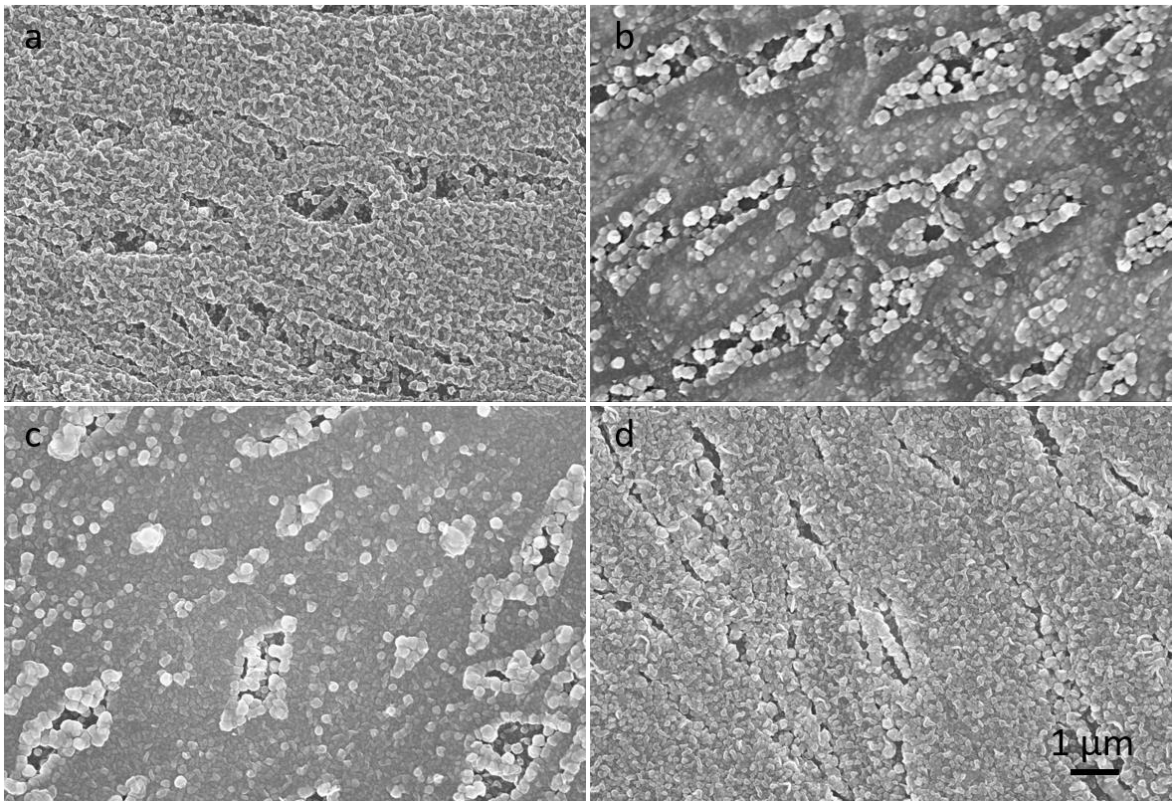


**Figure 58: Comparative SEM images of electrode surfaces after dip coating in 10 % 3TA (a), 10 % 4TA (b), 10 % DBTC (c) and 20 % DBTC (d) at 25000x magnification.**

The results of the ToF-SIMS and EDX analytics revealed that the 3TA 10 % coating forms a thin fluorine-containing surface layer, as can be seen by the strong and sharp $F^-$ signal peak in the SIMS depth profiles (fig. 59, left). Since the SIMS depth profiles or signal intensities do not represent a quantification of the elements or compounds, supplementary EDX investigations (fig. 59, right) were carried out which, in contrast to the SIMS spectra, only revealed a weak F signal. This allows the conclusion that the fluorine- or fluoride-containing layer is thinner than the information depth of the EDX signals. Another point of interest of the study was whether the amine group in the 3TA molecule also incorporates nitrogen into the resulting ASEI. Neither the ToF-SIMS nor the EDX could show any visible nitrogen signals, which means that 3TA is not suitable for producing a nitrogen-containing ASEI. Qualitatively speaking, the analyses of the 4TA coating (fig. 60) show great similarities to the previous coating. The SIMS depth profile also shows a sharp peak of the fluoride ion signal at the sample surface, but the fluorine related signals there and in the EDX are weaker compared to the signals of the natural passivation layer ($LiO_2H_2^-$ and $LiO^-$ resp. O and C), which suggests that the ASEI is also thin, but the composition has been less strongly affected by the coating.

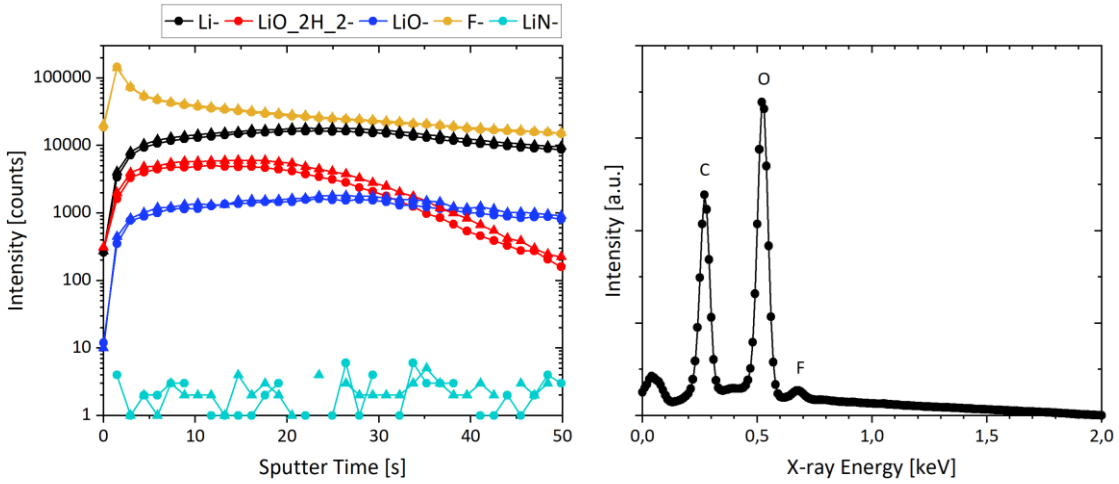


**Figure 59: ToF-SIMS depth profiles (left) and EDX spectrum (right) of a lithium electrode after dip coating in a 10 % 3TA solution.**

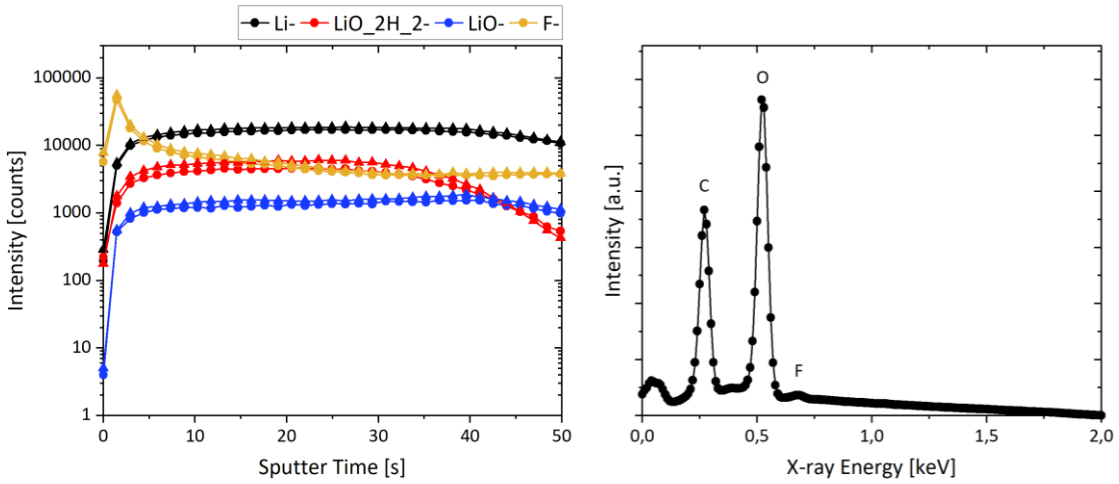


**Figure 60: ToF-SIMS depth profiles (left) and EDX spectrum (right) of a lithium electrode after dip coating in a 10 % 4TA solution.**

On the other hand, the DBTC 10 % coating only showed small changes in SIMS profiles compared to pristine Li-foil comprising slightly enhanced Br and Cl signals whilst these elements were almost not detectable by EDX (see fig. 61). It should be noted that in order to enable the detection of chlorine signals, the acceleration voltage of the electrons had to be increased from 2 kV to 4 kV compared to the 3TA and 4TA coatings, which, however, also increased the information depth of the EDX signals. In order to estimate the average X-ray emission depths, simulations were conducted using the software Casino v2.51. For samples with an input composition as indicated by the EDX spectra in figs. 59 and 60, in both cases the obtained average emission depth is 135 nm for 2 kV and 400 nm for 4 kV acceleration voltage. Furthermore, the higher acceleration voltage made the platinum coating of the samples visible as the Pt characteristic X-ray energy lies slightly above 2 kV. By specifying the material and the thickness of the coating in the evaluation program,

it can remove the platinum from the elemental quantification. The DBTC 20 % coating, of which the respective solution was close to saturation, exhibited a pronounced bromine-containing surface layer (fig 62, left). Although the coating molecule contains double the amount of chlorine compared to bromine, there is clearly lower chlorine incorporation, clearly indicating preferred bromination of the electrode surface.

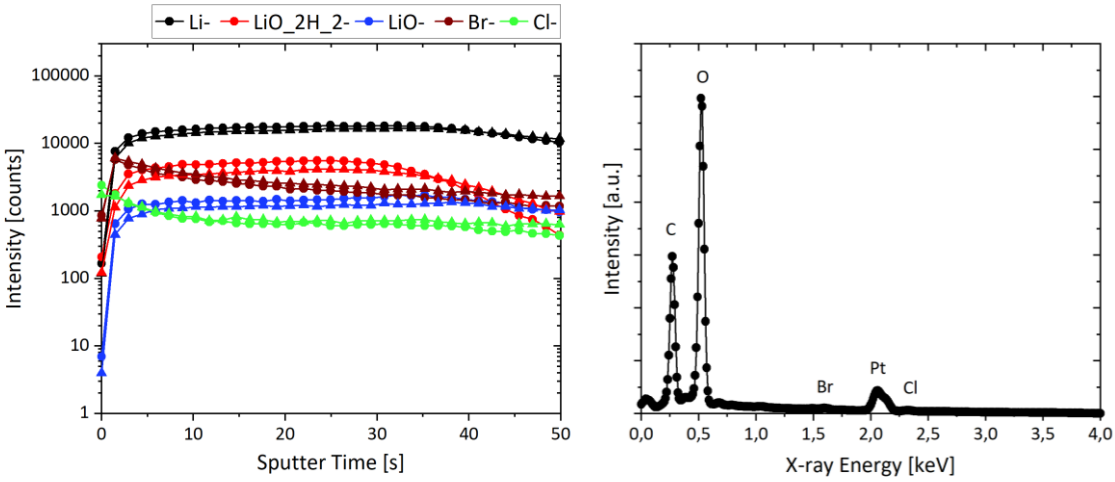


**Figure 61: ToF-SIMS depth profiles (left) and EDX spectrum (right) of a lithium electrode after dip coating in a 10 % DBTC solution.**

As depicted on the right of figure 62, these findings are confirmed by the EDX analysis that shows a distinct bromine (Br $L_\alpha$) signal at 1.5 eV. All the analyzed samples show very similar and parallelly progressing ToF-SIMS depth profiles meaning that the coatings are homogenous across the sample surface.

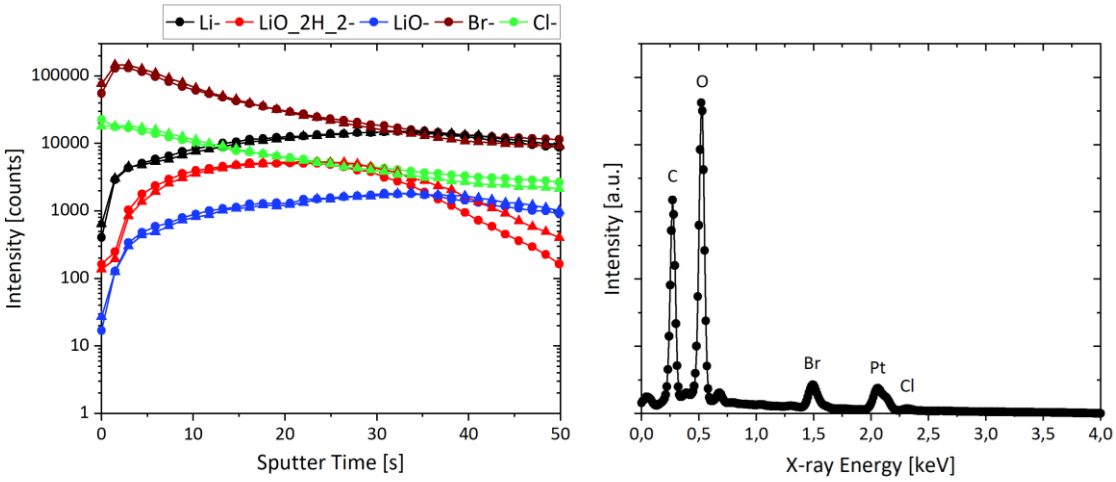


**Figure 62: ToF-SIMS depth profiles (left) and EDX spectrum (right) of a lithium electrode after dip coating in a 20 % DBTC solution.**

To quickly summarize, two fluorine-containing coating reagents and a chlorine- and bromine-containing substance were reviewed for coating lithium metal anodes. Comparing the two fluorine-containing coatings (3TA and 4TA), it was found that 3TA-coated electrodes performed better than

those coated with 4TA. The analysis by ToF-SIMS and EDX shows that in both methods the fluorine signals are more pronounced for the 3TA samples, which suggests that the higher fluorine content is linked to the improved electrochemistry. However, the SIMS profiles should not be interpreted quantitatively, as it is known from experience that fluorine and halogens are very easily ionized and therefore show a strong signal, while nitrogen, for example, is difficult to detect by ToF-SIMS. For this reason, it cannot be ruled out that nitrogen is present in the 3TA ASEI and may also have a positive influence. The DBTC coatings generally show a higher reproducibility than the fluorine-based coatings. The dip coating in the DBTC solutions mainly incorporated bromine into the surfaces of the electrodes, whereby it was also shown that with increased concentration of the coating solution, the cycle life of the cells increased and the overvoltage decreased. In particular, the electrodes treated with 20 % DBTC were the only samples on which strong signals of the corresponding halogen could be detected in the EDX. This may be due to the fact that DBTC shows a stronger reactivity than 3TA or 4TA anyway, as it is a brominating reagent *per se* (see reaction scheme in figure 63) and therefore the bromine is easily eliminated from the molecule.

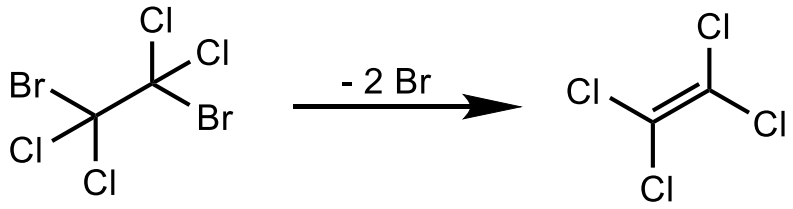


**Figure 63: Reaction scheme of bromine elimination from DBTC.**

In addition, the coating solution was close to the saturation limit, which may have led to the lithium serving as a kind of crystallization nucleus and thus "forcing" the DBTC to react even more strongly with lithium. The ionic conductivity or diffusivity of LiBr in comparison with LiF, however, do not seem to be a decisive factor for the SEI properties, as, depending on the source, LiBr ionic conductivity and diffusion coefficient is only slightly higher or practically the same as in LiF.[23,245]

## 4.4 Thin and homogenous ASEI by Dip Coating with Tris(*N*,*N*-tetramethylene)phosphoric acid triamide and Tert-pentanol

In the first part of this work, lithium electrodes were treated with a solution of tris(*N*,*N*-tetramethylene)phosphoric triamide (TNNT) and tert-pentanol in heptane. The basic hypothesis for this treatment was the consideration that the reaction of the lithium metal with the phosphorus- and nitrogen-containing molecule TNNT possibly leads to the incorporation of phosphorus and nitrogen compounds into the SEI. To increase the reactivity of the coating solution, an alcohol was added. *Tert*-pentanol was chosen because it is a short-chain alcohol, but its reactivity is limited by the

tertiary position of the alcohol group. In this way, a moderate, not too strong reaction with the lithium electrode should be tuned. TNNT is a derivative of the versatile solvent hexamethylphosphoramidate (HMPA), which, however, imposes severe health risks, which is why TNNT was chosen instead. Both molecule structures are depicted in figure 64. For the coating, 2 different variations were scanned for their properties: according to method i, the electrodes were rinsed with heptane after the 15-minute immersion bath in the reaction solution; according to method ii, the electrodes were carefully dried after the immersion bath. The first step in evaluating the modification of the lithium electrode is the construction of symmetrical cells for plating/stripping experiments, as this makes it easy to find out how the treated electrodes behave in comparison to untreated electrodes. The focus is on the overvoltage of the cell, which provides information about the cell resistance and can be used to estimate whether a short circuit or dendrite growth occurs (very low overvoltage) or whether the electrolyte is being consumed (very high overvoltage).

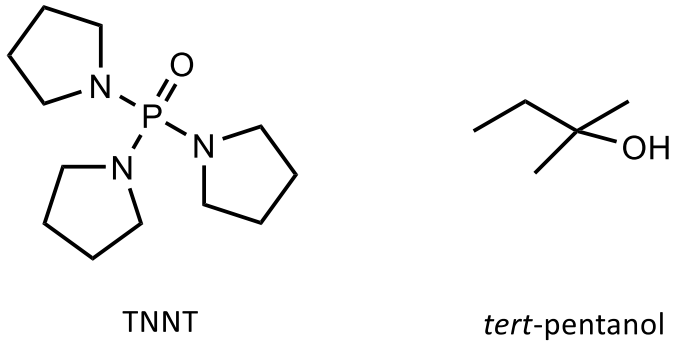


**Figure 64: Chemical structures of tris(*N*,*N*-tetramethylene)phosphoric acid triamide (TNNT, left) and *tert*-pentanol (right).**

In figure 65, the plating/stripping overvoltages of (a) a reference cell with pristine electrodes and symmetric cells using modified electrodes according (b) to method i and (c) to method ii are depicted. Both treatments were able to significantly improve the cycling behavior of the symmetric cells. The overpotential during simultaneous lithium deposition and dissolution was significantly reduced from up 50-80 mV in the reference cell to 22 mV (i) resp. 15 mV (ii) in the first cycles, and the areal resistances of cells were determined by Ohm's law to be 150 - 29 $\Omega cm^2$ (method ii); interestingly, for the latter method the resistances steadily decreased with the duration of the cycling experiments. Upon further comparison of the three voltage profiles, method ii shows the most stable cycling behavior compared to the pristine and rinsed electrodes as there are no high voltage peaks at the beginning or end of a half cycle which indicates high reversibility of the electrode reactions. Altogether, the coating after method ii enables stable cycling even at the highest current density (1 $mA/cm^2$) and an overall lifetime of almost 300 hours.

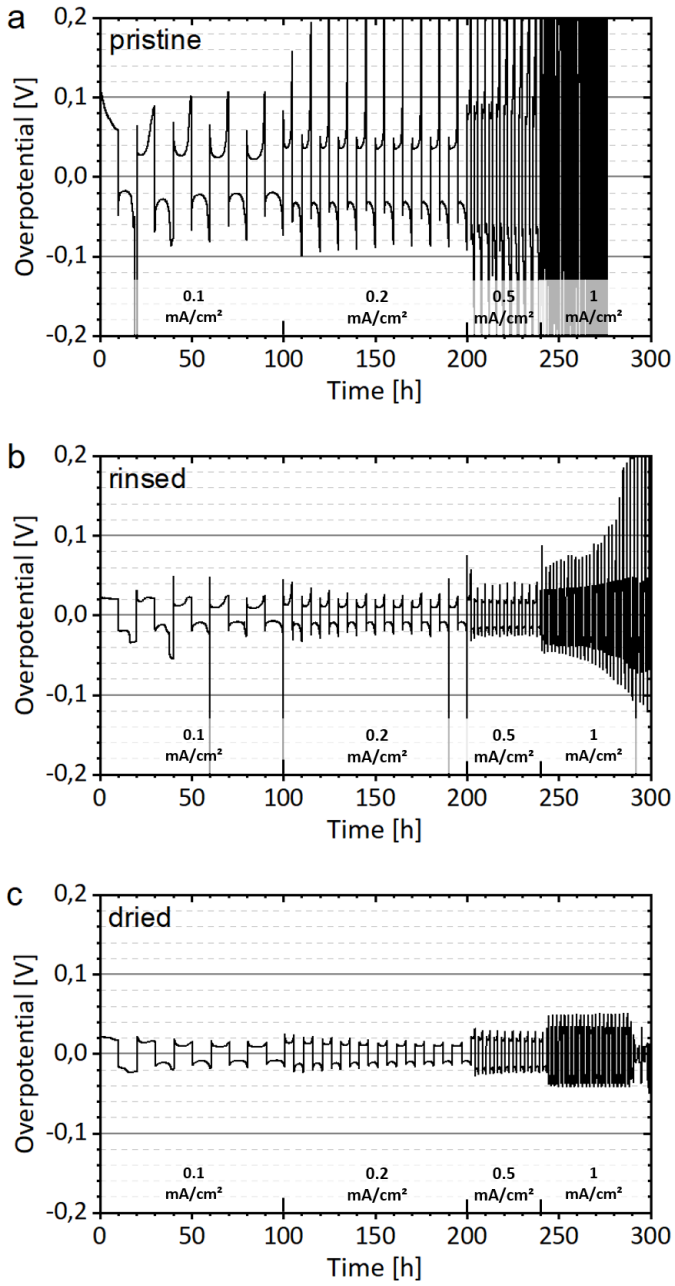


**Figure 65: Voltage profiles of symmetrical cells. The current density steps are being executed as follows: 0-100 h: 0.1 mA/cm²; 100-200 h: 0.2 mA/cm²; 200-240 h: 0.5 mA/cm²; 240+ h: 1 mA/cm². a) Pristine lithium electrodes. b) Electrodes modified by method i. c) Electrodes modified by method ii. All measurements were performed at $T$ = 25 °C.**

To gather more insights into the electrochemical processes in the symmetric cells, electrochemical impedance spectroscopy (EIS) was performed. Especially the question of what leads to the sinking cell resistance during cycling was of interest. In the known literature, however, there is no common sense about which half circles in the Nyquist impedance spectra corresponds to which electrochemical process, as for example, different publications assign the high frequency region to the SEI impedance[83,246], the charge transfer impedance/resistance[247] or even both.[248] In this work, the impedance data were analyzed under the hypothesis that the high frequency semicircle comprises both the charge transfer resistance (at the highest frequencies) and the SEI resistance

(at lower frequencies) leading to satisfactory fitting results. Figure 66 displays the impedance spectra of a symmetrical cell with electrodes prepared according to method ii. Initially, the Nyquist plot of the EIS data shows 2 distinct arcs which develop into 1 closed arc and 1 open arc after ca. 10 cycles. As already indicated by the overvoltage diagrams, the impedance data confirm that the cell resistance is sinking throughout the cycling experiment. Because the high frequency arcs comprise the SEI contribution to the impedance, these parts were analyzed in detail in order to answer the question why the cell resistance resp. SEI resistance is sinking over the experiment, as reasons for this could be a rising SEI conductivity as well as simply a growing surface area. According to the work of *He* et al.[248], the high frequency semicircles were analyzed using 2 constant phase elements as equivalent circuits for the SEI and charge transfer (ct) impedance. Overall, this revealed that the SEI areal impedance is decreasing from 57.2 $\Omega cm^2$ after the first cycle to 5.3 $\Omega cm^2$ after the $35^{th}$ cycle.

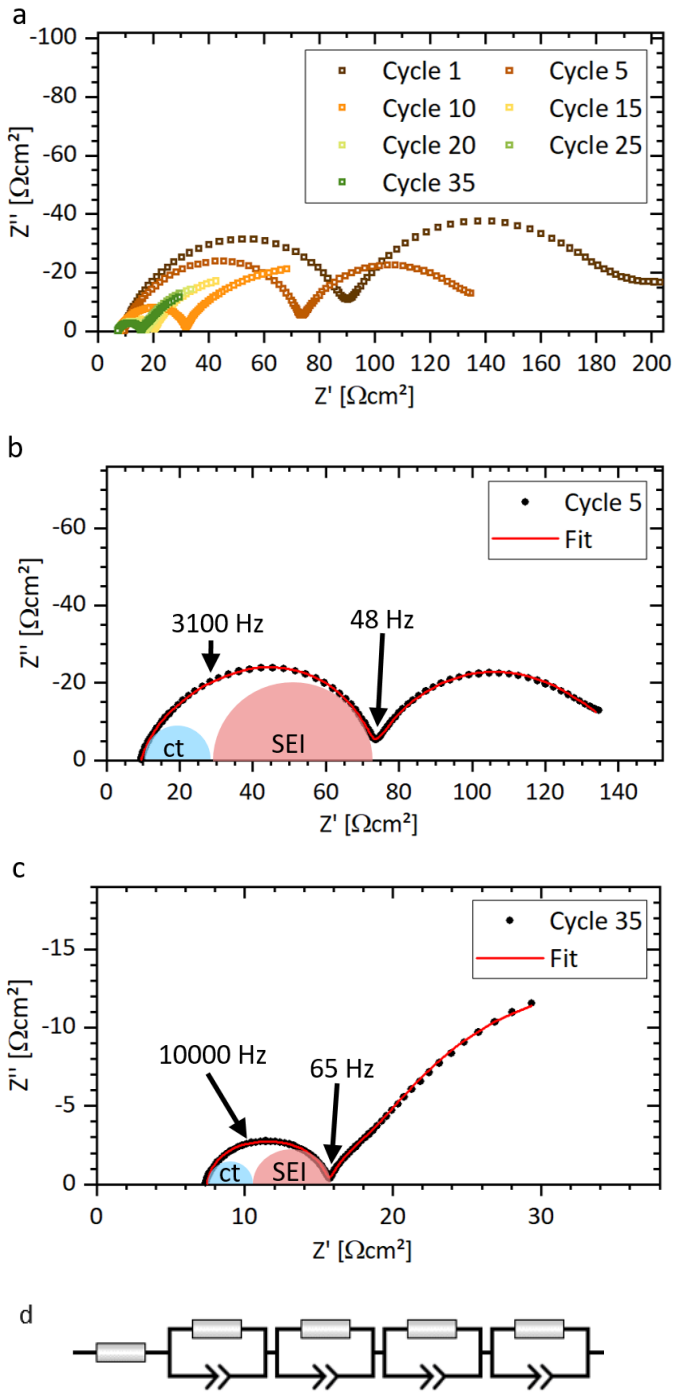


**Figure 66: a) Impedance spectra of a symmetric cell using electrodes modified by method ii. The EIS measurements were conducted after the indicated cycles. b) and c) Detailed depiction of the fitting information for the impedance spectra after cycle 5 and 35, resp. d) Model of the used equivalent circuit for the data fitting.**

Since it is not clear whether the reduced resistance comes from increased ionic conductivity of the SEI, its capacitance must be taken into consideration as well, as an increasing electrode surface *A* would lead to a sinking resistance *R* on the one hand, on the other hand it would lead the capacitance *C* to increase by the same factor as the resistance sinks according to their fundamental physical dependencies ($C = \varepsilon_0 \varepsilon_r \frac{A}{d}$ ; $R = \frac{1}{\sigma}\frac{d}{A}$).[246] Table 3 shows the detailed analysis of the SEI and charge transfer contributions which proves that the conductivity of the SEI is increasing over the cycling

experiment as the SEI areal resistance is decreasing significantly stronger (by a factor of 11 from 57.2 Ωcm² to 5.3 Ωcm²) than the SEI capacitance is increasing (by a factor of 3.6 from $2.24 \cdot 10^{-6}$ F to $8.02 \cdot 10^{-6}$ F). It should be noted that the areal resistances are calculated based on the geometric area of the electrodes ($A$ = 1.327 cm²) which should be considered the lower limit of the electrode surface area as an increasing surface area is expected.

**Table 3: Results of the charge transfer/SEI resistance/capacitance computations.**

| Cycle № | $R_{ct}$ /Ωcm² | $C_{ct}$ /F | $R_{SEI}$/Ωcm² | $C_{SEI}$/F |
|---|---|---|---|---|
| **1** | 20.8 | $1.38 \cdot 10^{-6}$ | 57.2 | $2.24 \cdot 10^{-6}$ |
| **5** | 19.4 | $1.48 \cdot 10^{-6}$ | 43.8 | $3.27 \cdot 10^{-6}$ |
| **10** | 8.2 | $1.57 \cdot 10^{-6}$ | 15.3 | $4.88 \cdot 10^{-6}$ |
| **15** | 5.2 | $1.75 \cdot 10^{-6}$ | 7.4 | $8.41 \cdot 10^{-6}$ |
| **20** | 3.2 | $2.52 \cdot 10^{-6}$ | 6.6 | $6.62 \cdot 10^{-6}$ |
| **25** | 2.7 | $2.84 \cdot 10^{-6}$ | 5.4 | $7.60 \cdot 10^{-6}$ |
| **35** | 2.9 | $2.83 \cdot 10^{-6}$ | 5.3 | $8.02 \cdot 10^{-6}$ |

In cooperation with the *Fraunhofer IWS* in Dresden, the modified electrodes were further characterized by employing them as anodes in lithium-sulfur batteries. For the tests, untreated anodes and anodes modified by method i (rinsed after dip coating) were compared regarding capacity retention and coulombic efficiency. Electrodes modified by method ii showed difficulties in storage and transport as they tended to stick to the transport cases despite careful drying leading to the destruction of the electrodes which is why method i was chosen for the Li-S cell tests. Figure 67 shows the results of these cycling experiments. The data clearly show that the artificial SEI that forms upon the surface reaction of lithium with TNNT and *tert*-pentanol has a positive influence on the performance of the lithium-sulfur cells.

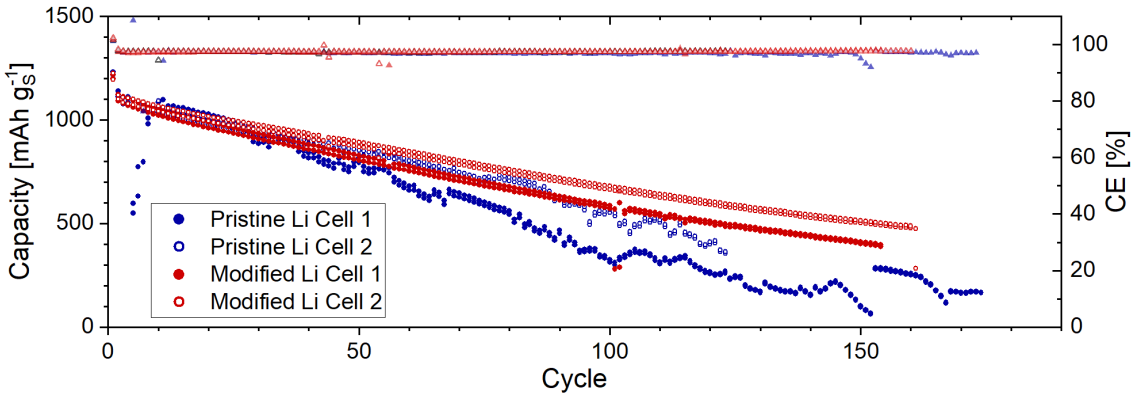


**Figure 67: Discharge capacity and Coulomb efficiency (CE) of two Li-S full cells with pristine lithium metal anodes and two Li-S full cells with lithium metal anodes modified according to method ii. Circular symbols indicate the discharge capacity and triangular symbols correspond to the Coulomb efficiency.**

Due to the improved lithium metal anodes, the Li-S cells show higher Coulomb efficiency and lower capacity fading, as the discharge capacity of the cells with pristine anodes is only 20.9 % and 33.0 % of their initial capacity, respectively, after 120 cycles. The use of the modified LMAs led to a higher capacity retention of 41.0 % resp. 48.2 % after the same amount of cycles. It is also worth mentioning that the change in discharge capacity appears to be much more uniform due to the treatment. In the untreated cells, the capacity jumps strongly up and down, which may indicate that the charging or discharging steps were partially interrupted prematurely due to suddenly increased overvoltage. This behavior is prevented by the surface modification of the anodes indicating a more stable anode/electrolyte interface.

In order to check whether the dip coating methods led to an altered surface chemistry and to verify the hypothesis that the TNNT molecules react with lithium metal forming a phosphorus and nitrogen containing SEI, the modified electrodes were examined by X-ray photoelectron spectroscopy (XPS) after the coating process. XPS can not only deliver information about the quantitative composition of the sample, it is also possible to distinguish individual chemical compounds through their distinctive binding energies. For example, the components of the natural lithium passivation layer show Li 1s binding energies of 53-55 eV while elemental lithium is not oxidized and therefore shows a lower binding energy of ca. 52.6 eV.[19] However, as the Li 1s signals of the natural passivation are overlapping each other and beyond that overlapping with the signals of possible ASEI species such as $Li_3N$ and $Li_3PO_4$, the XPS signals of the other characteristic elements like nitrogen or phosphorus must also be analyzed for comprehensive information regarding the chemical bonding states. Furthermore, the deeper ASEI layers towards the lithium bulk can be accessed and measured through sputtering.

Elemental quantification was conducted by the analysis of XPS survey spectra. As depicted in table 4, both dip coated electrodes showed no significant lithium signals on the surface. The pristine electrode, however, also showed quite low Li concentration of 11.2 % on the surface, whereby it is important to bear in mind that this is not necessarily lithium metal. Already after the first sputter step, all samples tend to have similar Li concentrations. Due to the natural passivation layer, pristine lithium only shows carbon and oxygen signals apart from the lithium signals. Compared to the pristine sample, both coatings led to strongly decreased oxygen signal intensity primarily on the surface while the treatment with organic molecules results in high carbon concentrations. Nevertheless, carbon signals quickly vanish through sputtering showing the artificial SEIs were very thin. Most importantly, the survey spectra verify the presence of nitrogen and phosphorus on the samples. For the method i, the respective atomic concentrations are even higher than on the sample modified by method ii pointing out that the 15 minutes of dip coating already led to a surface comprising 10.0 at% nitrogen and 5.9 at% phosphorus while in contrast the samples modified by method ii (dried) show higher N and P concentrations after the first sputter step.

Furthermore, the signal intensities of C, N and P decrease quicker in the rinsed sample indicating a thinner coating layer due to coating method i.

**Table 4: Element distributions on the analyzed lithium samples according to XPS. All data in atom%.**

| | Method i | | | Method ii | | | Pristine lithium | | |
|---|---|---|---|---|---|---|---|---|---|
| **Signal** | surf. | 1st sputt. | 2nd sputt. | surf. | 1st sputt. | 2nd sputt. | surf. | 1st sputt. | 2nd sputt. |
| **Li 1s** | - | 27.4 | 67.6 | - | 12.3 | 52.9 | 11.2 | 36.2 | 59.4 |
| **O 1s** | 16.8 | 39.5 | 28.4 | 15.5 | 13.7 | 33.1 | 63.6 | 44.2 | 32.5 |
| **C 1s** | 63.3 | 23.0 | - | 69.6 | 51.9 | 12.8 | 25.3 | 19.5 | 8.0 |
| **N 1s** | 10.0 | 2.6 | - | 8.1 | 7.5 | - | - | - | - |
| **P 2p** | 5.9 | 4.7 | - | 4.3 | 8.1 | 0.7 | - | - | - |

Figure 68 shows the Li 1s detail spectra of lithium electrodes treated by method i and ii which were measured after the 2nd sputtering step. In the left spectrum (method i) the photoelectron signals of lithium metal and associated plasmon-loss features are clearly visible. After the same sputter time, the sample prepared according to method ii (dried) shows less pronounced signals that can be associated to lithium metal, still, a shoulder towards lower binding energies indicates the presence of lithium metal nevertheless. These results show that the artificial SEI layer on top of the rinsed (method i) electrodes is thinner than on the dried (method ii) electrodes.

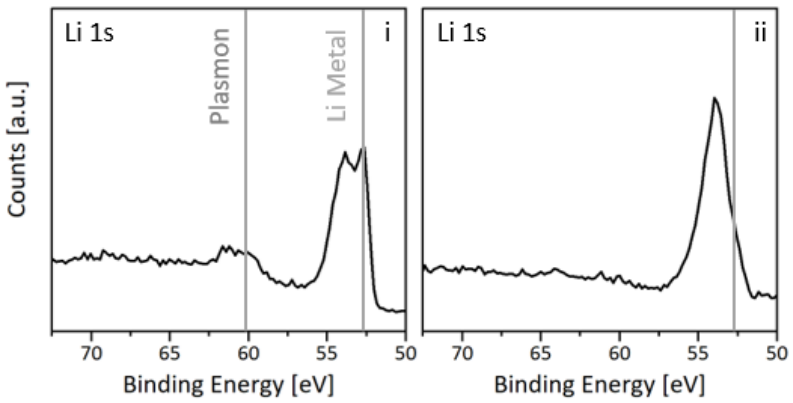


**Figure 68: Li 1s detail spectra of lithium foils after dip coating according to method i (left) and method ii (right). The spectra were measured after 2 sputter steps (3 min @ 1 kV, then 8 min @ 2 kV).**

The highest signal intensities of the N 1s spectra displayed in Figure 69 show at binding energies of 399 eV which can be attributed to organic bound nitrogen[249] similar to the bonding state in the TNNT molecule. Confirming the hypothesis that TNNT might react to lithium nitride upon contact with lithium metal, the surfaces of both samples already show N 1s signals at 397 eV which are

induced by the presence of $Li_3N$.[250] After the first sputtering step, these signals become even more pronounced.

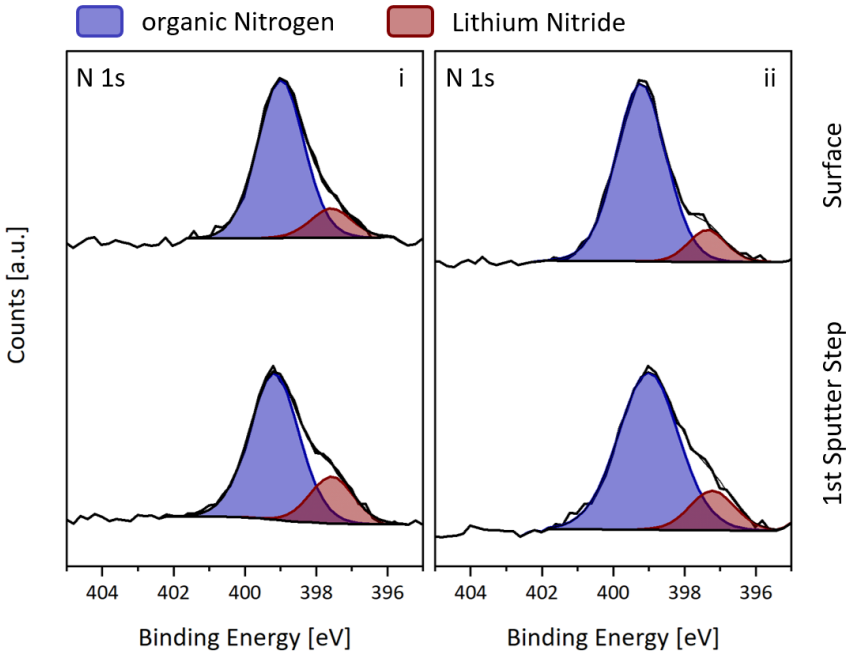


**Figure 69: N 1s detail spectra of lithium foils after dip coating according to method i (left) and method ii (right). The spectra were measured on the surface resp. after one sputter step (3 min @ 1 kV).**

Figure 70 shows the P 2p detail spectra where on the surface of both modified electrodes the dominating P 2p photoelectron signals are at a binding energy of ca. 133-134 eV which can be attributed to phosphate type species. After the 1st sputtering step, the presence of a second, further reduced phosphorus species can be found whose signal is much more pronounced in the dried sample (method ii) compared to method i. However, the presence of lithium phosphide cannot be proven as the measured binding energy of ca. 130 eV is too high for $Li_3P$ which is supposed to have a P 2p binding energy of 127-128 eV.[250] Since lithium phosphide will decompose upon contact with the smallest impurities even in ultra-high vacuum, its detection is known to be challenging.[68] Yet, the presence of the reduced phosphorus species proves that the phosphate-type phosphorus in TNNT is being reduced upon reaction with lithium metal.

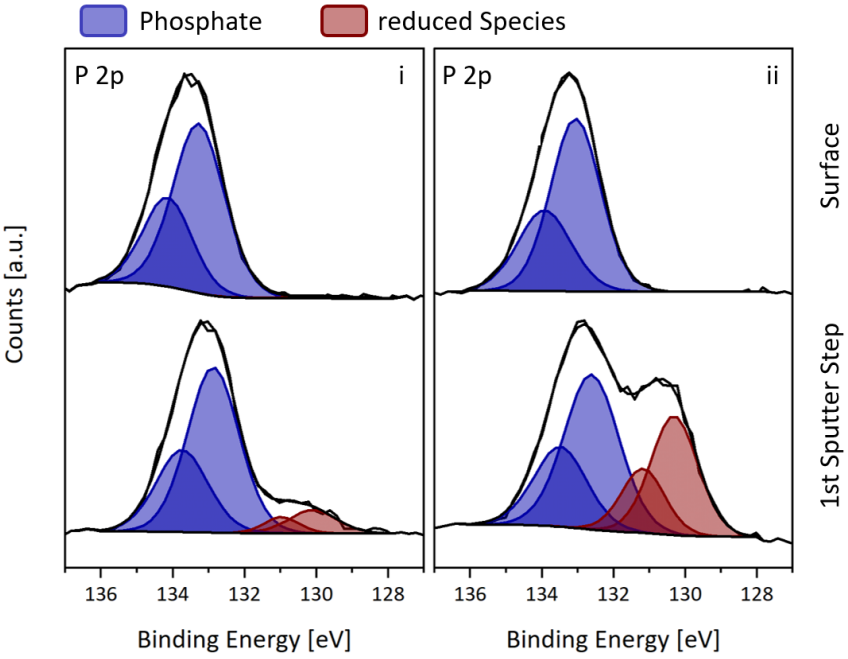


**Figure 70: P 2p detail spectra of lithium foils after dip coating according to method i (left) and method ii (right). The spectra were measured on the surface resp. after one sputter step (3 min @ 1 kV).**

To conclude the extensive characterization of the electrodes modified by dip coating, they were examined by ToF-SIMS to gain further insights into the structure, homogeneity and approximate thickness of the generated ASEIs. In order to make a statement about the homogeneity of the samples, 3 ToF-SIMS depth profiles were recorded at random locations for each sample or electrode. The three depth profiles of each sample shown in figure 71 a for method i and 71 b for method ii are almost identical for each sample which indicates a highly homogenous surface region. The clear presence of phosphorus ($P^-$) signals, consistent with the XPS results, prove that phosphorus derived from dip coating with TNNT was successfully incorporated into the ASEI. The progression of the signal intensities in the ToF-SIMS depth profiles further reveals the layered structure of the electrode surfaces, as the $P^-$ signal reaches its maximum first during sputtering, followed by the $LiO_2H_2^-$ secondary ion signal, which indicates the presence of LiOH. This course of events also agrees with the XPS results. As the $LiO_2H_2^-$ signal passes its maximum, the $LiH^-$ which corresponds to elemental lithium rises and reaches a maximum as reported for the native passivation layer on untreated lithium foils.[19] The fact that after longer sputtering time all signal intensities are decreasing also indicates an increasing lithium metal fraction. Contrary to the XPS measurements that clearly show the presence of organic bound nitrogen as well as lithium nitride, no significant intensity of signals typical for lithium nitride were possible to be detected by ToF-SIMS, as exemplarily shown for the $LiN^-$ ion signal. All in all, the qualitative results of the SIMS measurements are quite similar for both samples. However, direct comparison shows that for method i all signal intensities rise and decrease at earlier sputter times than for method ii confirming that rinsing the electrodes after dip coating leads to a thinner coating than letting it dry.

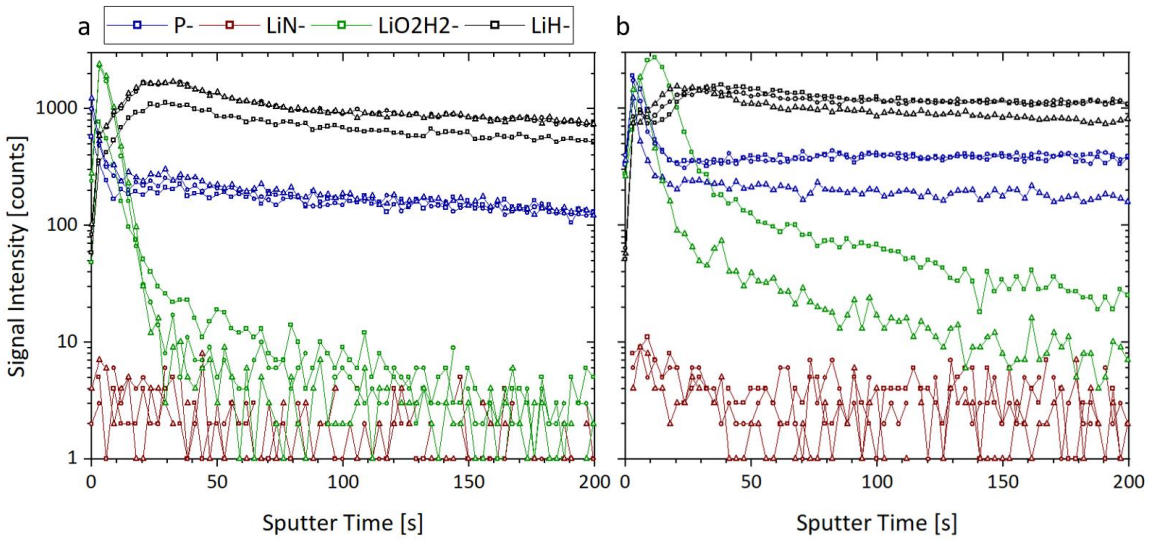


**Figure 71: a) ToF-SIMS depth profiles of a dip coated electrode sample treated according to method i. Comparing the three depth profiles measured at random locations of the samples shows that the resulting reaction layer is homogenous. b) ToF-SIMS depth profiles of a dip coated electrode sample treated according to method ii. While the resulting reaction layer (ASEI) is also homogenous, it is about twice as thick as the ASEI from method i.**

To summarize, the use of a TNNT and *tert*-pentanol containing solution for surface treatment, followed by gentle drying of the lithium metal electrodes, results in a significant reduction in cell resistance and improved cycle life in symmetrical cells. Also, the capacity retention in the investigated Li-S cells is higher with the rinsed coating compared with pristine anodes. The hypothesis that the SEI's ionic conductivity increases throughout plating/stripping experiments is supported by impedance measurements. This study aimed to determine whether this technique could initiate specific chemical reactions, such as the incorporation of desired reaction products, like the highly ion-conductive $Li_3N$, into the electrodes' surface. By conducting XPS and ToF-SIMS measurements, it was possible to demonstrate that this surface treatment method can integrate elements such as nitrogen and phosphorus into the lithium electrode's surface layer. XPS measurements provided evidence of this concept by detecting lithium nitride and reduced phosphorus species which must be originating from the decomposition of the TNNT molecule.

# 5 Summary and outlook

This dissertation focused on the development and evaluation of different liquid-based methods that can be scaled up for modifying lithium metal anodes. The modifications involve applying polymer coatings and polymer/solid electrolyte hybrid coatings through spin coating, as well as executing surface modifications of the solid electrolyte interphase (SEI) using reactive precursor chemicals through dip coating. To assess the impact of these coatings and modifications, symmetrical cells were used, and the chemical composition of the electrode surface was thoroughly analyzed. This comprehensive analysis helped gaining a better understanding of selecting suitable reagents, adjusting their reactivity, and optimizing the coating compositions.

In one study, a new concept involving spin coating combined solutions of polymers and metal complexes was explored. The use of these combined coatings led to improved electrochemical properties compared to using only polymers or metal complexes. However, the choice of solvent proved to be crucial, with DMF being unsuitable due to its reaction with lithium. Coatings with PS or PVDF and $In(acac)_3$ in THF showed significant improvements, although the solubility of PVDF in THF posed challenges and the PS coatings showed to be brittle. Another part of the research focused on developing hybrid LPSCl/polymer coatings for lithium metal anodes. PVDF presented difficulties due to either being insoluble in solvents or decomposing when dissolved. The use of PVDF-HFP, however, was possible for hybrid coatings and showed promising results. Polyethylene oxide (PEO) comprised the highest versatility and allowed coatings with a broad variety of solvents. Acetonitrile, ethyl acetate, and THF exhibited promising results in terms of low overpotential and long cycling stability.

For the electrode surface modifications by dip coating, the reactivity of the coating reagents played a crucial role, as observed in the study. Different chemicals displayed varying reactivity based on their molecular structure. The use of different solvents, such as heptane and THF, also affected the coatings' reactivity and performance. The choice of reagents and solvents played a significant role in achieving successful coatings, with NPCl/heptane and TDP/THF combinations showing strongly improved electrochemical properties and outstanding reproducibility for the NPCl/heptane dip coating. The high performance of such coated electrodes can be explained by the facile release of chlorine atoms from the NPCl molecule resulting in a LiCl rich artificial SEI without too many other contaminations. In contrast to this, the use of THF as solvent for the NPCl coating led to decomposition of the phosphazene ring and incorporation of THF into the ASEI resulting in too high reactivity. Similarly, the DDP molecule completely decomposes in contact with lithium resulting in a less well-defined ASEI compared to NPCl/heptane. SEM observations revealed additionally that the NPCl/heptane coating made the entire electrode surface available for the

electrochemical reactions while pristine and TDP/THF coated electrodes featured island-like lithium plating and stripping.

As the high LiCl content of the NPCl/heptane coatings obviously led to high lithium plating/stripping process stability, further comparative studies were conducted on halide containing coatings for lithium metal anodes. The fluorine-based coatings showed improved electrochemistry, with the 3TA-coated electrodes outperforming the 4TA-coated ones. The surface analytics revealed that both coatings comprised a thin, fluorine-containing surface layer while the 3TA modification presented stronger fluorine signals than the 4TA modification. The DBTC coatings exhibited higher reproducibility, and increased concentration of the coating solution improved cycle life and reduced overvoltage. The surface analytical methods showed here, that the DBTC dip coatings led to bromine containing ASEIs which confirmed the hypothesis already made for NPCl, meaning that a facile release of designated leaving groups (bromine in this case) is beneficial for the SEI modification while at the same time the by-product of bromine elimination (tetrachloroethene) is stable and can remain in the solution.

The use of TNNT and *tert*-pentanol in surface treatment led to reduced cell resistance, improved cycle life, and higher capacity retention in Li-S cells. Furthermore, it was proven by electrochemical impedance spectroscopy that the conductivity of the ASEI is increasing throughout the cycling experiment. XPS and ToF-SIMS analyses were able to demonstrate that by this treatment method, phosphorus and nitrogen originating from the TNNT molecule are integrated into the ASEI and are being reduced by lithium metal forming, among others, highly ion conductive lithium nitride. The results of this chapter were published in the *Journal of The Electrochemical Society* (DOI 10.1149/1945-7111/acc698).[200]

Amongst the vast number of publications concerning protected lithium metal anodes, where it is seldom explained why a compound is chosen for the electrode modification, these studies can act as a roadmap for creating specific ASEI compositions, helping to answer the question “how can I incorporate compound *XY* into the electrode surface to test its suitability?”. Answer: by coating the electrode with a chemical that will release *XY* easily and if necessary, tune the reactivity by the choice of solvents.

Regarding future research on the protection of lithium metal anodes based on this work, there are a couple of points worth digging further into: Since the connection between the degradation of the hybrid coating dispersions and the basicity of the solvent was only recognized in the very last steps of the process of compiling the dissertation, further work should be invested here. As the solubility of PVDF in DMF probably comes from its high dipole moment, other high polarity solvents with weaker Lewis basicity could be suitable for hybrid coatings, for example alkyl carbonates, cyclohexanone or lactones. In order to further research the possibilities of generating an artificial

SEI with an even higher $Li_3N$ content by dip coating, chemical compounds that consist to a large extent of nitrogen are the most suitable, as there are no reagents that can specifically perform a "nitriding" or "nitrogenation" reaction. However, the choice of nitrogen-rich compounds is severely limited by the fact that they can often react explosively, such as hydrazine or hydrazoid acid. Here, triazoles and tetrazoles would be suitable for dip coatings, but they could have a low reactivity due to the stabilization of the molecule by the aromatic ring structure. For further SEI modifications, e.g. to explore halogen-containing ASEIs in more depth, the toolbox of organic chemistry can be used to produce a LiI-containing ASEI by using the iodination reagent *N*-iodosuccinimide. Likewise, the analogues *N*-bromosuccinimide and *N*-chlorosuccinimide can be used for an extensive test series. In general, a modification of the lithium metal anode should aim to be as homogeneous and uniform as possible and to be electrochemically stable towards lithium metal. The implementation of binary lithium compounds is crucial here, as these are stable up respectively down to 0 V against $Li/Li^+$.[72]

# 6 References

(1) Thackeray, M. M.; Wolverton, C.; Isaacs, E. D. Electrical Energy Storage for Transportation-Approaching the Limits of, and Going beyond, Lithium-Ion Batteries. *Energy Environ. Sci.* **2012**, *5*, 7854–7863. https://doi.org/10.1039/c2ee21892e.

(2) Morioka, Y.; Narukawa, S.; Itou, T. State-of-the-Art of Alkaline Rechargeable Batteries. *J. Power Sources* **2001**, *100* (1–2), 107–116. https://doi.org/10.1016/S0378-7753(01)00888-6.

(3) Putois, F. Market for Nickel-Cadmium Batteries. *J. Power Sources* **1995**, *57* (1–2), 67–70. https://doi.org/10.1016/0378-7753(95)02243-0.

(4) Broussely, M.; Archdale, G. Li-Ion Batteries and Portable Power Source Prospects for the next 5-10 Years. *J. Power Sources* **2004**, *136*, 386–394. https://doi.org/10.1016/J.JPOWSOUR.2004.03.031.

(5) Ziegler, M. S.; Trancik, J. E. Re-Examining Rates of Lithium-Ion Battery Technology Improvement and Cost Decline. *Energy Environ. Sci.* **2021**, *14*, 1635. https://doi.org/10.1039/d0ee02681f.

(6) Janek, J.; Zeier, W. G. Challenges in Speeding up Solid-State Battery Development. *Nat. Energy* **2023**. https://doi.org/10.1038/s41560-023-01208-9.

(7) de Blas, I.; Mediavilla, M.; Capellán-Pérez, I.; Duce, C. The Limits of Transport Decarbonization under the Current Growth Paradigm. *Energy Strateg. Rev.* **2020**, *32*, 100543. https://doi.org/10.1016/J.ESR.2020.100543.

(8) Chakraborty, P.; Parker, R.; Hoque, T.; Cruz, J.; Du, L.; Wang, S.; Bhunia, S. Addressing the Range Anxiety of Battery Electric Vehicles with Charging En Route. *Sci. Rep.* **2022**, *12* (1), 1–15. https://doi.org/10.1038/s41598-022-08942-2.

(9) Wassiliadis, N.; Steinsträter, M.; Schreiber, M.; Rosner, P.; Nicoletti, L.; Schmid, F.; Ank, M.; Teichert, O.; Wildfeuer, L.; Schneider, J.; Koch, A.; König, A.; Glatz, A.; Gandlgruber, J.; Kröger, T.; Lin, X.; Lienkamp, M. Quantifying the State of the Art of Electric Powertrains in Battery Electric Vehicles: Range, Efficiency, and Lifetime from Component to System Level of the Volkswagen ID.3. *eTransportation* **2022**, *12*. https://doi.org/10.1016/J.ETRAN.2022.100167.

(10) Liu, J.; Bao, Z.; Cui, Y.; Dufek, E. J.; Goodenough, J. B.; Khalifah, P.; Li, Q.; Liaw, B. Y.; Liu, P.; Manthiram, A.; Meng, Y. S.; Subramanian, V. R.; Toney, M. F.; Viswanathan, V.

V.; Whittingham, M. S.; Xiao, J.; Xu, W.; Yang, J.; Yang, X. Q.; Zhang, J. G. Pathways for Practical High-Energy Long-Cycling Lithium Metal Batteries. *Nat. Energy* **2019**, *4* (3), 180–186. https://doi.org/10.1038/s41560-019-0338-x.

(11) Manthiram, A. An Outlook on Lithium Ion Battery Technology. *ACS Cent. Sci.* **2017**, *3* (10), 1063–1069. https://doi.org/10.1021/acscentsci.7b00288.

(12) Lin, L.; Qin, K.; Hu, Y. sheng; Li, H.; Huang, X.; Suo, L.; Chen, L. A Better Choice to Achieve High Volumetric Energy Density: Anode-Free Lithium-Metal Batteries. *Adv. Mater.* **2022**, *34* (23). https://doi.org/10.1002/ADMA.202110323.

(13) Janek, J.; Zeier, W. G. A Solid Future for Battery Development. *Nat. Energy* **2016**, *1* (9), 1–4. https://doi.org/10.1038/nenergy.2016.141.

(14) Albertus, P.; Babinec, S.; Litzelman, S.; Newman, A. Status and Challenges in Enabling the Lithium Metal Electrode for High-Energy and Low-Cost Rechargeable Batteries. *Nat. Energy* **2018**, *3*, 16–21. https://doi.org/10.1038/s41560-017-0047-2.

(15) Frith, J. T.; Lacey, M. J.; Ulissi, U. A Non-Academic Perspective on the Future of Lithium-Based Batteries. *Nat. Commun. 2023 141* **2023**, *14* (1), 1–17. https://doi.org/10.1038/s41467-023-35933-2.

(16) Galvez-Aranda, D. E.; Seminario, J. M. Ab Initio Molecular Dynamics of Li-Metal Anode in a Phosphate-Based Electrolyte: Solid Electrolyte Interphase Evolution. *J. Electrochem. Soc.* **2021**, *168*, 090528. https://doi.org/10.1149/1945-7111/ac22ca.

(17) Huang, Z.; Choudhury, S.; Paul, N.; Thienenkamp, J. H.; Lennartz, P.; Gong, H.; Müller-Buschbaum, P.; Brunklaus, G.; Gilles, R.; Bao, Z. Effects of Polymer Coating Mechanics at Solid-Electrolyte Interphase for Stabilizing Lithium Metal Anodes. *Adv. Energy Mater.* **2022**, *12* (5). https://doi.org/10.1002/AENM.202103187.

(18) Zheng, G.; Wang, C.; Pei, A.; Lopez, J.; Shi, F.; Chen, Z.; Sendek, A. D.; Lee, H. W.; Lu, Z.; Schneider, H.; Safont-Sempere, M. M.; Chu, S.; Bao, Z.; Cui, Y. High-Performance Lithium Metal Negative Electrode with a Soft and Flowable Polymer Coating. *ACS Energy Lett.* **2016**, *1* (6), 1247–1255. https://doi.org/10.1021/acsenergylett.6b00456.

(19) Otto, S.-K.; Moryson, Y.; Krauskopf, T.; Peppler, K.; Sann, J.; Janek, J.; Henss, A. In-Depth Characterization of Lithium-Metal Surfaces with XPS and ToF-SIMS: Toward Better Understanding of the Passivation Layer. *Chem. Mater* **2021**, *33*, 24. https://doi.org/10.1021/acs.chemmater.0c03518.

(20) Otto, S.-K.; Fuchs, T.; Moryson, Y.; Lerch, C.; Mogwitz, B.; Sann, J.; Janek, J.; Henss, A.

Storage of Lithium Metal: The Role of the Native Passivation Layer for the Anode Interface Resistance in Solid State Batteries. *ACS Appl. Energy Mater.* **2021**, *4*, 12798–12908. https://doi.org/10.1021/acsaem.1c02481.

(21) Peled, E. Film Forming Reaction at the Lithium/Electrolyte Interface. *J. Power Sources* **1983**, *9* (3), 253–266. https://doi.org/10.1016/0378-7753(83)87026-8.

(22) Peled, E.; Golodnitsky, D.; Ardel, G. Advanced Model for Solid Electrolyte Interphase Electrodes in Liquid and Polymer Electrolytes. *J. Electrochem. Soc.* **1997**, *144* (8), L208. https://doi.org/10.1149/1.1837858.

(23) Sang, J.; Yu, Y.; Wang, Z.; Shao, G. Theoretical Formulation of Li3a+bNaXb (X= Halogen) as Potential Artificial Solid Electrolyte Interphases (ASEI) to Protect Li Anode. *Phys. Chem. Chem. Phys.* **2020**, *22*, 12918. https://doi.org/10.1039/d0cp00151a.

(24) Pang, Q.; Liang, X.; Kochetkov, I. R.; Hartmann, P.; Nazar, L. F. Stabilizing Lithium Plating by a Biphasic Surface Layer Formed In Situ. *Angew. Chemie - Int. Ed.* **2018**, *57*, 9795–9798. https://doi.org/10.1002/anie.201805456.

(25) Mills, I.; Cvitas, T.; Homann, K.; Kallay, N.; Kuchitsu, K. *Quantities, Units and Symbols in Physical Chemistry*, 2nd Ed.; Blackwell Science Ltd: Oxford, 1993. https://doi.org/https://doi.org/10.1351/goldbook.

(26) Manthiram, A. A Reflection on Lithium-Ion Battery Cathode Chemistry. *Nat. Commun.* **2020**, *11*, 1550. https://doi.org/10.1038/s41467-020-15355-0.

(27) Xie, J.; Lu, Y.-C. A Retrospective on Lithium-Ion Batteries. *Nat. Commun.* **2020**, *11*, 2499. https://doi.org/10.1038/s41467-020-16259-9.

(28) Whittingham, M. S. Electrical Energy Storage and Intercalation Chemistry. *Science (80-. ).* **1976**, *192* (4244), 1126–1127. https://doi.org/10.1126/SCIENCE.192.4244.1126.

(29) Mizushima, K.; Jones, P. C.; Wiseman, P. J.; Goodenough, J. B. LixCoO2 (0<x≤1): A New Cathode Material for Batteries of High Energy Density. *Solid State Ionics* **1981**, *3–4*, 171–174. https://doi.org/10.1016/0167-2738(81)90077-1.

(30) Yoshino, A.; Sanechika, K.; Nakajuma, T. Secondary Battery. *JP9769585* **1985**.

(31) Diouf, B.; Pode, R. Potential of Lithium-Ion Batteries in Renewable Energy. *Renew. Energy* **2015**, *76*, 375–380. https://doi.org/10.1016/J.RENENE.2014.11.058.

(32) Wang, B.; Zhang, F.-L.; Zhou, X.-A.; Wang, P.; Wang, J.; Ding, H.; Dong, H.; Liang, W.-B.; Zhang, N.-S.; Li, S.-Y. Which of the Nickel-Rich NCM and NCA Is Structurally Superior as a Cathode Material for Lithium-Ion Batteries? *J. Mater. Chem.* **2021**, *9*, 13540.

https://doi.org/10.1039/d1ta01128f.

(33) Zubi, G.; Dufo-López, R.; Carvalho, M.; Pasaoglu, G. The Lithium-Ion Battery: State of the Art and Future Perspectives. *Renew. Sustain. Energy Rev.* **2018**, *89* (April 2017), 292–308. https://doi.org/10.1016/j.rser.2018.03.002.

(34) Li, W.; Erickson, E. M.; Manthiram, A. High-Nickel Layered Oxide Cathodes for Lithium-Based Automotive Batteries. *Nat. Energy* **2020**, *5* (1), 26–34. https://doi.org/10.1038/s41560-019-0513-0.

(35) Kim, Y.; Seong, W. M.; Manthiram, A. Cobalt-Free, High-Nickel Layered Oxide Cathodes for Lithium-Ion Batteries: Progress, Challenges, and Perspectives. *Energy Storage Mater.* **2021**, *34*, 250–259. https://doi.org/10.1016/j.ensm.2020.09.020.

(36) Mauger, A.; Julien, C. M. Critical Review on Lithium-Ion Batteries: Are They Safe? Sustainable? *Ionics (Kiel).* **2017**, *23*, 1933–1947. https://doi.org/10.1007/s11581-017-2177-8.

(37) Choi, J. W.; Aurbach, D. Promise and Reality of Post-Lithium-Ion Batteries with High Energy Densities. *Nat. Rev. Mater.* **2016**, *1*, 16013. https://doi.org/10.1038/natrevmats.2016.13.

(38) Randau, S.; Weber, D. A.; Kötz, O.; Koerver, R.; Braun, P.; Weber, A.; Ivers-Tiffée, E.; Adermann, T.; Kulisch, J.; Zeier, W. G.; Richter, F. H.; Janek, J. Benchmarking the Performance of All-Solid-State Lithium Batteries. *Nat. Energy* **2020**, *5* (3), 259–270. https://doi.org/10.1038/s41560-020-0565-1.

(39) Nitta, N.; Wu, F.; Lee, J. T.; Yushin, G. Li-Ion Battery Materials: Present and Future. *Mater. Today* **2015**, *18* (5), 252–264. https://doi.org/10.1016/J.MATTOD.2014.10.040.

(40) Lin, D.; Liu, Y.; Cui, Y. Reviving the Lithium Metal Anode for High-Energy Batteries. *Nat. Nanotechnol.* **2017**, *12* (3), 194–206. https://doi.org/10.1038/nnano.2017.16.

(41) Zheng, J. P.; Liang, R. Y.; Hendrickson, M.; Plichta, E. J. Theoretical Energy Density of Li-Air Batteries. *J. Electrochem. Soc.* **2008**, *155* (6), A432–A437. https://doi.org/10.1149/1.2901961.

(42) Li, G.; Chen, Z.; Lu, J. Lithium-Sulfur Batteries for Commercial Applications. *Chem* **2018**, *4* (1), 3–7. https://doi.org/10.1016/J.CHEMPR.2017.12.012.

(43) Zhou, G.; Chen, H.; Cui, Y. Formulation for High-Energy-Density Li-S Batteries Formulating Energy Density for Designing Practical Lithium-Sulfur Batteries. *Nat. Energy* **2022**, *7*, 312–319. https://doi.org/10.1038/s41560-022-01001-0.

(44) Mccloskey, B. D. Attainable Gravimetric and Volumetric Energy Density of Li−S and Li Ion Battery Cells with Solid Separator-Protected Li Metal Anodes. *J. Phys. Chem. Lett.* **2015**, *6*, 4581–4588. https://doi.org/10.1021/acs.jpclett.5b01814.

(45) Zhai, P. Y.; Huang, J. Q.; Zhu, L.; Shi, J. Le; Zhu, W.; Zhang, Q. Calendering of Free-Standing Electrode for Lithium-Sulfur Batteries with High Volumetric Energy Density. *Carbon N. Y.* **2017**, *111*, 493–501. https://doi.org/10.1016/J.CARBON.2016.10.035.

(46) Vilá, R. A.; Huang, W.; Cui, Y. Nickel Impurities in the Solid-Electrolyte Interphase of Lithium-Metal Anodes Revealed by Cryogenic Electron Microscopy. *Cell Reports Phys. Sci.* **2020**, *1* (9). https://doi.org/10.1016/J.XCRP.2020.100188.

(47) Lee, Y. G.; Fujiki, S.; Jung, C.; Suzuki, N.; Yashiro, N.; Omoda, R.; Ko, D. S.; Shiratsuchi, T.; Sugimoto, T.; Ryu, S.; Ku, J. H.; Watanabe, T.; Park, Y.; Aihara, Y.; Im, D.; Han, I. T. High-Energy Long-Cycling All-Solid-State Lithium Metal Batteries Enabled by Silver–Carbon Composite Anodes. *Nat. Energy* **2020**, *5*, 299–308. https://doi.org/10.1038/s41560-020-0575-z.

(48) Li, W.; Dahn, J. R.; Wainwright, D. S. Rechargeable Lithium Batteries with Aqueous Electrolytes. *Science (80-. ).* **1994**, *264* (5162), 1115–1118.

(49) Jiang, H.; Lin, X.; Wei, C.; Tian, Y.; An, Y.; Feng, J.; Tian, X. Lithium Dendrite Suppression by Facile Interfacial Barium Engineering for Stable 5 V-Class Lithium Metal Batteries with Carbonate-Based Electrolyte. *Chem. Eng. J.* **2021**, *414* (February), 128928. https://doi.org/10.1016/j.cej.2021.128928.

(50) Birdwhistell, R. K.; Ramette, R. W. Outmoded Terminology: The Normal Hydrogen Electrode. *Textb. forum* **1978**, *64* (10), 885.

(51) Wang, J.; Ge, B.; Li, H.; Yang, M.; Wang, J.; Liu, D.; Fernandez, C.; Chen, X.; Peng, Q. Challenges and Progresses of Lithium-Metal Batteries. *Chem. Eng. J.* **2021**, *420*, 129739. https://doi.org/10.1016/j.cej.2021.129739.

(52) Logan, E. R.; Louli, A. J.; Genovese, M.; Trussler, S.; Dahn, J. R. Investigating Parasitic Reactions in Anode-Free Li Metal Cells with Isothermal Microcalorimetry. *J. Electrochem. Soc.* **2021**, *168*, 060527. https://doi.org/10.1149/1945-7111/ac0947.

(53) Liu, Y. T.; Liu, S.; Li, G. R.; Gao, X. P. Strategy of Enhancing the Volumetric Energy Density for Lithium–Sulfur Batteries. *Adv. Mater.* **2021**, *33*, 2003955. https://doi.org/10.1002/ADMA.202003955.

(54) Fang, X.; Peng, H. A Revolution in Electrodes: Recent Progress in Rechargeable Lithium-

Sulfur Batteries. *Small* **2015**, *11* (13), 1488–1511. https://doi.org/10.1002/SMLL.201402354.

(55) Nanda, S.; Manthiram, A. Lithium Degradation in Lithium-Sulfur Batteries: Insights into Inventory Depletion and Interphasial Evolution with Cycling †. *Energy Environ. Sci* **2020**, *13*, 2501. https://doi.org/10.1039/d0ee01074j.

(56) Julien, C.; Mauger, A.; Vijh, A.; Zaghib, K. Lithium Batteries Science and Technology. *Springer Int. Publ. Switz.* **2016**, 29–34. https://doi.org/10.1007/978-3-319-19108-9.

(57) Wedepohl, K. H. *Sulfur in the Earth'S Crust, Its Origin and Natural Cycle.*; Elsevier B.V., 1984; Vol. 5. https://doi.org/10.1016/b978-0-444-42355-9.50007-4.

(58) Chung, W. J.; Griebel, J. J.; Kim, E. T.; Yoon, H.; Simmonds, A. G.; Ji, H. J.; Dirlam, P. T.; Glass, R. S.; Wie, J. J.; Nguyen, N. A.; Guralnick, B. W.; Park, J.; Somogyi, Á.; Theato, P.; Mackay, M. E.; Sung, Y. E.; Char, K.; Pyun, J. The Use of Elemental Sulfur as an Alternative Feedstock for Polymeric Materials. *Nat. Chem.* **2013**, *5* (6), 518–524. https://doi.org/10.1038/nchem.1624.

(59) Akhtar, N.; Sun, X.; Yasir Akram, M.; Zaman, F.; Wang, W.; Wang, A.; Chen, L.; Zhang, H.; Guan, Y.; Huang, Y. A Gelatin-Based Artificial SEI for Lithium Deposition Regulation and Polysulfide Shuttle Suppression in Lithium-Sulfur Batteries. *J. Energy Chem.* **2021**, *52*, 310–317. https://doi.org/10.1016/j.jechem.2020.04.046.

(60) Bhargav, A.; He, J.; Gupta, A.; Manthiram, A. Lithium-Sulfur Batteries: Attaining the Critical Metrics. *Joule* **2020**, *4* (2), 285–291. https://doi.org/10.1016/j.joule.2020.01.001.

(61) Li, M.; Li, X.; Tung, V.; Li, Y.; Lai, Z. Protection of Lithium Anode by a Highly Porous PVDF Membrane for High-Performance Li-S Battery. *ACS Appl. Energy Mater.* **2020**. https://doi.org/10.1021/acsaem.9b02211.

(62) Weller, C.; Thieme, S.; Härtel, P.; Althues, H.; Kaskel, S. Intrinsic Shuttle Suppression in Lithium-Sulfur Batteries for Pouch Cell Application. *J. Electrochem. Soc.* **2017**, *164* (14), A3766. https://doi.org/10.1149/2.0981714JES.

(63) Ogasawara, T.; Débart, A.; Holzapfel, M.; Nová, P.; Bruce, P. G. Rechargeable Li 2 O 2 Electrode for Lithium Batteries. *J. Am. Chem. Soc.* **2006**, *128*, 1390–1393. https://doi.org/10.1021/ja056811q.

(64) Liu, T.; Padmanabhan Vivek, J.; Zhao, E. W.; Lei, J.; Garcia-Araez, N.; Grey, C. P. Current Challenges and Routes Forward for Nonaqueous Lithium− Air Batteries. *Chem. Rev.* **2020**, *120*, 6558–6625. https://doi.org/10.1021/acs.chemrev.9b00545.

(65) Bender, C. L.; Hartmann, P.; Vračar, M.; Adelhelm, P.; Janek, J. On the Thermodynamics, the Role of the Carbon Cathode, and the Cycle Life of the Sodium Superoxide (NaO2) Battery. *Adv. Energy Mater.* **2014**, *4* (12). https://doi.org/10.1002/AENM.201301863.

(66) Schürmann, A.; Haas, R.; Murat, M.; Kuritz, N.; Balaish, M.; Ein-Eli, Y.; Janek, J.; Natan, A.; Schröder, D. Diffusivity and Solubility of Oxygen in Solvents for Metal/Oxygen Batteries: A Combined Theoretical and Experimental Study. *J. Electrochem. Soc.* **2018**, *165* (13), A3095–A3099. https://doi.org/10.1149/2.0601813jes.

(67) Ruhl, J.; Riegger, L. M.; Ghidiu, M.; Zeier, W. G. Impact of Solvent Treatment of the Superionic Argyrodite Li 6 PS 5 Cl on Solid-State Battery Performance. *Adv. Energy Sustain. Res.* **2021**, *2* (2), 2000077. https://doi.org/10.1002/aesr.202000077.

(68) Wenzel, S.; Weber, D. A.; Leichtweiss, T.; Busche, M. R.; Sann, J.; Janek, J. Interphase Formation and Degradation of Charge Transfer Kinetics between a Lithium Metal Anode and Highly Crystalline Li7P3S11 Solid Electrolyte. *Solid State Ionics* **2017**, *286* (August), 24–33. https://doi.org/10.1016/j.ssi.2015.11.034.

(69) Zhu, Y.; He, X.; Mo, Y. First Principles Study on Electrochemical and Chemical Stability of Solid Electrolyte–Electrode Interfaces in All-Solid-State Li-Ion Batteries. *J. Mater. Chem. A* **2016**, *4* (9), 3253–3266. https://doi.org/10.1039/C5TA08574H.

(70) Yao, X.; Huang, B.; Yin, J.; Peng, G.; Huang, Z.; Gao, C.; Liu, D.; Xu, X.; Yao, X.; Huang, B.; Yin, J.; Peng, G.; Huang, Z.; Gao, C.; Liu, D.; Xu, X. All-Solid-State Lithium Batteries with Inorganic Solid Electrolytes: Review of Fundamental Science. *Chinese Phys. B* **2016**, *25* (1), 18802. https://doi.org/10.1088/1674-1056/25/1/018802.

(71) Koerver, R.; Zhang, W.; De Biasi, L.; Schweidler, S.; Kondrakov, A. O.; Kolling, S.; Brezesinski, T.; Hartmann, P.; Zeier, W. G.; Janek, J. Chemo-Mechanical Expansion of Lithium Electrode Materials – on the Route to Mechanically Optimized All-Solid-State Batteries. *Energy Environ. Sci.* **2018**, *11* (8), 2142–2158. https://doi.org/10.1039/C8EE00907D.

(72) Zhu, Y.; He, X.; Mo, Y. Origin of Outstanding Stability in the Lithium Solid Electrolyte Materials : Insights from Thermodynamic Analyses Based on First- Principles Calculations. *ACS Appl. Energy Mater.* **2015**, *7*, 23685–23693. https://doi.org/10.1021/acsami.5b07517.

(73) Wenzel, S.; Leichtweiss, T.; Krüger, D.; Sann, J.; Janek, J. Interphase Formation on Lithium Solid Electrolytes — An in Situ Approach to Study Interfacial Reactions by Photoelectron Spectroscopy. *Solid State Ionics* **2015**, *278*, 98–105.

https://doi.org/10.1016/j.ssi.2015.06.001.

(74) Liu, Y.; Li, C.; Li, B.; Song, H.; Cheng, Z.; Chen, M.; He, P. Germanium Thin Film Protected Lithium Aluminum Germanium Phosphate for Solid-State Li Batteries. *Adv. Energy Mater.* **2018**, *8*, 1702374. https://doi.org/10.1002/aenm.201702374.

(75) Wu, L.; He, G.; Ding, Y. Ultrathin Al Foils to Fabricate Dendrite-Free Li-Al Anodes. *J. Mater. Chem. A* **2019**, *7* (44), 25415–25422. https://doi.org/10.1039/c9ta09464d.

(76) Hamann, C. H.; Vielstich, W. *Elektrochemie*, 4th ed.; Wiley-VCH Verlag GmbH & Co. KGaA: Weinheim, 2005.

(77) Gritzner, G.; Kuta, J. Recommendations on Reporting Electrode Potentials in Nonaqueous Solvents. *Electrochim. Acta* **1984**, *29* (6), 869–873. https://doi.org/10.1016/0013-4686(80)87041-1.

(78) Oh, S. K.; Kim, D.; Choi, A.; Kang, Y.; Ryu, K. H.; Jang, M. Two-Dimensional Phosphorene-Derived Protective Layers on a Lithium Metal Anode for Lithium-Oxygen Batteries. *ACS Nano* **2018**, *12* (5), 4419–4430. https://doi.org/10.1021/acsnano.8b00348.

(79) Yoon, I.; Jurng, S.; Abraham, D. P.; Lucht, B. L.; Guduru, P. R. Measurement of Mechanical and Fracture Properties of Solid Electrolyte Interaphase on Lithium Metal Anodes in Lithium Ion Batteries. *Energy Storage Mater.* **2019**, *25*, 296–304. https://doi.org/10.1016/j.ensm.2019.10.009.

(80) Lu, M.; Cheng, H.; Yang, Y. A Comparison of Solid Electrolyte Interphase (SEI) on the Artificial Graphite Anode of the Aged and Cycled Commercial Lithium Ion Cells. *Electrochim. Acta* **2008**, *53* (9), 3539–3546. https://doi.org/10.1016/J.ELECTACTA.2007.09.062.

(81) Agubra, V. A.; Fergus, J. W. The Formation and Stability of the Solid Electrolyte Interface on the Graphite Anode. *J. Power Sources* **2014**, *268*, 153–162. https://doi.org/10.1016/J.JPOWSOUR.2014.06.024.

(82) Hobold, G. M.; Lopez, J.; Guo, R.; Minafra, N.; Banerjee, A.; Shirley Meng, Y.; Shao-Horn, Y.; Gallant, B. M. Moving beyond 99.9% Coulombic Efficiency for Lithium Anodes in Liquid Electrolytes. *Nat. Energy* **2021**, *6*, 951–960. https://doi.org/10.1038/s41560-021-00910-w.

(83) Ran, Q.; Han, C.; Tang, A.; Chen, H.; Tang, Z.; Jiang, K.; Mai, Y.; Wang, J. Multifunctional Artificial Solid Electrolyte Interphase Layer for Lithium Metal Anode in Carbonate Electrolyte. *Solid State Ionics* **2020**, *344* (August 2019), 115095.

https://doi.org/10.1016/j.ssi.2019.115095.

(84) Hou, G.; Ci, C.; Salpekar, D.; Ai, Q.; Chen, Q.; Guo, H.; Chen, L.; Zhang, X.; Cheng, J.; Kato, K.; Vajtai, R.; Si, P.; Babu, G.; Ci, L.; Ajayan, P. M. Stable Lithium Metal Anode Enabled by an Artificial Multi-Phase Composite Protective Film. *J. Power Sources* **2020**, *448* (November 2019), 227547. https://doi.org/10.1016/j.jpowsour.2019.227547.

(85) Górecki, T. The Relations between the Shear Modulus, the Bulk Modulus and Young's Modulus for Polycrystalline Metallic Elements. *Mater. Sci. Eng.* **1980**, *43* (3), 225–230. https://doi.org/10.1016/0025-5416(80)90106-8.

(86) Monroe, C.; Newman, J. The Impact of Elastic Deformation on Deposition Kinetics at Lithium/Polymer Interfaces. *J. Electrochem. Soc.* **2005**, *152* (2), A396–A404. https://doi.org/10.1149/1.1850854.

(87) Liang, X.; Pang, Q.; Kochetkov, I. R.; Sempere, M. S.; Huang, H.; Sun, X.; Nazar, L. F. A Facile Surface Chemistry Route to a Stabilized Lithium Metal Anode. *Nat. Energy* **2017**, *2*, 17119. https://doi.org/10.1038/nenergy.2017.119.

(88) Liu, S.; Zhao, Q.; Zhang, X.; Liu, J.; Dai, L.; Wang, L.; Luo, J. A High Rate and Long Cycling Life Lithium Metal Anode with a Self-Repairing Alloy Coating. *J. Mater. Chem. A* **2020**, *8* (34), 17415–17419. https://doi.org/10.1039/d0ta06126c.

(89) Chae, O. B.; Adiraju, V. A. K.; Lucht, B. L. Performance Improvement of Lithium Metal Batteries Enabled By LiBF 3 CN as a New Electrolyte Additive. *J. Electrochem. Soc.* **2022**, *169*, 110506. https://doi.org/10.1149/1945-7111/ac9d67.

(90) Barr, T. L. An ESCA Study of the Termination of the Passivation of Elemental Metals1. *ESCA Study Elem. Met. Oxid. J. Phys. Chem.* **1978**, *82* (16), 1801.

(91) Churikov, A. V.; Nimon, E. S.; L´vov, A. L. Simulation of Ionic Transport in Passivating Films on the Lithium Electrode. *Russ. J. Electrochem.* **1998**, *34* (7), 591–599.

(92) Momma, T.; Nara, H.; Yamagami, S.; Tatsumi, C.; Osaka, T. Effect of the Atmosphere on Chemical Composition and Electrochemical Properties of Solid Electrolyte Interface on Electrodeposited Li Metal. *J. Power Sources* **2011**, *196* (15), 6483–6487. https://doi.org/10.1016/J.JPOWSOUR.2011.03.095.

(93) Peled, E. The Electrochemical Behavior of Alkali and Alkaline Earth Metals in Nonaqueous Battery Systems—The Solid Electrolyte Interphase Model. *J. Electrochem. Soc.* **1979**, *126* (12), 2047. https://doi.org/10.1149/1.2128859.

(94) Zhang, Z.; Li, Y.; Xu, R.; Zhou, W.; Li, Y.; Oyakhire, S. T.; Wu, Y.; Xu, J.; Wang, H.;

Yu, Z.; Boyle, D. T.; Huang, W.; Ye, Y.; Chen, H.; Wan, J.; Bao, Z.; Chiu, W.; Cui, Y. Capturing the Swelling of Solid-Electrolyte Interphase in Lithium Metal Batteries. *Science (80-. ).* **2022**, *375* (6576), 66–70. https://doi.org/10.1126/SCIENCE.ABI8703.

(95) Attia, P. M.; Chueh, W. C.; Harris, S. J. Revisiting the t 0.5 Dependence of SEI Growth. *J. Electrochem. Soc.* **2020**, *167*, 090535. https://doi.org/10.1149/1945-7111/ab8ce4.

(96) Kindermann, F. M.; Keil, J.; Frank, A.; Jossen, A. A SEI Modeling Approach Distinguishing between Capacity and Power Fade. *J. Electrochem. Soc.* **2017**, *164* (12), E287–E294. https://doi.org/10.1149/2.0321712jes.

(97) Kamyab, N.; Weidner, J. W.; White, R. E. Mixed Mode Growth Model for the Solid Electrolyte Interface (SEI). *J. Electrochem. Soc.* **2019**, *166* (2), A334–A341. https://doi.org/10.1149/2.1101902jes.

(98) Nakamura, T.; Amezawa, K.; Kulisch, J.; Zeier, W. G.; Janek, J. Guidelines for All-Solid-State Battery Design and Electrode Buffer Layers Based on Chemical Potential Profile Calculation. *ACS Appl. Mater. Interfaces* **2019**, *11* (22), 19968–19976. https://doi.org/10.1021/ACSAMI.9B03053/SUPPL_FILE/AM9B03053_SI_002.XLSX.

(99) Single, F.; Latz, A.; Horstmann, B. Identifying the Mechanism of Continued Growth of the Solid–Electrolyte Interphase. *ChemSusChem* **2018**, *11* (12), 1950–1955. https://doi.org/10.1002/CSSC.201800077.

(100) Menkin, S.; O'Keefe, C. A.; Gunnarsdottir, A. B.; Dey, S.; Pesci, F.; Shen, Z.; Aguadero, A.; Grey, C. P. Towards an Understanding of the SEI Formation and Lithium Preferential Plating on Copper. *ECS Meet. Abstr.* **2020**, *MA2020-02* (45), 3773–3773. https://doi.org/10.1149/ma2020-02453773mtgabs.

(101) Guo, R.; Gallant, B. M. Li 2 O Solid Electrolyte Interphase: Probing Transport Properties at the Chemical Potential of Lithium. *Chem. Lett.* **2020**, *32*, 5525–5533. https://doi.org/10.1021/acs.chemmater.0c00333.

(102) Lorger, S.; Usiskin, R.; Maier, J. Transport and Charge Carrier Chemistry in Lithium Oxide. *J. Electrochem. Soc.* **2019**, *166* (10), A2215–A2220. https://doi.org/10.1149/2.1121910jes.

(103) Yildirim, H.; Kinaci, A.; Chan, M. K. Y.; Greeley, J. P. First-Principles Analysis of Defect Thermodynamics and Ion Transport in Inorganic SEI Compounds: LiF and NaF. *ACS Appl. Mater. Interfaces* **2015**, *7*, 18985–18996. https://doi.org/10.1021/acsami.5b02904.

(104) Churikov, A. V. Ion Transport Mechanism in Solid Electrolyte Films on Lithium. *Tech.*

*Phys.* **2005**, *50* (11), 1490–1496. https://doi.org/10.1134/1.2131960/METRICS.

(105) He, M.; Guo, R.; Hobold, G. M.; Gao, H.; Gallant, B. M. The Intrinsic Behavior of Lithium Fluoride in Solid Electrolyte Interphases on Lithium. *Appl. Phys. Sci.* **2019**, *117* (1), 73–79. https://doi.org/10.1073/pnas.1911017116.

(106) Walter, E.; Spotte-Smith, C.; Kam, R. L.; Barter, D.; Xie, X.; Hou, T.; Dwaraknath, S.; Blau, S. M.; Persson, K. A. Toward a Mechanistic Model of Solid− Electrolyte Interphase Formation and Evolution in Lithium-Ion Batteries. *ACS Energy Lett* **2022**, *7*, 1446–1453. https://doi.org/10.1021/acsenergylett.2c00517.

(107) Guo, R.; Wang, D.; Zuin, L.; Gallant, B. M. Reactivity and Evolution of Ionic Phases in the Lithium Solid−Electrolyte Interphase. *ACS Energy Lett* **2021**, *6*, 877–885. https://doi.org/10.1021/acsenergylett.1c00117.

(108) Fiedler, C.; Luerssen, B.; Rohnke, M.; Sann, J.; Janek, J. XPS and SIMS Analysis of Solid Electrolyte Interphases on Lithium Formed by Ether-Based Electrolytes. *J. Electrochem. Soc.* **2017**, *164* (14), A3742–A3749. https://doi.org/10.1149/2.0851714jes.

(109) Soto, F. A.; Ma, Y.; Martinez De La Hoz, J. M.; Seminario, J. M.; Balbuena, P. B. Formation and Growth Mechanisms of Solid-Electrolyte Interphase Layers in Rechargeable Batteries. *Chem. Mater.* **2015**, *27*, 7990–8000. https://doi.org/10.1021/acs.chemmater.5b03358.

(110) Krauss, F. T.; Pantenburg, I.; Roling, B. Transport of Ions, Molecules, and Electrons across the Solid Electrolyte Interphase: What Is Our Current Level of Understanding? *Adv. Mater. Interfaces* **2022**, *9* (8). https://doi.org/10.1002/admi.202101891.

(111) Von Kolzenberg, L.; Werres, M.; Tetzloff, J.; Horstmann, B. Transition between Growth of Dense and Porous Films: Theory of Dual-Layer SEI †. *Phys. Chem. Chem. Phys.* **2022**, *24*, 18469. https://doi.org/10.1039/d2cp00188h.

(112) Attia, P. M.; Das, S.; Harris, S. J.; Bazant, M. Z.; Chueh, W. C. Electrochemical Kinetics of SEI Growth on Carbon Black: Part I. Experiments. *J. Electrochem. Soc.* **2016**, *166* (4), E97–E106. https://doi.org/10.1149/2.0231904jes.

(113) Das, S.; Attia, P. M.; Chueh, W. C.; Bazant, M. Z. Electrochemical Kinetics of SEI Growth on Carbon Black: Part II. Modeling. *J. Electrochem. Soc.* **2019**, *166* (4), E107–E118. https://doi.org/10.1149/2.0241904jes.

(114) Li, Y.; Li, Y.; Sun, Y.; Butz, B.; Yan, K.; Koh, A. L.; Zhao, J.; Pei, A.; Cui, Y.; Nano, S. Revealing Nanoscale Passivation and Corrosion Mechanisms of Reactive Battery

Materials in Gas Environments. *Nano Lett* **2017**, *17*, 22. https://doi.org/10.1021/acs.nanolett.7b02630.

(115) Wang, W.; Yue, X.; Meng, J.; Wang, J.; Wang, X.; Chen, H.; Fu, J.; Zhou, Y.; Chen, J.; Fu, Z. Lithium Phosphorus Oxynitride as an Efficient Protective Layer on Lithium Metal Anodes for Advanced Lithium-Sulfur Batteries. *Energy Storage Mater.* **2019**, *18*, 414–422. https://doi.org/10.1016/j.ensm.2018.08.010.

(116) Camacho-Forero, L. E.; Smith, T. W.; Balbuena, P. B. Effects of High and Low Salt Concentration in Electrolytes at Lithium−Metal Anode Surfaces. *J. Phys. Chem. C* **2017**, *121*, 182–194. https://doi.org/10.1021/acs.jpcc.6b10774.

(117) Frenck, L.; Sethi, G. K.; Maslyn, J. A.; Balsara, N. P. Factors That Control the Formation of Dendrites and Other Morphologies on Lithium Metal Anodes. *Front. Energy Res.* **2019**, *7* (November), 115. https://doi.org/10.3389/fenrg.2019.00115.

(118) Monroe, C.; Newman, J. Dendrite Growth in Lithium-Polymer Systems. *J. Electrochem. Soc.* **2003**, *150* (10), A1377–A1384. https://doi.org/10.1149/1.1606686.

(119) Ding, F.; Xu, W.; Graff, G. L.; Zhang, J.; Sushko, M. L.; Chen, X.; Shao, Y.; Engelhard, M. H.; Nie, Z.; Xiao, J.; Liu, X.; Sushko, P. V.; Liu, J.; Zhang, J. G. Dendrite-Free Lithium Deposition via Self-Healing Electrostatic Shield Mechanism. *J. Am. Chem. Soc.* **2013**, *135* (11), 4450–4456. https://doi.org/10.1021/ja312241y.

(120) Fleury, V.; Chazalviel, J. N.; Rosso, M.; Sapoval, B. The Role of the Anions in the Growth Speed of Fractal Electrodeposits. *J. Electroanal. Chem.* **1990**, *290* (1–2), 249–255. https://doi.org/10.1016/0022-0728(90)87434-L.

(121) Bai, P.; Guo, J.; Wang, M.; Kushima, A.; Su, L.; Li, J.; Brushett, F. R.; Bazant, M. Z. Interactions between Lithium Growths and Nanoporous Ceramic Separators. *Joule* **2018**, *2* (11), 2434–2449. https://doi.org/10.1016/J.JOULE.2018.08.018.

(122) Cipolla, A.; Barchasz, C.; Mathieu, B.; Chavillon, B.; Martinet, S. Effect of Electrochemical and Mechanical Properties of SEI on Dendritic Growth during Lithium Deposition on Lithium Metal Electrode. *J. Power Sources* **2022**, *545*, 231898.

(123) Steiger, J.; Kramer, D.; Mönig, R. Microscopic Observations of the Formation, Growth and Shrinkage of Lithium Moss during Electrodeposition and Dissolution. *Electrochim. Acta* **2014**, *136*, 529–536. https://doi.org/10.1016/J.ELECTACTA.2014.05.120.

(124) Steiger, J.; Richter, G.; Wenk, M.; Kramer, D.; Mönig, R. Comparison of the Growth of Lithium Filaments and Dendrites under Different Conditions. *Electrochem. commun.*

**2015**, *50*, 11–14. https://doi.org/10.1016/J.ELECOM.2014.11.002.

(125) Sand, H. J. S. III. On the Concentration at the Electrodes in a Solution, with Special Reference to the Liberation of Hydrogen by Electrolysis of a Mixture of Copper Sulphate and Sulphuric Acid . *London, Edinburgh, Dublin Philos. Mag. J. Sci.* **1901**, *1* (1), 45–79. https://doi.org/10.1080/14786440109462590.

(126) Su, L.; Manthiram, A. Lithium-Metal Batteries via Suppressing Li Dendrite Growth and Improving Coulombic Efficiency. *Small Struct.* **2022**, *3* (10), 2200114. https://doi.org/10.1002/SSTR.202200114.

(127) Bai, P.; Li, J.; Brushett, F. R.; Bazant, M. Z. Transition of Lithium Growth Mechanisms in Liquid Electrolytes. *Energy Environ. Sci.* **2016**, *9* (10), 3221–3229. https://doi.org/10.1039/c6ee01674j.

(128) Maraschky, A.; Akolkar, R. Mechanism Explaining the Onset Time of Dendritic Lithium Electrodeposition via Considerations of the Li + Transport within the Solid Electrolyte Interphase. *J. Electrochem. Soc.* **2018**, *165* (14), 696–703. https://doi.org/10.1149/2.0601814jes.

(129) Aurbach, D.; Pollak, E.; Elazari, R.; Salitra, G.; Kelley, C. S.; Affinito, J. On the Surface Chemical Aspects of Very High Energy Density , Rechargeable Li – Sulfur Batteries On the Surface Chemical Aspects of Very High Energy Density , Rechargeable Li – Sulfur Batteries. *J. Electrochem. Soc.* **2009**, *156* (8), A694–A702. https://doi.org/10.1149/1.3148721.

(130) Qie, L.; Zu, C.; Manthiram, A. A High Energy Lithium-Sulfur Battery with Ultrahigh-Loading Lithium Polysulfide Cathode and Its Failure Mechanism. *Adv. Energy Mater.* **2016**, *6*, 1502459. https://doi.org/10.1002/aenm.201502459.

(131) Mikhaylik, Y. V; Akridge, J. R. Polysulfide Shuttle Study in the Li / S Battery System. *J. Electrochem. Soc.* **2004**, *151* (11), A1969–A1976. https://doi.org/10.1149/1.1806394.

(132) Akridge, J. R.; Mikhaylik, Y. V.; White, N. Li/S Fundamental Chemistry and Application to High-Performance Rechargeable Batteries. *Solid State Ionics* **2004**, *175* (1–4), 243–245. https://doi.org/10.1016/J.SSI.2004.07.070.

(133) Luo, J.; Lee, R. C.; Jin, J. T.; Weng, Y. T.; Fang, C. C.; Wu, N. L. A Dual-Functional Polymer Coating on a Lithium Anode for Suppressing Dendrite Growth and Polysulfide Shuttling in Li-S Batteries. *Chem. Commun.* **2017**, *53* (5), 963–966. https://doi.org/10.1039/c6cc09248a.

(134) Kamphaus, E. P.; Balbuena, P. B. Effects of Dimethyl Disulfide Cosolvent on Li-S Battery Chemistry and Performance. *Chem. Mater.* **2019**, *31* (7), 2377–2389. https://doi.org/10.1021/acs.chemmater.8b04821.

(135) Mikhaylik, Y. V. ELECTROLYTES FOR LITHIUM SULFUR CELLS. *US Pat. 7354680 B2* **2008**, *2* (12).

(136) Duangdangchote, S.; Krittayavathananon, A.; Phattharasupakun, N.; Joraleechanchai, N.; Sawangphruk, M. Insight into the Effect of Additives Widely Used in Lithium-Sulfur Batteries. *Chem. Commun.* **2019**, *55* (93), 13951–13954. https://doi.org/10.1039/c9cc06504k.

(137) Manthiram, A.; Fu, Y.; Chung, S.; Zu, C.; Su, Y. Rechargeable Lithium − Sulfur Batteries. *Chem. Rev.* **2014**, *114*, 11751–11787. https://doi.org/10.1021/cr500062v.

(138) Komaba, S.; Kumagai, N.; Kataoka, Y. Influence of Manganese(II), Cobalt(II), and Nickel(II) Additives in Electrolyte on Performance of Graphite Anode for Lithium-Ion Batteries. *Electrochim. Acta* **2002**, *47* (8), 1229–1239. https://doi.org/10.1016/S0013-4686(01)00847-7.

(139) Amine, K.; Chen, Z.; Zhang, Z.; Liu, J.; Lu, W.; Qin, Y.; Lu, J.; Curtis, L.; Sun, Y. K. Mechanism of Capacity Fade of MCMB/Li1.1[Ni1/3Mn1/3Co1/3]0.9O2cell at Elevated Temperature and Additives to Improve Its Cycle Life. *J. Mater. Chem.* **2011**, *21* (44), 17754–17759. https://doi.org/10.1039/C1JM11584G.

(140) Joshi, T.; Eom, K.; Yushin, G.; Fuller, T. F. Effects of Dissolved Transition Metals on the Electrochemical Performance and SEI Growth in Lithium-Ion Batteries. *J. Electrochem. Soc.* **2014**, *161* (12), A1915–A1921. https://doi.org/10.1149/2.0861412jes.

(141) Zheng, H.; Sun, Q.; Liu, G.; Song, X.; Battaglia, V. S. Correlation between Dissolution Behavior and Electrochemical Cycling Performance for LiNi 1/3Co 1/3Mn 1/3O 2-Based Cells. *J. Power Sources* **2012**, *207*, 134–140. https://doi.org/10.1016/J.JPOWSOUR.2012.01.122.

(142) Betz, J.; Brinkmann, J. P.; Nölle, R.; Lürenbaum, C.; Kolek, M.; Stan, M. C.; Winter, M.; Placke, T. Cross Talk between Transition Metal Cathode and Li Metal Anode: Unraveling Its Influence on the Deposition/Dissolution Behavior and Morphology of Lithium. *Adv. Energy Mater.* **2019**, *9* (21). https://doi.org/10.1002/AENM.201900574.

(143) Zhang, X.-Q.; Wang, X.-M.; Li, B.-Q.; Shi, P.; Huang, J.-Q.; Chen, A.; Zhang, Q. Crosstalk Shielding of Transition Metal Ions for Long Cycling Lithium-Metal Batteries †. *J. Mater. Chem. A* **2020**, *8*, 4283. https://doi.org/10.1039/c9ta12269a.

(144) Langdon, J.; Manthiram, A. Crossover Effects in Batteries with High-Nickel Cathodes and Lithium-Metal Anodes. *Adv. Funct. Mater.* **2021**, *31*, 2010267. https://doi.org/10.1002/ADFM.202010267.

(145) Langdon, J.; Manthiram, A. Crossover Effects in Lithium-metal Batteries with a Localized High Concentration Electrolyte and High-nickel Cathodes. *Adv. Mater.* **2022**, 2205188. https://doi.org/10.1002/ADMA.202205188.

(146) Zeng, W.; Cheng, M. M. C.; Ng, S. K. Y. Effects of Transition Metal Cation Additives on the Passivation of Lithium Metal Anode in Li–S Batteries. *Electrochim. Acta* **2019**, *319*, 511–517. https://doi.org/10.1016/j.electacta.2019.06.177.

(147) Bi, X.; Amine, K.; Lu, J. The Importance of Anode Protection towards Lithium Oxygen Batteries. *J. Mater. Chem. A* **2020**, *8*, 3563–3573. https://doi.org/10.1039/c9ta12414d.

(148) Haas, R.; Murat, M.; Weiss, M.; Janek, J.; Natan, A.; Schröder, D. Understanding the Transport of Atmospheric Gases in Liquid Electrolytes for Lithium-Air Batteries. *J. Electrochem. Soc.* **2021**, *168*, 070504. https://doi.org/10.1149/1945-7111/ac0d66.

(149) Wang, E.; Dey, S.; Liu, T.; Menkin, S.; Grey, C. P. Effects of Atmospheric Gases on Li Metal Cyclability and Solid-Electrolyte Interphase Formation. *ACS Energy Lett* **2020**, *5*, 1088–1094. https://doi.org/10.1021/acsenergylett.0c00257.

(150) Lee, H.; Lee, D. J.; Lee, J. N.; Song, J.; Lee, Y.; Ryou, M. H.; Park, J. K.; Lee, Y. M. Chemical Aspect of Oxygen Dissolved in a Dimethyl Sulfoxide-Based Electrolyte on Lithium Metal. *Electrochim. Acta* **2014**, *123*, 419–425. https://doi.org/10.1016/J.ELECTACTA.2014.01.042.

(151) Qiu, F.; Zhang, X.; Qiao, Y.; Zhang, X.; Deng, H.; Shi, T.; He, P.; Zhou, H. An Ultra-Stable and Enhanced Reversibility Lithium Metal Anode with a Sufficient O2 Design for Li-O2 Battery. *Energy Storage Mater.* **2018**, *12*, 176–182. https://doi.org/10.1016/j.ensm.2017.12.011.

(152) Haas, R.; Janek, J. The Influence of Oxygen Dissolved in the Liquid Electrolyte on Lithium Metal Anodes. *J. Electrochem. Soc.* **2022**, *169* (11), 110527. https://doi.org/10.1149/1945-7111/AC9D6B.

(153) Chen, K.; Huang, G.; Ma, J. L.; Wang, J.; Yang, D. Y.; Yang, X. Y.; Yu, Y.; Zhang, X. B. The Stabilization Effect of CO2 in Lithium–Oxygen/CO2 Batteries. *Angew. Chemie Int. Ed.* **2020**, *59* (38), 16661–16667. https://doi.org/10.1002/ANIE.202006303.

(154) Cho, M. H.; Trottier, J.; Gagnon, C.; Hovington, P.; Clément, D.; Vijh, A.; Kim, C. S.;

Guerfi, A.; Black, R.; Nazar, L.; Zaghib, K. The Effects of Moisture Contamination in the Li-O2 Battery. *J. Power Sources* **2014**, *268*, 565–574. https://doi.org/10.1016/J.JPOWSOUR.2014.05.148.

(155) Huang, S.; Cui, Z.; Zhao, N.; Sun, J.; Guo, X. Influence of Ambient Air on Cell Reactions of Li-Air Batteries. *Electrochim. Acta* **2016**, *191*, 473–478. https://doi.org/10.1016/J.ELECTACTA.2016.01.102.

(156) Ha, S.; Kim, Y.; Koo, D.; Ha, K.-H.; Park, Y.; Kim, D.-M.; Son, S.; Yim, T.; Lee, K. T. Investigation into the Stability of Li Metal Anodes in Li-O 2 Batteries with a Redox Mediator †. *J. Mater. Chem. A* **2017**, *5*, 10609–10621. https://doi.org/10.1039/c7ta02210g.

(157) Bergner, B. J.; Schürmann, A.; Peppler, K.; Garsuch, A.; Janek, J. TEMPO: A Mobile Catalyst for Rechargeable Li-O 2 Batteries. *J. Am. Chem. Soc.* **2014**, *136*, 15054–15064. https://doi.org/10.1021/ja508400m.

(158) Bergner, B. J.; Hofmann, C.; Schürmann, A.; Schröder, D.; Peppler, K.; Schreiner, P. R.; Janek, J. Understanding the Fundamentals of Redox Mediators in Li-O 2 Batteries: A Case Study on Nitroxides †. *Phys. Chem. Chem. Phys* **2015**, *17*, 31769–31779. https://doi.org/10.1039/c5cp04505c.

(159) Manthiram, A.; Yu, X.; Wang, S. Lithium Battery Chemistries Enabled by Solid-State Electrolytes. *Nat. Rev. Mater.* **2017**, *2* (4), 1–16. https://doi.org/10.1038/natrevmats.2016.103.

(160) Zhang, R.; Strauss, F.; Jiang, L.; Casalena, L.; Li, L.; Janek, J.; Kondrakov, A.; Brezesinski, T. Transition-Metal Interdiffusion and Solid Electrolyte Poisoning in All-Solid-State Batteries Revealed by Cryo-TEM. *Chem. Commun.* **2023**, *59*, 4600–4603. https://doi.org/10.1039/d3cc00516j.

(161) Guo, F.; Wu, C.; Chen, H.; Zhong, F.; Ai, X.; Yang, H.; Qian, J. Dendrite-Free Lithium Deposition by Coating a Lithiophilic Heterogeneous Metal Layer on Lithium Metal Anode. *Energy Storage Mater.* **2020**, *24* (January), 635–643. https://doi.org/10.1016/j.ensm.2019.06.010.

(162) Qu, S.; Jia, W.; Wang, Y.; Li, C.; Yao, Z.; Li, K.; Liu, Y.; Zou, W.; Zhou, F.; Wang, Z.; Li, J. Air-Stable Lithium Metal Anode with Sputtered Aluminum Coating Layer for Improved Performance. *Electrochim. Acta* **2019**, *317*, 120–127. https://doi.org/10.1016/j.electacta.2019.05.138.

(163) Tang, W.; Yin, X.; Kang, S.; Chen, Z.; Tian, B.; Teo, S. L.; Wang, X.; Chi, X.; Loh, K. P.; Lee, H.; Zheng, G. W. Lithium Silicide Surface Enrichment : A Solution to Lithium Metal

Battery. *Adv. Mater.* **2018**, *30*, 1801745. https://doi.org/10.1002/adma.201801745.

(164) Kang, D.; Hart, N.; Koh, J.; Ma, L.; Liang, W.; Xu, J.; Sardar, S.; Lemmon, J. P. Rearrange SEI with Artificial Organic Layer for Stable Lithium Metal Anode. *Energy Storage Mater.* **2020**, *24* (March), 618–625. https://doi.org/10.1016/j.ensm.2019.06.014.

(165) Guoxing Li, Qingquan Huang, Xin He, Yue Gao, Daiwei Wang, Seong H. Kim, D. W. Self-Formed Hybrid Interphase Layer on Lithium Metal for High-Performance Lithium–Sulfur Batteries. *ACS Nano* **2018**, *12*, 1500–1507. https://doi.org/10.1021/acsnano.7b08035.

(166) Nazri, G. PREPARATION, STRUCTURE AND IONIC CONDUCTIVITY OF LITHIUM PHOSPHIDE. *Solid State Ionics* **1989**, *34*, 97–102.

(167) von Alpen, U. Li3N: A Promising Li Ionic Conductor. *J. Solid State Chem.* **1979**, *29*, 379–392.

(168) Ma, G.; Wen, Z.; Wu, M.; Shen, C.; Wang, Q.; Jin, J.; Wu, X. A Lithium Anode Protection Guided Highly-Stable Lithium–Sulfur Battery. *Chem. Commun.* **2014**, *50*, 14209–14212. https://doi.org/10.1039/C4CC05535G.

(169) Lin, L.; Liang, F.; Zhang, K.; Mao, H.; Yang, J.; Qian, Y. Lithium Phosphide/Lithium Chloride Coating on Lithium for Advanced Lithium Metal Anode. *J. Mater. Chem. A Mater. energy Sustain.* **2018**, *6*, 15859–15867. https://doi.org/10.1039/C8TA05102J.

(170) Zhang, X. Q.; Cheng, X. B.; Chen, X.; Yan, C.; Zhang, Q. Fluoroethylene Carbonate Additives to Render Uniform Li Deposits in Lithium Metal Batteries. *Adv. Funct. Mater.* **2017**, *27* (10). https://doi.org/10.1002/adfm.201605989.

(171) Zheng, J.; Ju, Z.; Zhang, B.; Nai, J.; Liu, T.; Liu, Y.; Xie, Q.; Zhang, W.; Wang, Y.; Tao, X. Lithium Ion Diffusion Mechanism on the Inorganic Components of the Solid-Electrolyte Interphase. *J. Mater. Chem. A* **2021**, *9*, 10251–10259. https://doi.org/10.1039/d0ta11444h.

(172) Edström, K.; Herstedt, M.; Abraham, D. P. A New Look at the Solid Electrolyte Interphase on Graphite Anodes in Li-Ion Batteries. *J. Power Sources* **2006**, *153* (2), 380–384. https://doi.org/10.1016/j.jpowsour.2005.05.062.

(173) Xu, N.; Shi, J.; Liu, G.; Yang, X.; Zheng, J.; Zhang, Z.; Yang, Y. Research Progress of Fluorine-Containing Electrolyte Additives for Lithium Ion Batteries. *J. Power Sources Adv.* **2021**, *7*, 100043. https://doi.org/10.1016/j.powera.2020.100043.

(174) Teufl, T.; Pritzl, D.; Hartmann, L.; Solchenbach, S.; Mendez, M. A.; Gasteiger, H. A.

Implications of the Thermal Stability of FEC-Based Electrolytes for Li-Ion Batteries. *J. Electrochem. Soc.* **2023**, *170*, 020531. https://doi.org/10.1149/1945-7111/acbc52.

(175) Lu, Y.; Tu, Z.; Archer, L. A. Stable Lithium Electrodeposition in Liquid and Nanoporous Solid Electrolytes. *Nat. Mater.* **2014**, *13* (10), 961–969. https://doi.org/10.1038/nmat4041.

(176) Chen, L.; Chen, K.-S.; Chen, X.; Ramirez, G.; Huang, Z.; Geise, N. R.; Steinrü, H.-G.; Fisher, B. L.; Shahbazian-Yassar, R.; Toney, M. F.; Hersam, M. C.; Elam, J. W. Novel ALD Chemistry Enabled Low-Temperature Synthesis of Lithium Fluoride Coatings for Durable Lithium Anodes. *ACS Appl. Mater. Interfaces* **2018**, *10*, 26972–26981. https://doi.org/10.1021/acsami.8b04573.

(177) Guan, P.; Liu, L.; Lin, X. Simulation and Experiment on Solid Electrolyte Interphase (SEI) Morphology Evolution and Lithium-Ion Diffusion. *J. Electrochem. Soc.* **2015**, *162* (9), A1798–A1808. https://doi.org/10.1149/2.0521509jes.

(178) Pathak, R.; Chen, K.; Gurung, A.; Reza, K. M.; Bahrami, B.; Pokharel, J.; Baniya, A.; He, W.; Wu, F.; Zhou, Y.; Xu, K.; Qiao, Q. Q. Fluorinated Hybrid Solid-Electrolyte-Interphase for Dendrite-Free Lithium Deposition. *Nat. Commun.* **2020**, *11*, 93. https://doi.org/10.1038/s41467-019-13774-2.

(179) Harrup, M. K.; Rollins, H. W.; Jamison, D. K.; Dufek, E. J.; Gering, K. L.; Luther, T. A. Unsaturated Phosphazenes as Co-Solvents for Lithium-Ion Battery Electrolytes. *J. Power Sources* **2015**, *278*, 794–801. https://doi.org/10.1016/j.jpowsour.2014.07.109.

(180) Dagger, T.; Rad, B. R.; Schappacher, F. M.; Winter, M. Comparative Performance Evaluation of Flame Retardant Additives for Lithium Ion Batteries – I. Safety, Chemical and Electrochemical Stabilities. *Energy Technol.* **2018**, *6* (10), 2011–2022. https://doi.org/10.1002/ENTE.201800132.

(181) Li, H.; Wen, Z.; Wu, D.; Ji, W.; He, Z.; Wang, F.; Yang, Y.; Zhang, P.; Zhao, J. Achieving a Stable Solid Electrolyte Interphase and Enhanced Thermal Stability by a Dual-Functional Electrolyte Additive toward a High-Loading LiNi 0.8 Mn 0.1 Co 0.1 O 2 /Lithium Pouch Battery. *ACS Appl. Mater. Interfaces* **2021**, *13*, 57142–57152. https://doi.org/10.1021/acsami.1c17209.

(182) Chen, Y.; Mao, Y.; Hao, X.; Cao, Y.; Wang, W. A Stable Fluorine-Containing Solid Electrolyte Interface toward Dendrite-Free Lithium-Metal Anode for Lithium-Sulfur Batteries. *ChemElectroChem* **2021**, *8* (8), 1500–1506. https://doi.org/10.1002/CELC.202100062.

(183) Liu, Y. F.; Wang, H. R.; Li, J. Y.; Chen, M. J.; Chen, H.; Lu, B. Y.; Ma, Q.; Wu, X. W.;

Zeng, X. X. Mixed Lithium Fluoride-Nitride Ionic Conducting Interphase for Dendrite-Free Lithium Metal Anode. *Appl. Surf. Sci.* **2021**, *541*, 148294. https://doi.org/10.1016/j.apsusc.2020.148294.

(184) He, X.; Schmohl, S.; Wiemhöfer, H. D. Comparative Study of Interfacial Behavior for Polyphosphazene Based Polymer Electrolytes and LiPF 6 in EC/DMC against Lithium Metal Anodes. *Polym. Test.* **2019**, *76* (February), 505–512. https://doi.org/10.1016/j.polymertesting.2019.04.012.

(185) Jankowsky, S.; Hiller, M. M.; Stolina, R.; Wiemh, H. Performance of Polyphosphazene Based Gel Polymer Electrolytes in Combination with Lithium Metal Anodes. *J. Power Sources* **2015**, *273*, 574–579. https://doi.org/10.1016/j.jpowsour.2014.09.077.

(186) Bai, W.-L.; Zhang, Z.; Chen, X.; Zhang, Q.; Xu, Z.-X.; Zhai, G.-Y.; Lin, X.; Liu, X.; Tsega, T. T.; Zhao, C.; Wang, K.-X.; Chen, J.-S. Phosphazene-Derived Stable and Robust Artificial SEI for Protecting Lithium Anodes of Li-O 2 Batteries †. *Chem. Commun* **2020**, *56*, 12566. https://doi.org/10.1039/d0cc05303a.

(187) Zhang, X.; Sun, C. Recent Advances in Dendrite-Free Lithium Metal Anodes for High-Performance Batteries. *Phys. Chem. Chem. Phys* **2022**, *24*, 19996. https://doi.org/10.1039/d2cp01655a.

(188) Liu, Y.; Xu, X.; Kapitanova, O. O.; Evdokimov, P. V.; Song, Z.; Matic, A.; Xiong, S. Electro-Chemo-Mechanical Modeling of Artificial Solid Electrolyte Interphase to Enable Uniform Electrodeposition of Lithium Metal Anodes. *Adv. Energy Mater.* **2022**, *12* (9), 1–8. https://doi.org/10.1002/aenm.202103589.

(189) Pan, J.; Zhang, Q.; Xiao, X.; Cheng, Y.-T.; Qi, Y. Design of Nanostructured Heterogeneous Solid Ionic Coatings through a Multiscale Defect Model. *ACS Appl. Mater. Interfaces* **2016**, *8*, 5687–5693. https://doi.org/10.1021/acsami.5b12030.

(190) Zhang, Q.; Pan, J.; Lu, P.; Liu, Z.; Verbrugge, M. W.; Sheldon, B. W.; Cheng, Y.-T.; Qi, Y.; Xiao, X. Synergetic Effects of Inorganic Components in Solid Electrolyte Interphase on High Cycle Efficiency of Lithium Ion Batteries. *Nano Lett.* **2016**, *16*, 2011–2016. https://doi.org/10.1021/acs.nanolett.5b05283.

(191) G.A. Nazri, R.A. Conell, C. J. Preparation and Physical Properties of Lithium Phosphide-Lithium Chloride, a Solid Electrolyte for Solid State Lithium Batteries. *Solid State Ionics* **1996**, *86* (88), 99–105.

(192) Wagner, B. J. Composite Solid Ion Conductors. *High Conduct. Solid Ion. Conduct.* **1989**, 146–165. https://doi.org/https://doi.org/10.1142/9789814434294_0007.

(193) Ouyang, Y.; Guo, Y.; Li, D.; Wei, Y.; Zhai, T.; Li, H. Single Additive with Dual Functional-Ions for Stabilizing Lithium Anodes. *ACS Appl. Mater. Interfaces* **2019**, *11* (12), 11360–11368. https://doi.org/10.1021/acsami.8b21420.

(194) Zu, C.; Yu, H.; Li, H. Enabling the Thermal Stability of Solid Electrolyte Interphase in Li-Ion Battery. *InfoMat* **2021**, *3* (6), 648–661. https://doi.org/10.1002/INF2.12190.

(195) Zhang, H.; Eshetu, G. G.; Judez, X.; Li, C.; Rodriguez-Martínez, L. M.; Armand, M. Elektrolytadditive Für Lithiummetallanoden Und Wiederaufladbare Lithiummetallbatterien: Fortschritte Und Perspektiven. *Angew. Chemie* **2018**, *130* (46), 15220–15246. https://doi.org/10.1002/ANGE.201712702.

(196) Kim, H.; Lee, J. T.; Lee, D. C.; Oschatz, M.; Cho, W. Il; Kaskel, S.; Yushin, G. Enhancing Performance of Li-S Cells Using a Li-Al Alloy Anode Coating. *Electrochem. commun.* **2013**, *36*, 38–41. https://doi.org/10.1016/J.ELECOM.2013.09.002.

(197) Shen, X.; Cheng, X.; Shi, P.; Huang, J.; Zhang, X.; Yan, C.; Li, T.; Zhang, Q. Lithium–Matrix Composite Anode Protected by a Solid Electrolyte Layer for Stable Lithium Metal Batteries. *J. Energy Chem.* **2019**, *37*, 29–34. https://doi.org/10.1016/j.jechem.2018.11.016.

(198) Sun, B.; Lang, J.; Liu, K.; Hussain, N.; Fang, M.; Wu, H. Promoting a Highly Stable Lithium Metal Anode by Superficial Alloying with an Ultrathin Indium Sheet. *Chem. Commun.* **2019**, *55* (11), 1592–1595. https://doi.org/10.1039/C8CC08934E.

(199) Tu, Y.; Ma, Q.; Wang, A.; Zhang, X.; Li, G.; Luo, J.; Liu, X. Skin Care Design for Lithium Metal Protection with Cosmetics Introduction. *J. Energy Chem.* **2020**, *48*, 383–389. https://doi.org/10.1016/j.jechem.2020.01.036.

(200) Krauskopf, B.; Otto, S.-K.; Moryson, Y.; Hoffmann, F.; Sann, J.; Janek, J. Thin and Homogenous Surface Functionalization of Lithium Metal Anodes by Defined Molecular Treatment. *J. Electrochem. Soc.* **2023**, *170* (3), 030537. https://doi.org/10.1149/1945-7111/ACC698.

(201) Tang, S.; Zhang, X.; Li, Y.; Tian, J.; Zhao, Y.; Mai, L.; Wang, L.; Cao, Y.-C.; Zhang, W. A Fast Ionic Conductor and Stretchable Solid Electrolyte Artificial Interphase Layer for Li Metal Protection in Lithium Batteries. *J. Alloys Compd.* **2020**, 155839. https://doi.org/10.1016/j.jallcom.2020.155839.

(202) Zhang, Y. J.; Wang, W.; Tang, H.; Bai, W. Q.; Ge, X.; Wang, X. L.; Gu, C. D.; Tu, J. P. An Ex-Situ Nitridation Route to Synthesize Li3N-Modified Li Anodes for Lithium Secondary Batteries. *J. Power Sources* **2015**, *277*, 304–311. https://doi.org/10.1016/j.jpowsour.2014.12.023.

(203) Kozen, A. C.; Lin, C. F.; Pearse, A. J.; Schroeder, M. A.; Han, X.; Hu, L.; Lee, S. B.; Rubloff, G. W.; Noked, M. Next-Generation Lithium Metal Anode Engineering via Atomic Layer Deposition. *ACS Nano* **2015**, *9* (6), 5884–5892. https://doi.org/10.1021/acsnano.5b02166.

(204) Chen, K.; Pathak, R.; Gurung, A.; Adhamash, E. A.; Bahrami, B.; He, Q.; Qiao, H.; Smirnova, A. L.; Wu, J. J.; Qiao, Q.; Zhou, Y. Flower-Shaped Lithium Nitride as a Protective Layer via Facile Plasma Activation for Stable Lithium Metal Anodes. *Energy Storage Mater.* **2019**, *18*, 389–396. https://doi.org/10.1016/j.ensm.2019.02.006.

(205) Moryson, Y.; Hartmann, H.; Otto, S.-K.; Fang, X.; Rohnke, M.; Janek, J. Protective Coating for the Lithium Metal Anode Prepared by Plasma Polymerization. *ACS Appl. Energy Mater.* **2023**, *6* (12), 6656–6665. https://doi.org/10.1021/acsaem.3c00681.

(206) Zhang, Y. J.; Liu, X. Y.; Bai, W. Q.; Tang, H.; Shi, S. J.; Wang, X. L.; Gu, C. D.; Tu, J. P. Magnetron Sputtering Amorphous Carbon Coatings on Metallic Lithium : Towards Promising Anodes for Lithium Secondary Batteries. *J. Power Sources* **2014**, *266*, 43–50. https://doi.org/10.1016/j.jpowsour.2014.04.147.

(207) Jing, H.; Kong, L.; Liu, S.; Li, G.; Gao, X. Protected Lithium Anode with Porous Al2O3 Layer for Lithium–Sulfur Battery. *J. Mater. Chem. A* **2015**, *3*, 12213–12219. https://doi.org/10.1039/c5ta01490e.

(208) Wang, L.; Zhang, L.; Wang, Q.; Li, W.; Wu, B.; Jia, W.; Wang, Y.; Li, J.; Li, H. Long Lifespan Lithium Metal Anodes Enabled by Al2O3 Sputter Coating. *Energy Storage Mater.* **2018**, *10* (August 2017), 16–23. https://doi.org/10.1016/j.ensm.2017.08.001.

(209) Wu, M.; Chang, H. Self-Assembly of NiO-Coated ZnO Nanorod Electrodes with Core − Shell Nanostructures as Anode Materials for Rechargeable Lithium- Ion Batteries. *J. Phys. Chem. Solids* **2013**, *117*, 2590–2599. https://doi.org/10.1021/jp3079327.

(210) Takada, K.; Ohta, N.; Zhang, L.; Fukuda, K.; Sakaguchi, I.; Ma, R.; Osada, M.; Sasaki, T. Interfacial Modification for High-Power Solid-State Lithium Batteries. *Solid State Ionics* **2008**, *179*, 1333–1337. https://doi.org/10.1016/j.ssi.2008.02.017.

(211) Zhu, B.; Jin, Y.; Hu, X.; Zheng, Q.; Zhang, S.; Wang, Q.; Zhu, J. Poly(Dimethylsiloxane) Thin Film as a Stable Interfacial Layer for High-Performance Lithium-Metal Battery Anodes. *Adv. Mater.* **2017**, *29*, 1603755. https://doi.org/10.1002/adma.201603755.

(212) Becking, J.; Gröbmeyer, A.; Kolek, M.; Rodehorst, U.; Schulze, S.; Winter, M.; Bieker, P.; Stan, M. C. Lithium-Metal Foil Surface Modification: An Effective Method to Improve the Cycling Performance of Lithium-Metal Batteries. *Adv. Mater. Interfaces* **2017**, *4* (16),

1–9. https://doi.org/10.1002/admi.201700166.

(213) Ryou, M. H.; Lee, Y. M.; Lee, Y.; Winter, M.; Bieker, P. Mechanical Surface Modification of Lithium Metal: Towards Improved Li Metal Anode Performance by Directed Li Plating. *Adv. Funct. Mater.* **2015**, *25* (6), 834–841. https://doi.org/10.1002/ADFM.201402953.

(214) Lopez, J.; Pei, A.; Oh, J. Y.; Wang, G. J. N.; Cui, Y.; Bao, Z. Effects of Polymer Coatings on Electrodeposited Lithium Metal. *J. Am. Chem. Soc.* **2018**, *140* (37), 11735–11744. https://doi.org/10.1021/jacs.8b06047.

(215) Kozen, A. C.; Lin, C. F.; Zhao, O.; Lee, S. B.; Rubloff, G. W.; Noked, M. Stabilization of Lithium Metal Anodes by Hybrid Artificial Solid Electrolyte Interphase. *Chem. Mater.* **2017**, *29* (15), 6298–6307. https://doi.org/10.1021/acs.chemmater.7b01496.

(216) Du, H.; Li, S.; Qu, H.; Lu, B.; Wang, X.; Chai, J. Stable Cycling of Lithium-Sulfur Battery Enabled by a Reliable Gel Polymer Electrolyte Rich in Ester Groups. *J. Memb. Sci.* **2018**, *550* (October 2017), 399–406. https://doi.org/10.1016/j.memsci.2018.01.017.

(217) Min, S.; Su, I.; Sun, Y.; Song, J.; Chung, S.; Kim, D. Cycling Characteristics of Lithium Metal Batteries Assembled with a Surface Modi Fi Ed Lithium Electrode. *J. Power Sources* **2013**, *244*, 363–368. https://doi.org/10.1016/j.jpowsour.2012.12.106.

(218) Weiss, M.; Seidlhofer, B.; Geiß, M.; Geis, C.; Busche, M. R.; Becker, M.; Vargas-barbosa, N. M.; Silvi, L.; Zeier, W. G.; Der, D. S.; Janek, J. Unraveling the Formation Mechanism of Solid − Liquid Electrolyte Interphases on LiPON Thin Films. *ACS Appl. Mater. Interfaces* **2019**, *11*, 9539–9547. https://doi.org/10.1021/acsami.8b19973.

(219) Wang, L.; Zhang, L.; Wang, Q.; Li, W.; Wu, B.; Jia, W.; Wang, Y.; Li, J.; Li, H. Long Lifespan Lithium Metal Anodes Enabled by Al2O3 Sputter Coating. *Energy Storage Mater.* **2018**, *10*, 16–23. https://doi.org/10.1016/j.ensm.2017.08.001.

(220) Wang, L.; Wang, Q.; Jia, W.; Chen, S.; Gao, P.; Li, J. Li Metal Coated with Amorphous Li 3 PO 4 via Magnetron Sputtering for Stable and Long-Cycle Life Lithium Metal Batteries. *J. Power Sources* **2017**, *342*, 175–182. https://doi.org/10.1016/j.jpowsour.2016.11.097.

(221) Chung, K.; Kim, W.; Choi, Y. Lithium Phosphorous Oxynitride as a Passive Layer for Anodes in Lithium Secondary Batteries. *J. Electroanal. Chem.* **2004**, *566*, 263–267. https://doi.org/10.1016/j.jelechem.2003.11.035.

(222) Lu, Y.; Gu, S.; Hong, X.; Rui, K.; Huang, X.; Jin, J.; Chen, C.; Yang, J.; Wen, Z. Pre-Modified Li3PS4 Based Interphase for Lithium Anode towards High-Performance Li-S

Battery. *Energy Storage Mater.* **2018**, *11* (September 2017), 16–23. https://doi.org/10.1016/j.ensm.2017.09.007.

(223) Barai, P.; Fuchs, T.; Trevisanello, E.; Kim, H. K.; Richter, F. H.; Janek, J.; Srinivasan, V. Reaction Current Heterogeneity at the Interface between a Lithium Electrode and Polymer/Ceramic Composite Electrolytes. *ACS Appl. Energy Mater.* **2023**, *6* (4), 2160–2177. https://doi.org/10.1021/ACSAEM.2C03059/ASSET/IMAGES/LARGE/AE2C03059_0011.JPEG.

(224) Sen, S.; Trevisanello, E.; Niemöller, E.; Niemöller, N.; Shi, B.-X.; Simon, F. J.; Richter, F. H.; Janek, J. The Role of Polymers in Lithium Solid-State Batteries with Inorganic Solid Electrolytes. *J. Mater. Chem. A HIGHLIGHT Publ.* **2021**, *9*, 18701–18732. https://doi.org/10.1039/d1ta02796d.

(225) Wu, H. L.; Haasch, R. T.; Perdue, B. R.; Apblett, C. A.; Gewirth, A. A. The Effect of Water-Containing Electrolyte on Lithium-Sulfur Batteries. *J. Power Sources* **2017**, *369*, 50–56. https://doi.org/10.1016/J.JPOWSOUR.2017.09.044.

(226) Lacey, M. J. Influence of the Electrolyte on the Internal Resistance of Lithium−Sulfur Batteries Studied with an Intermittent Current Interruption Method. *ChemElectroChem* **2017**, *4* (8), 1997–2004. https://doi.org/10.1002/CELC.201700129.

(227) Pei, H.; Guo, W.; Guo, R.; Li, Y.; Fang, C.; Zhang, Y.; Liu, W.; Wang, Y.; Xie, J. The Stability of Polymers in Liquid Li-S Battery. *J. Electrochem. Soc.* **2019**, *166* (3), A5215–A5220. https://doi.org/10.1149/2.0291903jes.

(228) Wang, S.; Zhang, X.; Liu, S.; Xin, C.; Xue, C.; Richter, F.; Li, L.; Fan, L.; Lin, Y.; Shen, Y.; Janek, J.; Nan, C. W. High-Conductivity Free-Standing Li6PS5Cl/Poly(Vinylidene Difluoride) Composite Solid Electrolyte Membranes for Lithium-Ion Batteries. *J. Mater.* **2020**, *6* (1), 70–76. https://doi.org/10.1016/j.jmat.2019.12.010.

(229) Zhang, Y.; Chen, R.; Wang, S.; Liu, T.; Xu, B.; Zhang, X.; Wang, X.; Shen, Y.; Lin, Y. H.; Li, M.; Fan, L. Z.; Li, L.; Nan, C. W. Free-Standing Sulfide/Polymer Composite Solid Electrolyte Membranes with High Conductance for All-Solid-State Lithium Batteries. *Energy Storage Mater.* **2020**, *25*, 145–153. https://doi.org/10.1016/j.ensm.2019.10.020.

(230) Marshall, J. E.; Zhenova, A.; Roberts, S.; Petchey, T.; Zhu, P.; Dancer, C. E. J.; McElroy, C. R.; Kendrick, E.; Goodship, V. On the Solubility and Stability of Polyvinylidene Fluoride. *Polymers (Basel).* **2021**, *13* (9), 1–31. https://doi.org/10.3390/polym13091354.

(231) Zhang, X.; Liu, T.; Zhang, S.; Huang, X.; Xu, B.; Lin, Y.; Xu, B.; Li, L.; Nan, C.-W.;

Shen, Y. Synergistic Coupling between Li 6.75 La 3 Zr 1.75 Ta 0.25 O 12 and Poly(Vinylidene Fluoride) Induces High Ionic Conductivity, Mechanical Strength, and Thermal Stability of Solid Composite Electrolytes. *J. Am. Chem. Soc.* **2017**, *139*, 13779–13785. https://doi.org/10.1021/jacs.7b06364.

(232) Nikiforov, G. B.; Roesky, H. W.; Koley, D. A Survey of Titanium Fluoride Complexes , Their Preparation , Reactivity , and Applications. *Coord. Chem. Rev.* **2014**, *258–259*, 16–57. https://doi.org/10.1016/j.ccr.2013.09.002.

(233) Maercker, A. Etherspaltungen Mit Organoalkalimetall-Verbindungen Und Alkalimetallen. *Angew. Chemie* **1987**, *99* (10), 1002–1019. https://doi.org/10.1002/ANGE.19870991006.

(234) Huang, C.-J.; Thirumalraj, B.; Tao, H.-C.; Shitaw, K. N.; Sutiono, H.; Hagos, T. T.; Tadesse Beyene, T.; Kuo, L.-M.; Wang, C.-C.; Wu, S.-H.; Su, W.-N.; Hwang, B. J. Decoupling the Origins of Irreversible Coulombic Efficiency in Anode-Free Lithium Metal Batteries. *Nat. Commun.* **2021**, *12*, 1452. https://doi.org/10.1038/s41467-021-21683-6.

(235) Jankowsky, S.; Hiller, M. M.; Wiemhöfer, H. Preparation and Electrochemical Performance of Polyphosphazene Based Salt-in-Polymer Electrolyte Membranes for Lithium Ion Batteries. *J. Power Sources* **2014**, *253*, 256–262. https://doi.org/10.1016/j.jpowsour.2013.11.120.

(236) Wren, A. G.; Phillips, R. W.; Tolentino, L. U. Surface Reactions of Chlorine Molecules and Atoms with Water and Sulfuric Acid at Low Temperatures. *J. Colloid Interface Sci.* **1979**, *70* (3), 544–557. https://doi.org/10.1016/0021-9797(79)90062-6.

(237) Sydam, R.; Deepa, M. A New Organo-Inorganic Hybrid of Poly(Cyclotriphosphazene-4,4′-Bipyridinium)Chloride with a Large Electrochromic Contrast. *J. Mater. Chem. C* **2013**, *1* (47), 7930–7940. https://doi.org/10.1039/C3TC31486C.

(238) Green, B.; Ridley, D. C.; Sherwood, P. M. A. X-Ray Photoelectron Spectroscopy of Some Dimethylamino-Substituted Cyclotri Phosphazenes. *J. Chem. Soc. Dalt. Trans.* **1973**, 1042–1044.

(239) Bhatia, Q. S.; Burrell, M. C. X-Ray Photoelectron and Static Secondary-Ion Mass Spectroscopic Studies of Segmented Block Copoly(Ether-Ester)S. *Polymer (Guildf).* **1991**, *32* (11), 1948–1956. https://doi.org/10.1016/0032-3861(91)90157-E.

(240) Boulanger, P.; Pireauxt, J. J.; Verbist, J. J.; Delhalle, J. X-Ray Photoelectron Spectroscopy Characterization of Amorphous and Crystalline Poly(Tetrahydrofuran): Experimental and Theoretical Study. *Polymer (Guildf).* **1994**, *35* (24), 5185–5193.

(241) Briggs, D.; Beamson, G. Primary and Secondary Oxygen-Induced C1s Binding Energy Shifts in X-Ray Photoelectron Spectroscopy of Polymers. *Anal. Chem.* **1992**, *64*, 1729–1736.

(242) Bruce, P. G.; Vincent, C. A. Polymer Electrolytes. *J. CHEM. SOC. FARADAY TRANS* **1993**, *89* (17), 3187–3203.

(243) Bieker, G.; Winter, M.; Bieker, P. Electrochemical in Situ Investigations of SEI and Dendrite Formation on the Lithium Metal Anode. *Phys. Chem. Chem. Phys.* **2015**, *17* (14), 8670–8679. https://doi.org/10.1039/C4CP05865H.

(244) Wood, K. N.; Kazyak, E.; Chadwick, A. F.; Chen, K. H.; Zhang, J. G.; Thornton, K.; Dasgupta, N. P. Dendrites and Pits: Untangling the Complex Behavior of Lithium Metal Anodes through Operando Video Microscopy. *ACS Cent. Sci.* **2016**, *2* (11), 790–801. https://doi.org/https://doi.org/10.1021/acscentsci.6b00260.

(245) Armstrong, R. D.; Landles, K. Lithium Ion Conducting Solids for Ambient Applications. *J. Appl. Electrochem.* **1982**, *12*, 533–535.

(246) Drvarič Talian, S.; Bobnar, J.; Sinigoj, A. R.; Humar, I.; Gaberšček, M. Transmission Line Model for Description of the Impedance Response of Li Electrodes with Dendritic Growth. *J. Phys. Chem. C* **2019**, *123* (46), 27997–28007. https://doi.org/10.1021/acs.jpcc.9b05887.

(247) Pang, Q.; Liang, X.; Shyamsunder, A.; Nazar, L. F. An In Vivo Formed Solid Electrolyte Surface Layer Enables Stable Plating of Li Metal. *Joule* **2017**, *1* (4), 871–886. https://doi.org/10.1016/j.joule.2017.11.009.

(248) He, Y.; Fan, W.; Zhang, Y.; Wang, Z.; Li, X.; Liu, Z.-G.; Lü, Z. Understanding the Relationships between Morphology, SEI Composition and Coulombic Efficiency of Lithium Metal. *ACS Appl. Mater. Interfaces* **2020**, *12*, 22268–22277. https://doi.org/10.1021/acsami.0c00789.

(249) Artyushkova, K. Misconceptions in Interpretation of Nitrogen Chemistry from X-Ray Photoelectron Spectra. *J. Vaccum Sci. Technol. A* **2020**, *38*, 031002. https://doi.org/10.1116/1.5135923.

(250) Schwöbel, A.; Hausbrand, R.; Jaegermann, W. Interface Reactions between LiPON and Lithium Studied by In-Situ X-Ray Photoemission. *Solid State Ionics* **2015**, *273*, 51–54. https://doi.org/10.1016/j.ssi.2014.10.017.

# 7 Appendix

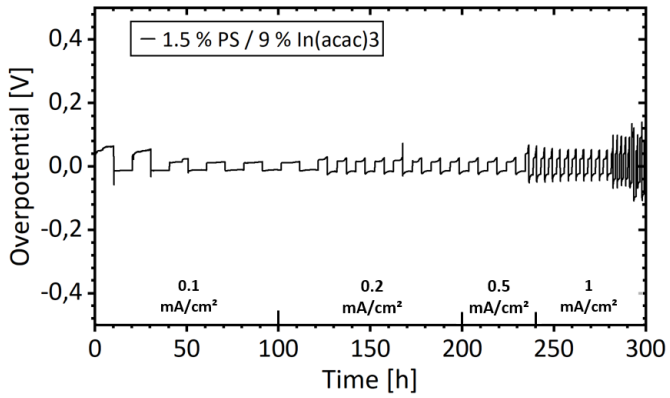


**Figure A1: Overpotential profile of a symmetrical cell using electrodes spin coated with PS and $In(acac)_3$ using THF as solvent. Measurement was performed at $T$ = 25 °C.**

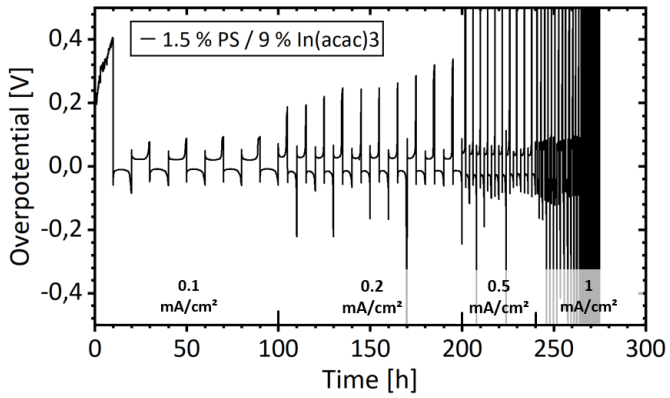


**Figure A2: Overpotential profile of a symmetrical cell using electrodes spin coated with PS and $In(acac)_3$ using THF as solvent. Measurement was performed at $T$ = 25 °C.**

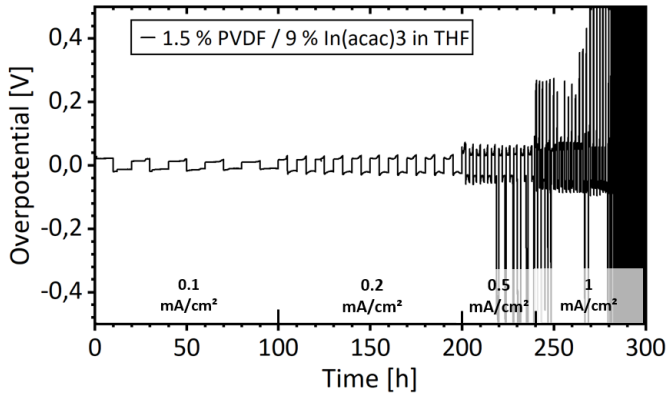


**Figure A3: Overpotential profile of a symmetrical cell using electrodes spin coated with PVDF and $In(acac)_3$ using THF as solvent. Measurement was performed at $T$ = 25 °C.**

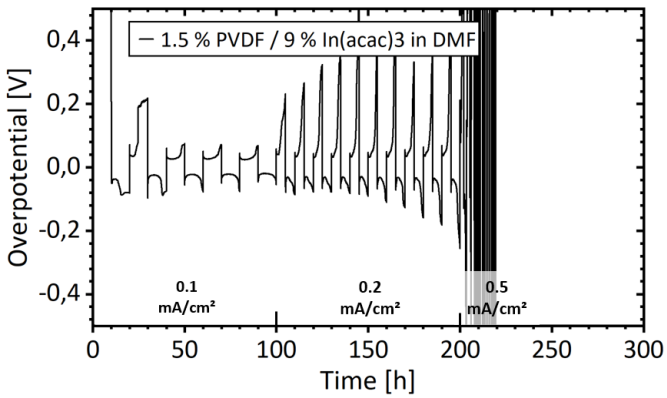


**Figure A4: Overpotential profile of a symmetrical cell using electrodes spin coated with PVDF and $In(acac)_3$ using DMF as solvent. Measurement was performed at $T$ = 25 °C.**

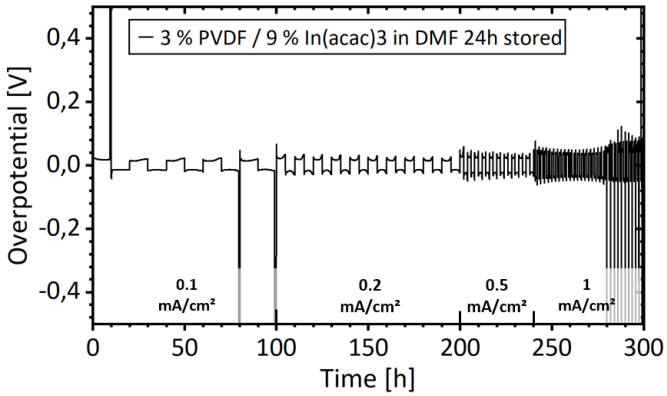


**Figure A5: Overpotential profile of a symmetrical cell using electrodes spin coated with PVDF and $In(acac)_3$ using DMF as solvent. Cycling was started after 24 h resting time. Measurement was performed at $T$ = 25 °C.**

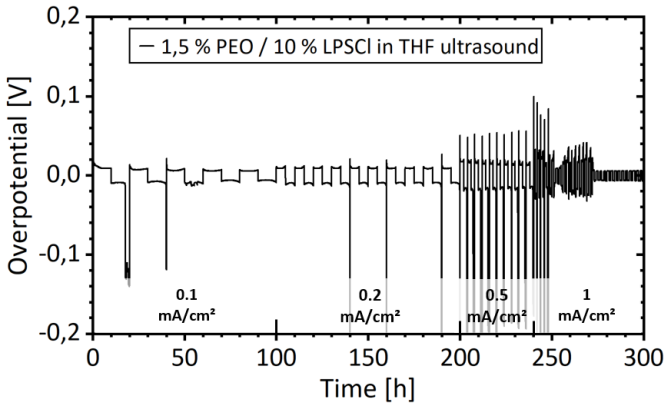


**Figure A6: Overpotential profile of a symmetrical cell using electrodes spin coated with 2 x 5 droplets ultrasonicated PEO 1.5:10 in THF. Measurement was performed at $T$ = 25 °C.**

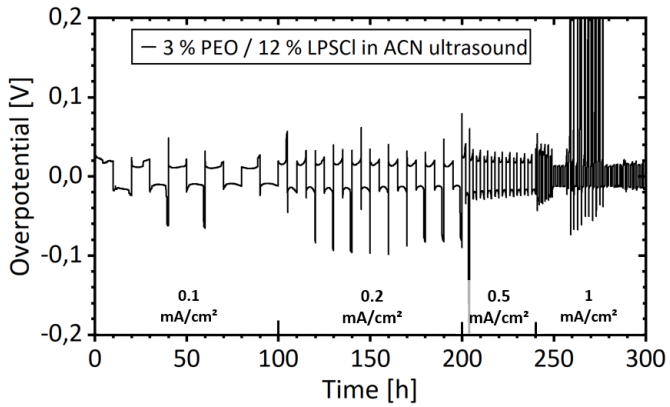


**Figure A7: Overpotential profile of a symmetrical cell using electrodes spin coated with 2 x 5 droplets ultrasonicated PEO 3:12 in acetonitrile. Measurement was performed at $T$ = 25 °C.**

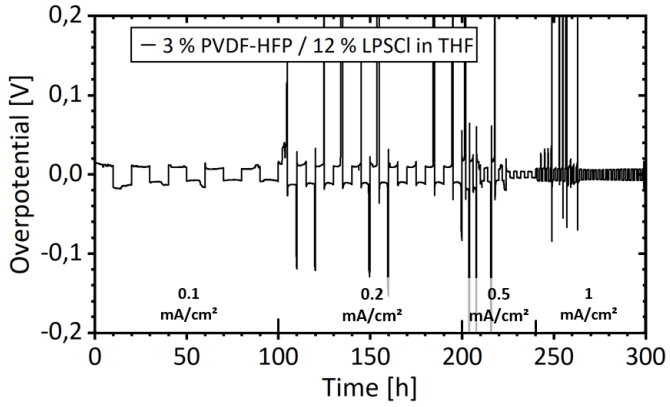


**Figure A8: Overpotential profile of a symmetrical cell using electrodes spin coated with PVDF-HFP 3:12 in THF. Measurement was performed at $T$ = 25 °C.**

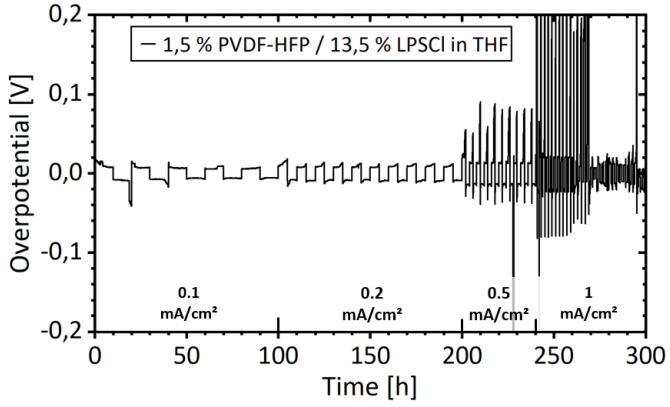


**Figure A9: Overpotential profile of a symmetrical cell using electrodes spin coated with PVDF-HFP 1.5:13.5 in THF. Measurement was performed at $T$ = 25 °C.**

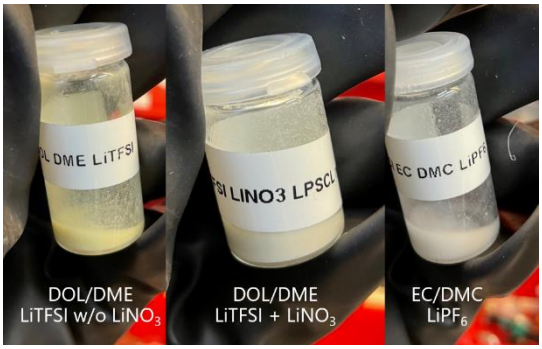


**Figure A10: LPSCl submerged in different liquid electrolytes. The argyrodite in DME/DOL/LiTFSI without lithium nitrate shows slight yellow discoloration whereas this could possibly come from moisture content in the liquid electrolyte.**

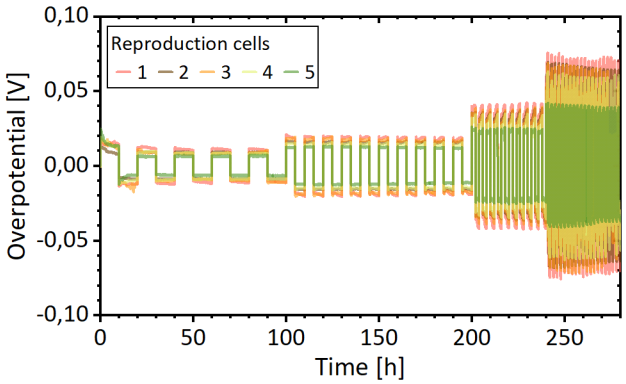


**Figure A11: Overpotential of 5 symmetric cells using two Li metal electodes after dip coating in 16.7 % NPCl in heptane. The high uniformity of the cycling behavior can clearly be seen. Measurements were performed at *T* = 25 °C.**

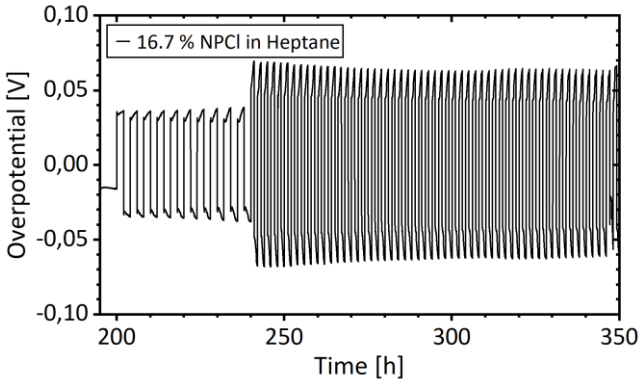


**Figure A12: Overpotential of a symmetric cell using two Li metal electodes after dip coating in 16.7 % NPCl in heptane. Enlarged display of the high current density part of figure 40. Measurement was performed at *T* = 25 °C.**

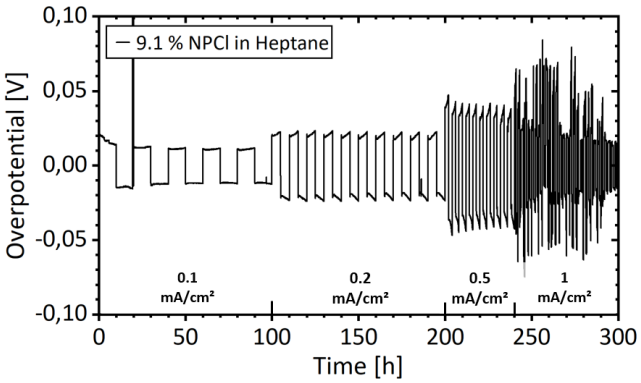


**Figure A13: Overpotential of a symmetric cell using two Li metal electodes after dip coating in 9.1 % NPCl in heptane. Measurement was performed at *T* = 25 °C.**

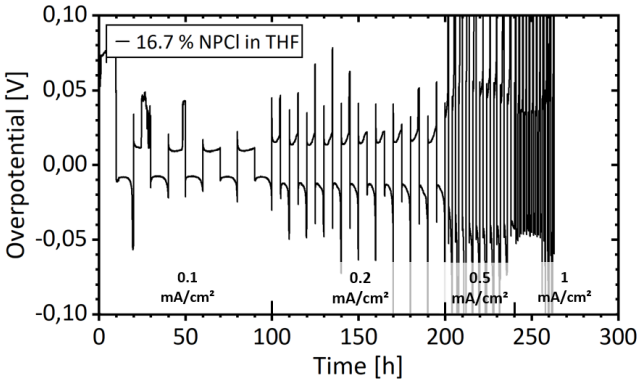


**Figure A14: Overpotential of a symmetric cell using two Li metal electodes after dip coating in 16.7 % NPCl in THF. Measurement was performed at *T* = 25 °C.**

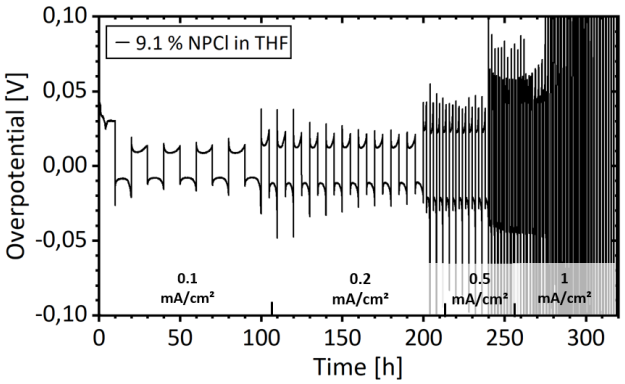


**Figure A15: Overpotential of a symmetric cell using two Li metal electodes after dip coating in 9.1 % NPCl in THF. Measurement was performed at *T* = 25 °C.**

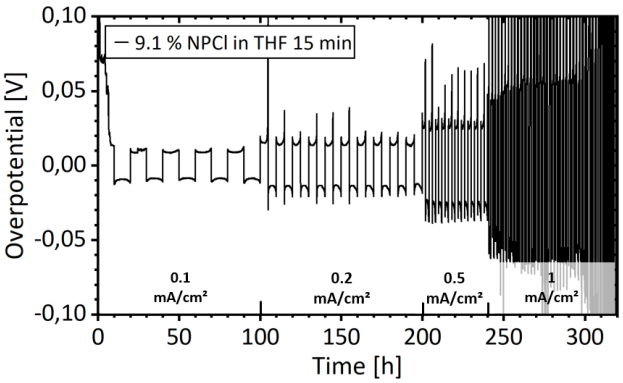


**Figure A16: Overpotential of a symmetric cell using two Li metal electodes after dip coating in 9.1 % NPCl in THF for 15 minutes. Measurement was performed at *T* = 25 °C.**

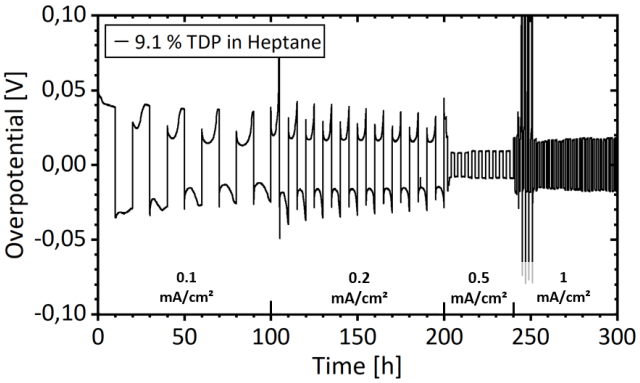


**Figure A17: Overpotential of a symmetric cell using two Li metal electodes after dip coating in 9.1 % TDP in heptane. Measurement was performed at *T* = 25 °C.**

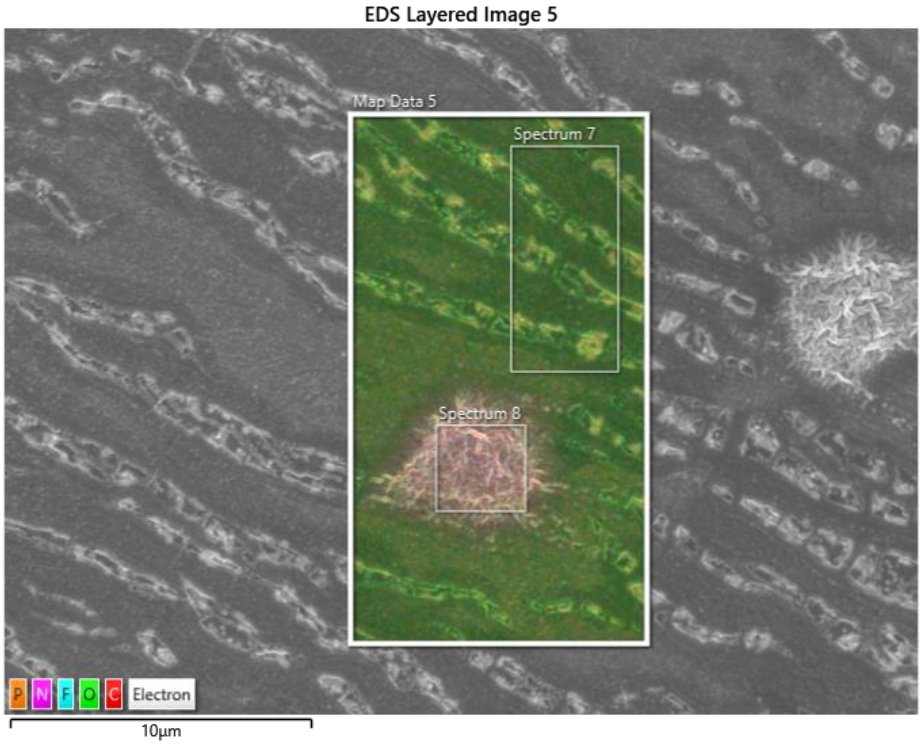


**Figure A18: SEM/EDX overlay picture of an electrode after coating with 16.7 % TDP in THF.**

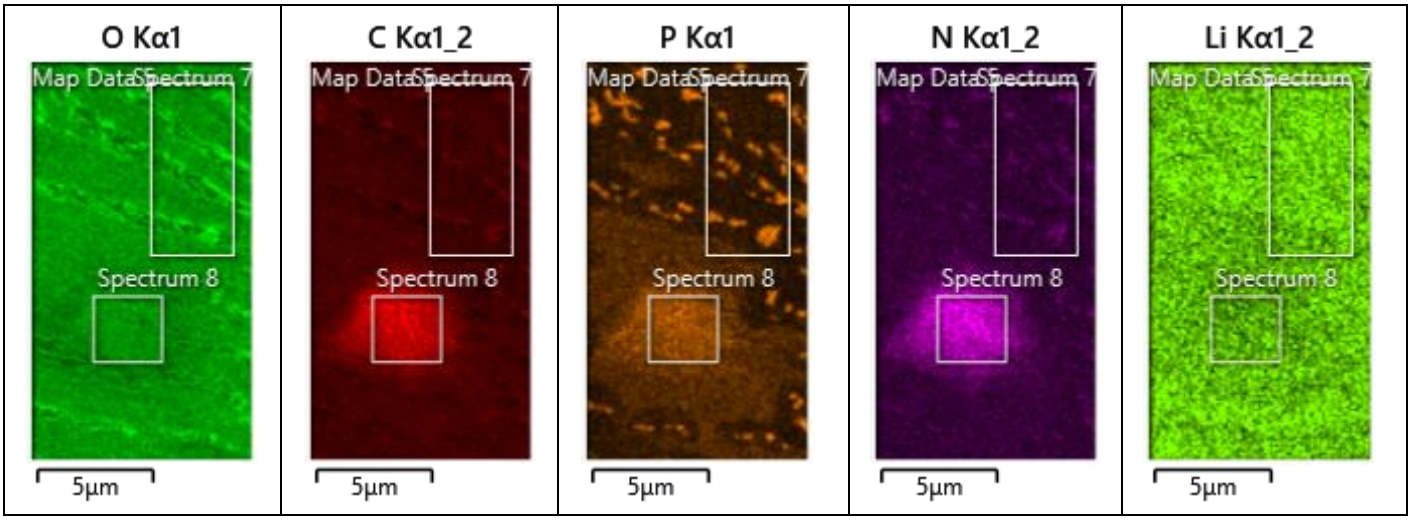


**Figure A19: EDX element spectra of the overlay area from A18. The strong C, N and P signals at the rectangle marked as "Spectrum 8" led to the conclusion that these structures are TDP residuals. The spotwise reaction of the reagent with the Lithium metal can also clearly be seen.**

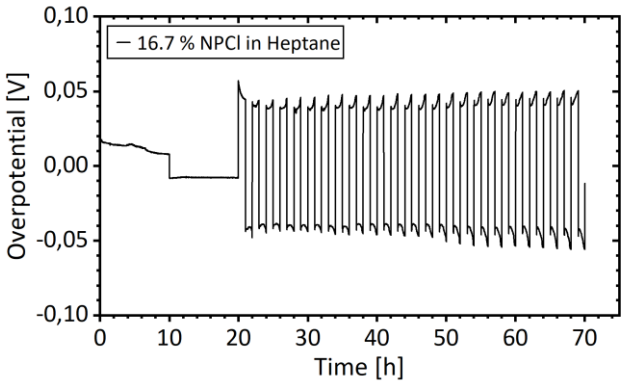


**Figure A20: Overpotential of a symmetric cell using two Li metal electodes after dip coating in 16.7 % NPCl in heptane. For use as SEM sample, the cell was cycled for one cycle at 0.1 mA/cm² followed by 25 cycles at 1 mA/cm². Measurement was performed at *T* = 25 °C.**

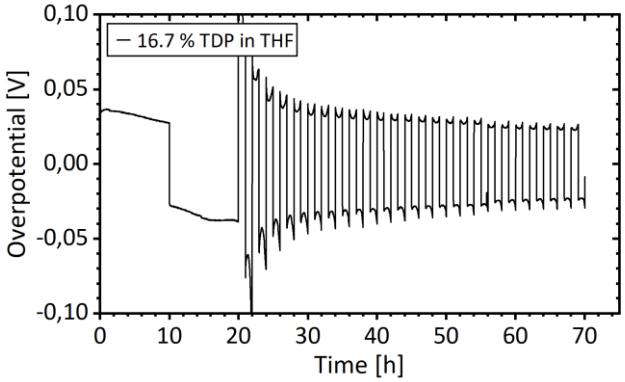


**Figure A21: Overpotential of a symmetric cell using two Li metal electodes after dip coating in 16.7 % TDP in THF. For use as SEM sample, the cell was cycled for one cycle at 0.1 mA/cm² followed by 25 cycles at 1 mA/cm². Measurement was performed at *T* = 25 °C.**

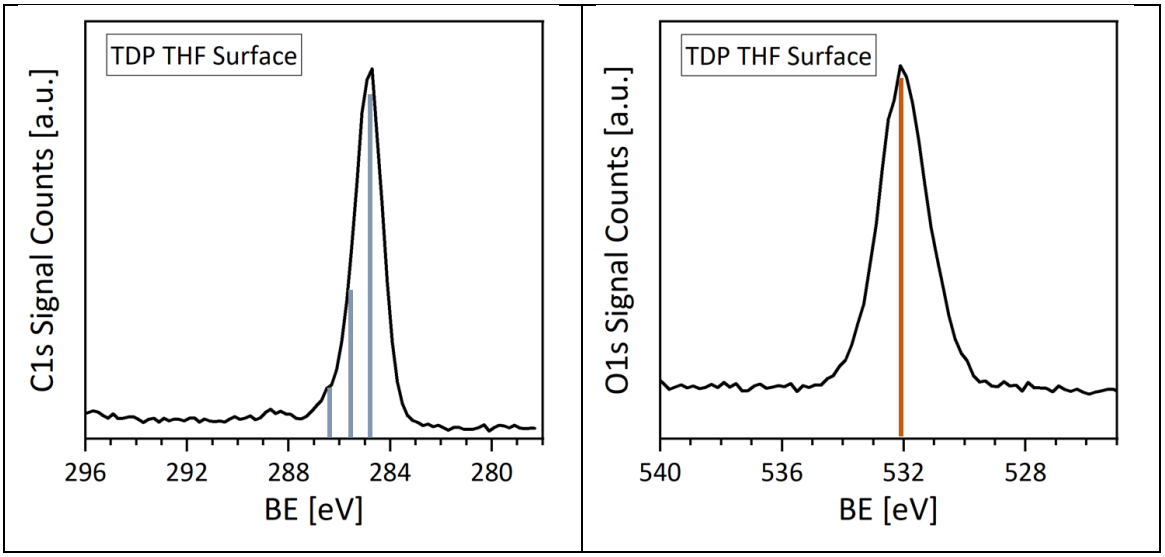


**Figure A22: Left: C 1s surface spectrum of TDP/THF coated lithium. The highest peak at ~ 284.8 eV is attributed to adventitious carbon while the two other indicated peaks at roughly 285.5 and 286.5 eV are attributed to C-O and C-O-C bound species.[241] Right: O 1s surface spectrum of TDP/THF coated lithium. The peak at 532 eV can be attributed to hydroxide type species.**

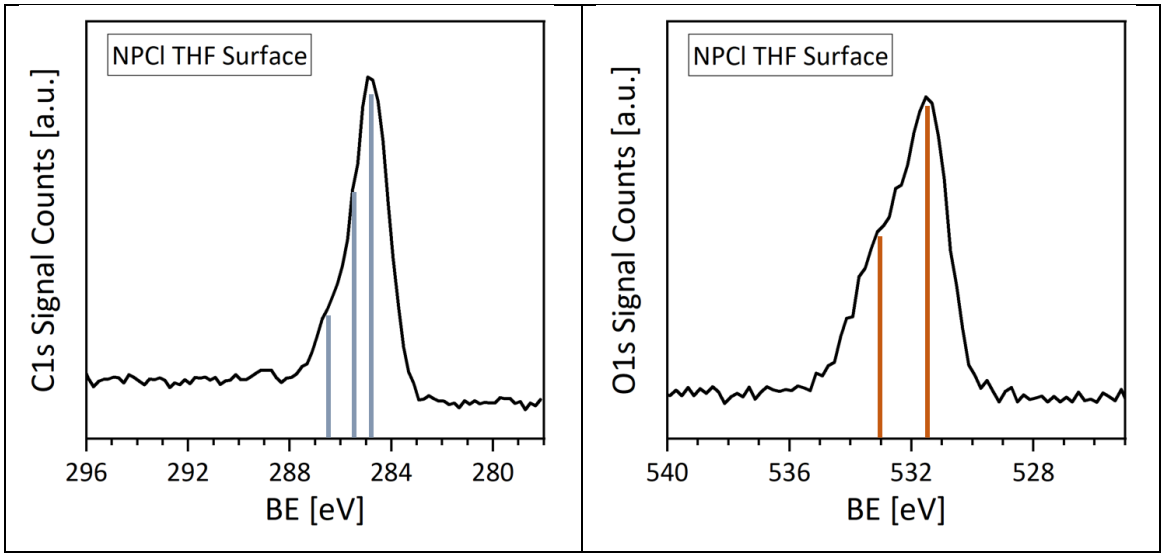


**Figure A23: Left: C 1s surface spectrum of NPCl/THF coated lithium. The highest peak at ~ 284.8 eV is attributed to adventitious carbon while the two other indicated peaks at roughly 285.5 and 286.5 eV are attributed to C-O and C-O-C bound species.[241] Right: O 1s surface spectrum of NPCl/THF coated lithium. The peak at slightly below 532 eV can be attributed to hydroxide type species and the peak at 533 eV belongs to C-O species.**

# 8 Acknowledgements/Danksagung

Hiermit möchte ich allen Personen, die mich im Laufe der Promotion unterstützt haben, meinen herzlichen Dank aussprechen.

Prof. Dr. Dr. h.c. Jürgen Janek für die Möglichkeit, Teil seiner großartigen Arbeitsgruppe zu sein und über dieses spannende Thema meine Doktorarbeit anzufertigen, sowie für die Unterstützung und Ideen in den zahlreichen Gesprächen.

Dr. Joachim Sann für die weitere Betreuung der Arbeit und die immer schnelle Erreichbarkeit. Danke für die vielen Gespräche, das Feedback, für alle Vorschläge und Ratschläge.

Dr. Anja Henß, Dr. Bjoern Luerßen, PD Dr. Marcus Rohnke, Dr. Boris Mogwitz und Dr. Klaus Peppler für die Unterstützung und die Beantwortung aller möglichen kleinen und großen Fragen.

Dr. Fabian Stöhr für die zahllosen interdisziplinären Unterredungen, in denen wir uns stets gegenseitig vom hohen Wert der wissenschaftlichen Arbeit überzeugen konnten.

Dr. Svenja-Katharina Otto, Yannik Moryson, Luise Riegger, Kilian Vettori und Steffen Schröder für das wunderbare Arbeitsklima im Büro B65, für die Pflege der Pflanzen im Büro, für jede kleine Unterhaltung und natürlich auch für den fachlichen Austausch.

Anika Siebert und Lukas Schneider für die Unterstützung im Labor und dafür, dass ich ihre Bachelorarbeiten betreuen durfte.

Meiner Frau Marie, meinen Eltern und meinen Freunden für jede Unterstützung, jedes schöne Erlebnis und jedes gute Wort abseits der Uni.

Danke!